NASA TN D-1525

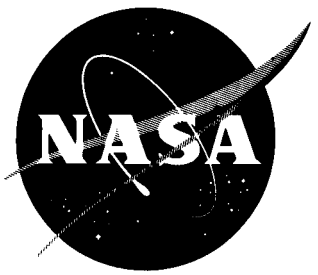

TECHNICAL NOTE

D-1525

INFLUENCE OF WEIGHT PARAMETERS ON THE PROPULSION REQUIREMENTS OF ORBIT-LAUNCHED VEHICLES

By Dietrich W. Fellenz and Ronald J. Harris

George C. Marshall Space Flight Center
Huntsville, Alabama

NATIONAL AERONAUTICS AND SPACE ADMINISTRATION

WASHINGTON

May 1963

TABLE OF CONTENTS

LIST OF ILLUSTRATIONS

LIST OF ILLUSTRATIONS (Cont'd)

LIST OF ILLUSTRATIONS (Cont'd)

LIST OF ILLUSTRATIONS (Cont'd)

LIST OF ILLUSTRATIONS (Cont'd)

DEFINITION OF SYMBOLS (Concluded)

SYMBOL	DEFINITION
v^*	Comparative velocity; m/sec
W_o	Initial or gross weight; force units
W_n	Effective structural weight; force units
W_8	Used propellant weight; force units
W_{gd}	Gross payload weight; force units
ϑ	Flight path angle measured from the local vertical (positive down), [deg]
β	Thrust vector orientation angle measured from the velocity vector to the thrust vector (positive down), [deg]
ψ	Central angle measured from ignition [deg]
ϵ_n	Effective structural ratio of stage $= \frac{W_n}{W_o}$
ζ	Propellant ratio of individual stage $= \frac{W_8}{W_o}$
λ_{gd}	Gross payload ratio of individual stage $= \frac{W_{gd}}{W_o}$
$\mu_\oplus$	Gravitational constant of earth

Subscripts

o	Initial
$\oplus$	Earth
id	Ideal
b	Burnout

NATIONAL AERONAUTICS AND SPACE ADMINISTRATION

TECHNICAL NOTE D-1525

INFLUENCE OF WEIGHT PARAMETERS ON THE PROPULSION REQUIREMENTS OF ORBIT-LAUNCHED VEHICLES

By

Dietrich W. Fellenz and Ronald J. Harris

SUMMARY

The effects of thrust-to-weight ratio and structural weight assumptions on payload performance have been investigated for orbit launched vehicles with lunar or escape missions. The propulsion systems considered were high-energy chemical and nuclear heat-exchanger systems. It is shown that the assumption of structural weights as being composed of terms proportional to thrust level and propellant loading is necessary and practical for the discussion of the influence of thrust-to-weight ratio on payload performance.

Results are given in parametric form showing payload ratio and related performance parameters as functions of thrust-to-weight ratio, representative engine and tankage specific weights for both propulsion systems and for tangential and circumferential thrust orientations and for different altitudes. The curves permit the rapid determination of maximum payload conditions as well as the discussion of performance parameters of off-optimum configurations.

INTRODUCTION

An area of considerable interest in the design of orbit-launched space vehicles is the wide range of feasible values for thrust-to-weight ratio. The constraint imposed by wind conditions on ground-launch vehicles is removed as is the constraint that the thrust-to-weight ratio must be greater than one at ignition. The upper limit of possible thrust-to-weight ratios for an orbit-launched vehicle is determined primarily by its structural design and the maximum tolerable burnout acceleration; whereas, the lower limit is established by acceptable velocity losses or travel time. The basic problem then is to determine, for a given vehicle system, the thrust-to-weight ratio which yields maximum payload.

The general effects of thrust-to-weight ratio on the trajectory and performance characteristics of space vehicles have been widely discussed in the literature. It is obvious that low thrust results in longer burning time and higher velocity losses. High specific impulse also leads to increased burning time and velocity losses. In the latter case, however, the propulsion system is more efficient because of the higher exhaust velocity and the consequent reduction of the required propellant ratio. In Reference 1 the importance of thrust vector orientation in the determination of the optimum thrust-to-weight ratio is recognized and the cases of radial and circumferential thrust are compared, concluding that the latter is the more efficient mode. The results of one of the earliest attempts to find the optimum thrust vector orientation are given in Reference 2. In this and a later paper by the same author, Reference 3, both of which are based on the assumption of constant acceleration, it was concluded that the tangential thrust vector control mode is a very close approximation of optimal conditions. It is further stated in Reference 3 that an even closer approximation can be made by assuming a "throw-off angle" (equivalent to β in this report) of a certain magnitude and tapering this angle to zero at burnout. The advantage of using the tangential thrust orientation mode as compared with the circumferential is confirmed in Reference 4. The same modes were investigated in Reference 5, considering mission requirements up to three times the initial orbital speed. It is shown therein that the tangential mode is close to optimum, especially if a hyperbolic excess after escape must be attained.

A generalized presentation of the trajectory parameters for the case of low thrust-to-weight ratios (on the order of 0.01) and constant tangential thrust is given in reference 6. Further discussions of the problems of departure from orbit and low thrust trajectories can be found in references 7 and 8.

All of the investigations mentioned above centered around the evaluation of the mass ratio required for a particular mission as a function of specific impulse and steering program. For the inclusion of high or low thrust levels, simplifying modifications of the equations of motion were usually introduced.

The mass ratio of a vehicle, however, does not readily lend itself for the discussion of payload performance, if the structural parameters are unknown, and also does not permit the discussion of the influence of the initial thrust-to-weight ratio on payload performance. This was possible only when assumptions for structural weights were introduced in reference 9. This study assumes, however, that the structural weight consists mainly of engine weight and neglects propellant tankage weight. This assumption is justified for the electrical propulsion systems analyzed in reference 9, where the engine weight per unit thrust is several orders of magnitude higher than those of typical chemical and nuclear heat exchanger propulsion systems. For a vehicle employing one of the latter systems, it is also necessary to consider those structural weights which are proportional to the required propellant loading. One of the first steps in this direction was made in reference 10, which discusses the effect of initial thrust-to-weight ratio on the payload performance of a wide spectrum of conceivable propulsion systems, ranging from low-energy chemical to electrical propulsion. Representative engine and tankage specific weights were assumed for each system and payload and optimum thrust-to-weight ratio were calculated for the escape from earth orbit mission. Since the effect of variations in engine and tankage weights was not included in reference 10, the results are not readily adaptable to vehicle configurations whose weight characteristics are different from those assumed. Furthermore, the velocity requirements for the assumed mission were derived from analytical approximations.

The purpose of the present analysis is to determine the optimum thrust-to-weight ratio, corresponding to maximum payload, for space vehicles departing from earth orbit on lunar or escape missions, considering engine and propellant tankage specific weights as parameters.

As mentioned previously it is necessary to specify the structural weight characteristics of the vehicle before the payload weight can be calculated from the cutoff weight. The range of engine and tankage specific weights assumed was based on current characteristics of both high-energy chemical and nuclear heat exchanger propulsion systems. The specific impulse was assumed to be 420 seconds for the chemical systems and 765 seconds for the nuclear systems.

Calculations were made by numerical integration on the IBM 7090 digital computer. The equations of motion are related to a spherical, rotating earth. Only planar trajectories were considered and all aerodynamic and pertubative forces were neglected. Thrust is assumed to remain constant throughout flight. Although the tangential thrust vector control mode has been shown to be nearer to the optimum conditions, the circumferential mode was also investigated for comparison purposes.

The authors of this report are indebted to Dr. H.G.L. Krause and D.R. Saxton for their advice and constructive criticism, to L.G. Singleton for the programming of the equations, and to L.R. Cohen for his assistance in the construction of the graphs.

ANALYSIS

From the wide spectrum of mission profiles involving orbit-launched vehicles, lunar missions of specified transfer time and escape missions were selected for consideration. Two specific thrust orientation modes were considered: thrust tangential to the flight path, $\beta = 0^\circ$, and circumferential thrust where the thrust is always perpendicular to the local radius vector so that $\beta = 90^\circ - \vartheta$.

The impulsive velocity requirements for injection into a lunar transfer trajectory having an 80 kilometer (43.17 nautical mile) periselenum were calculated using the method shown in FIGURE 1. This method is based on the sphere of influence concept, reducing the n-body problem to two two-body problems. These velocity requirements were programmed into a trajectory computation procedure in such a manner that the vehicle velocity at the end of each calculation step is compared with the impulsive injection velocity required at the same altitude for a specific transfer time. When these velocities match, the parameters of interest are printed.

Only transfer times between 70 hours and 49.75 hours (corresponding to escape) were considered.

The impulsive velocities given in FIGURE 1 were calculated assuming horizontal injection ($\vartheta = 90°$), whereas the flight path angle at injection in the present analysis was not restricted to this condition. Consequently, a slightly higher injection velocity is required if transfer time is held constant. However, the velocity requirements given in FIGURE 1 are somewhat conservative. Both of these influences are of the same order of magnitude and are assumed to compensate each other.

Referring to the sketch below, the equations of motion of the vehicle flying out of orbit are:

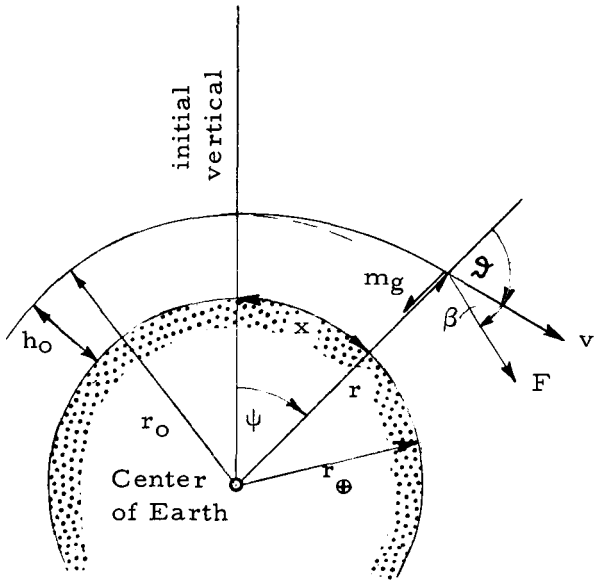

$$\dot{v} = \frac{F \cos \beta}{m} - g \cos \vartheta$$

$$\dot{\vartheta} = \frac{F \sin \beta}{m v} + \left(\frac{g}{v} - \frac{v}{r} \right) \sin \vartheta$$

The thrust orientation angle is dependent on the control mode used. For the tangential mode,

$$\beta = 0^\circ$$

and for the circumferential mode,

$$\beta = 90^\circ - \vartheta$$

Numerical integration of the equations of motion determines velocity and flight path angle since

$$v = \int \dot{v}\, dt$$

$$\vartheta = \int \dot{\vartheta}\, dt$$

The range and altitude are then calculated by the relations

$$x = \int \frac{r_\oplus}{r} v \sin\vartheta \, dt$$

$$h = h_o + \int v \cos\vartheta \, dt$$

The central angle is found from

$$\psi = \int \frac{\dot{x}}{r_\oplus} \, dt$$

It should be noted that the initial thrust-to-weight ratio is hidden in the general equations of motion since at $t = 0$,

$$\frac{F}{m} = \left(\frac{F}{W_o}\right) g_n$$

The most important variable in the equations of motion, as far as payload performance is concerned, is the burning time required to achieve preset burnout conditions. Before an evaluation can be made of payload performance, however, the weight characteristics of the vehicle must be defined. Following the approach used in Reference 11, the effective net structural weight of the stage is assumed to be composed of three weight groups proportional to the thrust, propellant loading and initial weight of the stage respectively. The first weight group is composed of the engine, propulsion system hardware, and certain structural members which may be assumed proportional to thrust. The

second group consists of the propellant tankage and any propellant residuals which may be assumed proportional to the propellant loading. While propellant residuals are obviously not a part of the stage structure, they are part of the dead weight of the stage and are normally included in the effective net structural weight. The third weight group, which is assumed to be proportional to the initial weight of the vehicle, is composed of astrionic gear, interstage structure, and various miscellaneous equipment. Thus the effective net structural weight of a stage can be expressed as

$$W_n = AF + BW_8 + CW_0$$

The parameters A, B, and C are structural specific weight factors equivalent to those defined in Reference 11. They are:

$$A = \frac{\text{Weight proportional to } F}{F}$$

$$B = \frac{\text{Weight proportional to } W_8}{W_8}$$

$$C = \frac{\text{Weight proportional to } W_0}{W_0}$$

In terms of nondimensional ratios, the effective net structural weight is

$$\epsilon_n = A\,(F/W_0) + B\zeta + C$$

In the present analysis, C was assumed to be zero. This assumption does not affect the determination of the optimum thrust-to-weight ratio but does affect the payload curves as will be explained later.

The relation between stage payload, propellant loading and net structural weight is

$$W_{gd} = W_o - W_s - W_n$$

or in dimensionless terms

$$\lambda_{gd} = 1 - \zeta - \epsilon_n$$

This can be further expressed as

$$\lambda_{gd} = 1 - \zeta\,(B+1) - A\,(F/W_o) - C$$

For constant thrust and specific impulse, the propellant ratio is given by

$$\zeta = \left(\frac{F}{W_o}\right) \frac{t_b}{I_{sp}}$$

Hence,

$$\lambda_{gd} = 1 - \frac{F}{W_o}\left(\frac{B+1}{I_{sp}}\, t_b + A\right) - C$$

so that the influence of thrust-to-weight ratio on payload becomes evident. Since the burning time and hence the propellant ratio are determined from the numerical integration of the equations of motion, it remains only to assume representative structural weights in order to evaluate the payload ratio. It should be noted that since C is a constant in the above equation, it can be assumed zero in the determination of the optimum thrust-to-weight ratio as mentioned earlier.

For a mission with a given impulsive velocity requirement and an assumed specific impulse and thrust level, the maximum payload ratio and corresponding optimum thrust-to-weight ratio are determined by the tradeoff between burning time and net effective structural weight. With very large thrust-to-weight ratios, approaching an impulsive kick, the burning time and hence the velocity losses are comparatively low but the propulsion system weight usually comprises a significant percentage of the total stage weight. For low thrust-to-weight ratios, burning time and velocity losses are higher, while the propulsion system weight is relatively small and in some cases may be neglected. Thus, for a given vehicle system, there is an optimum thrust-to-weight ratio somewhere between these two extreme cases which results in a maximum payload.

A vehicle departing from orbit gains considerable potential energy before reaching injection conditions, especially in the case of low thrust or high specific impulse systems. It is therefore necessary, in calculating velocity losses, to compare the gain in total energy with the energy supplied by the vehicle stage. The sum of the potential energy

$$E_{pot} = m \int_{r_o}^{r} \frac{\mu_\oplus}{r^2} \, dr = m \, \mu_\oplus \left(\frac{1}{r_o} - \frac{1}{r} \right)$$

and the kinetic energy

$$E_{kin} = \frac{mv^2}{2}$$

is expressed as velocity called the comparative velocity,

$$v^* = \sqrt{\frac{2}{m} (E_{kin} + E_{pot})}$$

or

$$v^* = \sqrt{v^2 + 2 \, \mu_\oplus \left(\frac{1}{r_o} - \frac{1}{r} \right)}$$

The increase in comparative velocity during ascent from $r = r_o$ to $r = r_b$ is

$$\Delta v^* = v^*_{r_b} - v^*_{r_o}$$

or

$$\Delta v^* = \sqrt{v_B^2 + 2 \mu_\oplus \left(\frac{1}{r_o} - \frac{1}{r_b} \right)} - v_o$$

The velocity loss due to gravity is then

$$\Delta v_{loss} = \Delta v_{id} - \Delta v^*$$

Since,

$$\Delta v_{id} = g_n I_{sp} \ln \frac{1}{1 - \zeta}$$

then,

$$\Delta v_{loss} = g_n I_{sp} \ln \frac{1}{1-\zeta} - \Delta v^*$$

For the special case of going from circular velocity at r_o to escape velocity, the relations simplify to

$$\Delta v^* = \sqrt{\frac{\mu_\oplus}{r_o}} \left(\sqrt{2}-1\right) = 0.414 \sqrt{\frac{\mu_\oplus}{r_o}}$$

$$\Delta v_{loss} = g_n I_{sp} \ln \frac{1}{1-\zeta} - 0.414 \sqrt{\frac{\mu_\oplus}{r_o}}$$

ASSUMPTIONS

The basic assumptions made in the analysis are summarized as follows:

1. Acceleration with constant thrust out of a circular earth orbit with tangential and circumferential thrust vector control modes

2. Initial orbital altitudes:

h_o = 185.2 km (100 N. M.)
h_o = 370.4 km (200 N. M.)
h_o = 555.6 km (300 N. M.)

3. Acceleration of a single stage to local conditions required for lunar transfer to an 80km periselenum with free-flight times of 70, 65, 60, 55, and 49.75 (equivalent to escape) hours

4. Structural specific weights for high-energy chemical stages with I_{sp} = 420 sec were varied parametrically over the following ranges:

$0.01 < A < 0.05$
$0.03 < B < 0.09$

5. Structural specific weights for nuclear heat-exchanger stages using liquid hydrogen as a propellant with I_{sp} = 765 sec were varied parametrically over the following ranges:

$$0.09 < A < 0.60$$
$$0.08 < B < 0.14$$

6. Mean spherical earth model with:

$$\mu_{\oplus} = 398,613.52 \text{ km}^3/\text{sec}^2$$

$$r_{\oplus} = 6371.104 \text{ km}$$

DISCUSSION OF RESULTS

The results of the analysis, shown in FIG 2 through 68 are separated according to the assumed values of I_{sp}. The high-energy chemical results are given first, followed by identical data for the nuclear heat-exchanger systems. The major portion of the analysis was directed toward the escape mission and its equivalent lunar mission.

It was found that the propellant ratio required for lunar missions, with transfer times other than escape transfer, differs from the escape propellant ratio by a value that, for all practical purposes, is dependent only on transfer time and specific impulse FIG 68. This increment is independent of the initial thrust-to-weight ratio, initial orbital altitude, and thrust orientation mode within the accuracy that the propellant ratio curves can be read.

The major emphasis in this study was placed on the influence of structural weight on the optimum thrust-to-weight ratio. The majority of the curves presented (FIG 3-11, 19-27, 33-44, and 52-63) show the functional relation between the payload and thrust-to-weight ratios. The upper limit of thrust-to-weight ratio was selected arbitrarily, while the lower limit was determined by the maximum injection altitude assumed in FIG 1. For F/W_o values lower than about 0.08 and I_{sp} = 765 sec, the maximum altitude assumed was exceeded before escape velocity was achieved. The curves are relatively flat in the region of the maximum payload ratio so the performance is not severely penalized if the thrust-to-weight ratio is slightly above or below optimum. The curves are very steep on each end, however, indicating that the thrust-to-weight ratio must be confined to a narrow

region for near optimum payload performance. It should be emphasized that, as mentioned earlier, the magnitude of the payload ratio λ shown in the curves was calculated assuming C = 0, since the magnitude of C does not affect the optimum thrust-to-weight ratio. A non-zero value of C detracts from the value of the payload ratio shown and simply shifts each curve downward so that the actual payload in a practical case is

$$\lambda_{gd} = \lambda_{c=o} - C$$

The optimum points on each set of payload ratio curves were plotted separately in FIG 12, 28, 45, and 64 to allow a rapid evaluation of the effect of the structural parameters on optimum conditions. It should be noted that in all cases considered the tangential thrust vector control mode results in higher payload ratios. The difference between this mode and the circumferential mode disappears at the higher thrust-to-weight ratios, however, as would be expected. The results generally agree with those shown in reference 10 for the structural weight parameters assumed therein.

Within the range of structural weight parameters assumed in this study, the optimum thrust-to-weight ratio is shown (see FIG 12, 28, 45, and 64) to be within the following approximate areas:

High energy chemical vehicles $0.25 < F/W_o < 0.60$
Nuclear heat-exchanger vehicles $0.10 < F/W_o < 0.30$

From FIG 1 it can be seen that the difference in injection velocity between the missions of various transfer times considered in this analysis is relatively small, compared to the total velocity required. Consequently, for a given vehicle the difference in tankage weight required for the various transfer times considered can be neglected so that the difference in payload can be attributed only to the difference in the propellant required. Under this assumption, FIG 68 shows the increment of payload ratio between the escape mission and the other transfer times considered.

Further results showing related parameters that do not require discussion include: curves for central angle, burning time, altitude, flight path angle, and velocity losses. The curves for burning time (FIG 15 and 48) and flight path angle at escape (FIG 17 and 50) can be considered valid for all initial orbital altitudes investigated, since the variation of these parameters with the initial orbital altitude is negligible.

Brief calculations were made to determine the effect of variation of specific impulse at constant parameters. Although not shown, results indicated that the effect on the optimum thrust-to-weight ratio of a ten-per cent variation in specific impulse is negligible, the payload ratio curves simply being shifted.

CONCLUSIONS AND RECOMMENDATIONS

From the results of this study, it can be concluded that the payload performance of vehicles escaping from orbit is quite sensitive to the initial thrust-to-weight ratio. It is shown that the optimum thrust-to-weight ratio is dependent on the vehicle structural weight parameters, the optimum value decreasing with increasing specific engine weight. The specific tankage weight has a secondary influence on the magnitude of the optimum thrust-to-weight ratio; however, it certainly does influence the magnitude of the obtainable payload ratio.

Propulsion systems with higher specific impulse usually have higher specific engine weights, offsetting part of the advantage of the improved efficiency. In addition, those systems that use hydrogen for propellant mass flow have comparatively high specific tank weights due to the low bulk density of the propellant, which again reduces the payload ratio that can be achieved. In the case of the nuclear heat exchanger system, the increase in specific impulse over that of an oxygen/hydrogen system is sufficient to show a real performance advantage. The actual application of any higher specific impulse propulsion system, however, would be decided on operational considerations like state of development, maximum allowable trip times, in addition to the consideration of the performance aspect.

The method used in this study can be extended to investigate the propulsion system thrust requirements of vehicles either braking into or leaving lunar and planetary orbits. In cases where both maneuvers are performed by the same propulsion system operating at different acceleration levels (such as braking into and leaving an orbit about the moon), the system has to be optimized with respect to the overall mission, i.e., for each individual maneuver the system may be required to operate at off-optimum conditions.

REFERENCES

1. Tsien, H.S., Take-Off from Satellite Orbit. American Rocket Society, Paper No. 93-53, 1953.

2. Lawden, D.F., Optimal Programming of Rocket Thrust Direction. Astronautica Acta, Vol. 1., pp. 41-56, 1955.

3. Lawden, D.F., Optimal Escape from a Circular Orbit. Astronautica Acta, Vol. 4, No. 3, pp. 218-233, 1958.

4. Benney, D.J., Escape from a Circular Orbit Using Tangential Thrust. Jet Propulsion, Vol. 28, No. 3, pp. 167-169, March 1958.

5. Moeckel, W.E., Trajectories with Constant Tangential Thrust in Central Gravitational Fields. NASA Technical Report. TR R-53, 1959.

6. Perkins, F.M., Flight Mechanics of Low-Thrust Spacecraft. Journal of the Aerospace Sciences, Vol. 26, No. 5, pp. 291-297, May 1959.

7. Levin, E., Lunar and Interplanetary Trajectories, Low Acceleration Transfer Orbits. Handbook of Astronautical Engineering, Editor H.H. Koelle, McGraw Hill, 1961.

8. Ehricke, K.A., Special Cases of Powered Trajectories, Handbook of Astronautical Engineering. Editor H.H. Koelle, McGraw Hill, 1961.

9. Moeckel, W.E., Propulsion Methods in Astronautics. Advances in Aeronautical Sciences, Pergamon Press, Vol. 2, pp. 1078-1097, 1959.

10. Ruppe, H.O., On the Problem of Optimum Acceleration for Orbit-Launched Vehicles. NASA MSFC Internal Note M-FPO-4-61, May 1962.

11. Krause, H.G.L., General Theory of Multistaged Rockets and Performance Theory of an N-Stage Satellite Carrier With a Specific Turning Program. ARS-Preprint 2073-61, October 1961.

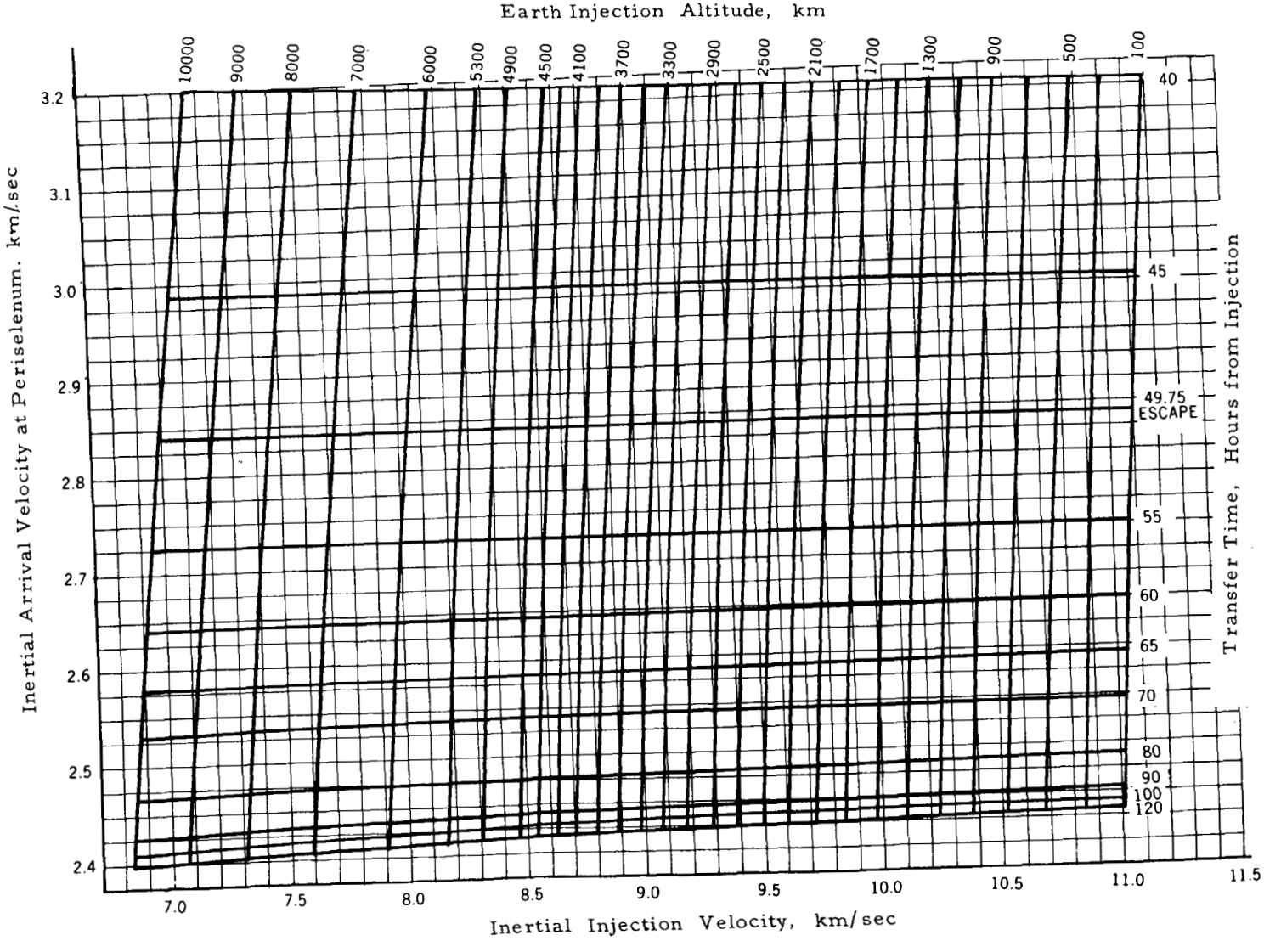

FIGURE 1. LUNAR MISSION VELOCITY REQUIREMENTS FOR AN 80-km PERISELENUM

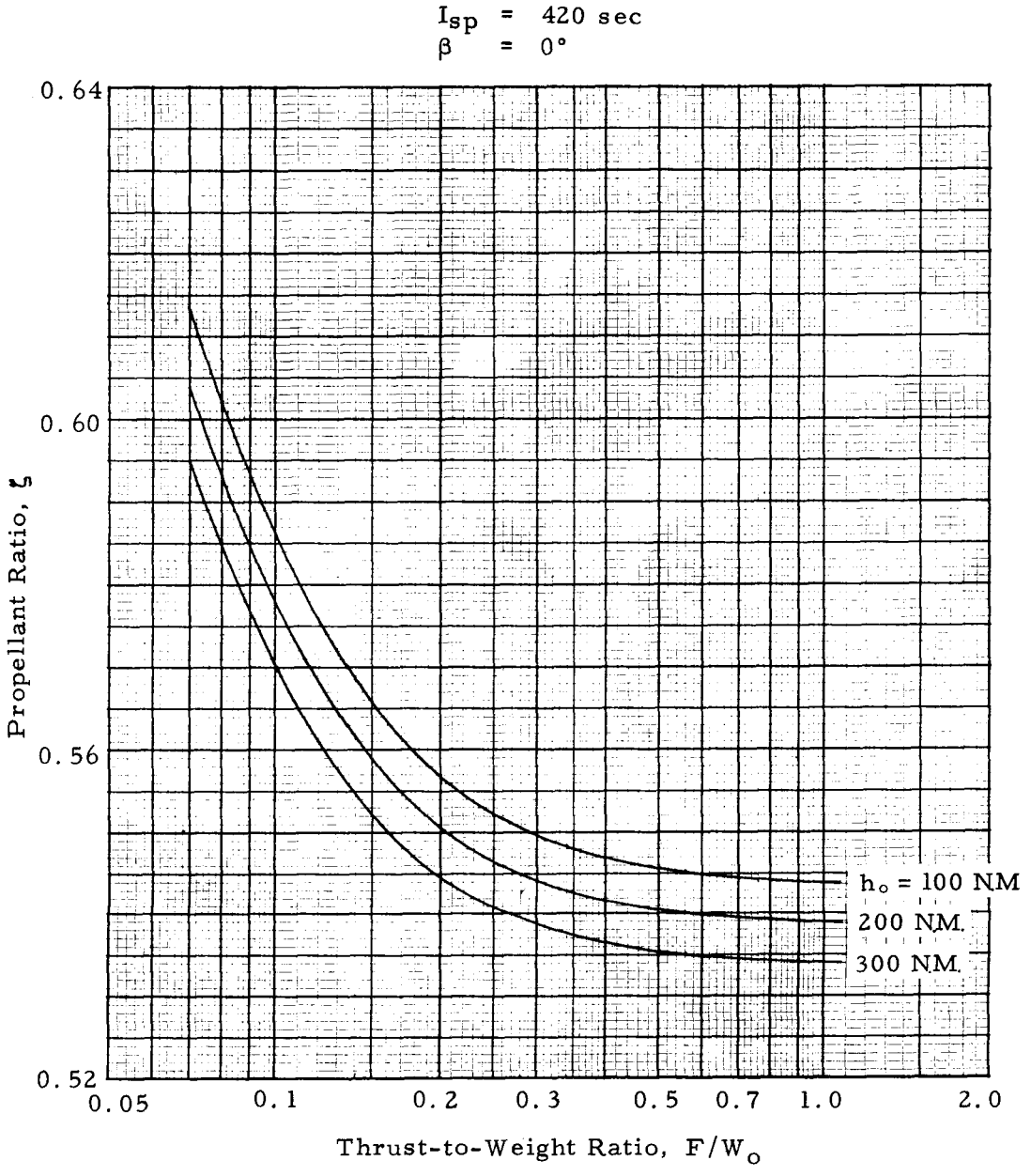

FIGURE 2. PROPELLANT CONSUMPTION REQUIRED FOR ESCAPE

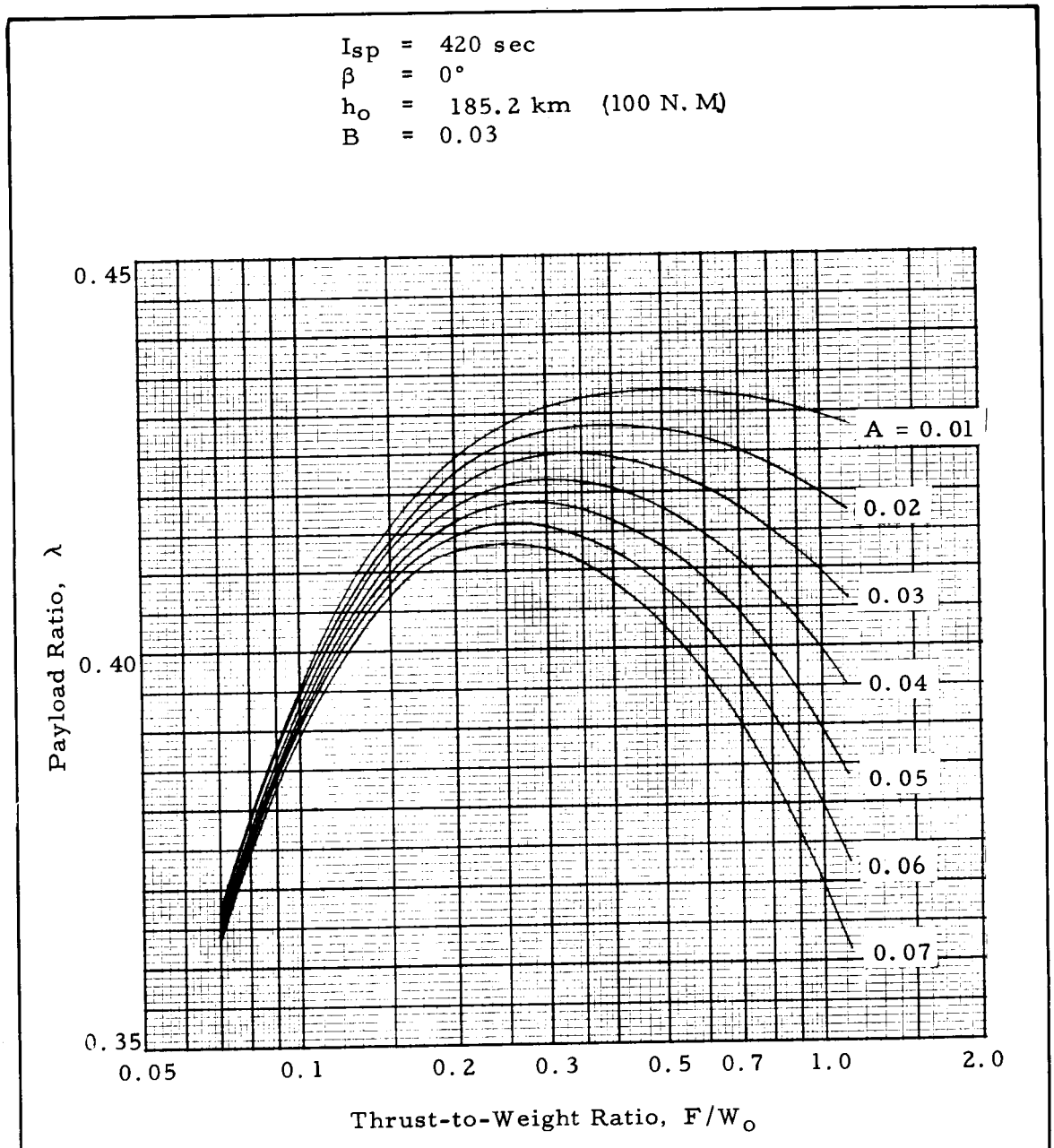

FIGURE 3. PAYLOAD RATIO AT ESCAPE

I_{sp} = 420 sec
β = 0°
h_o = 185.2 km (100 N. M.)
B = 0.06

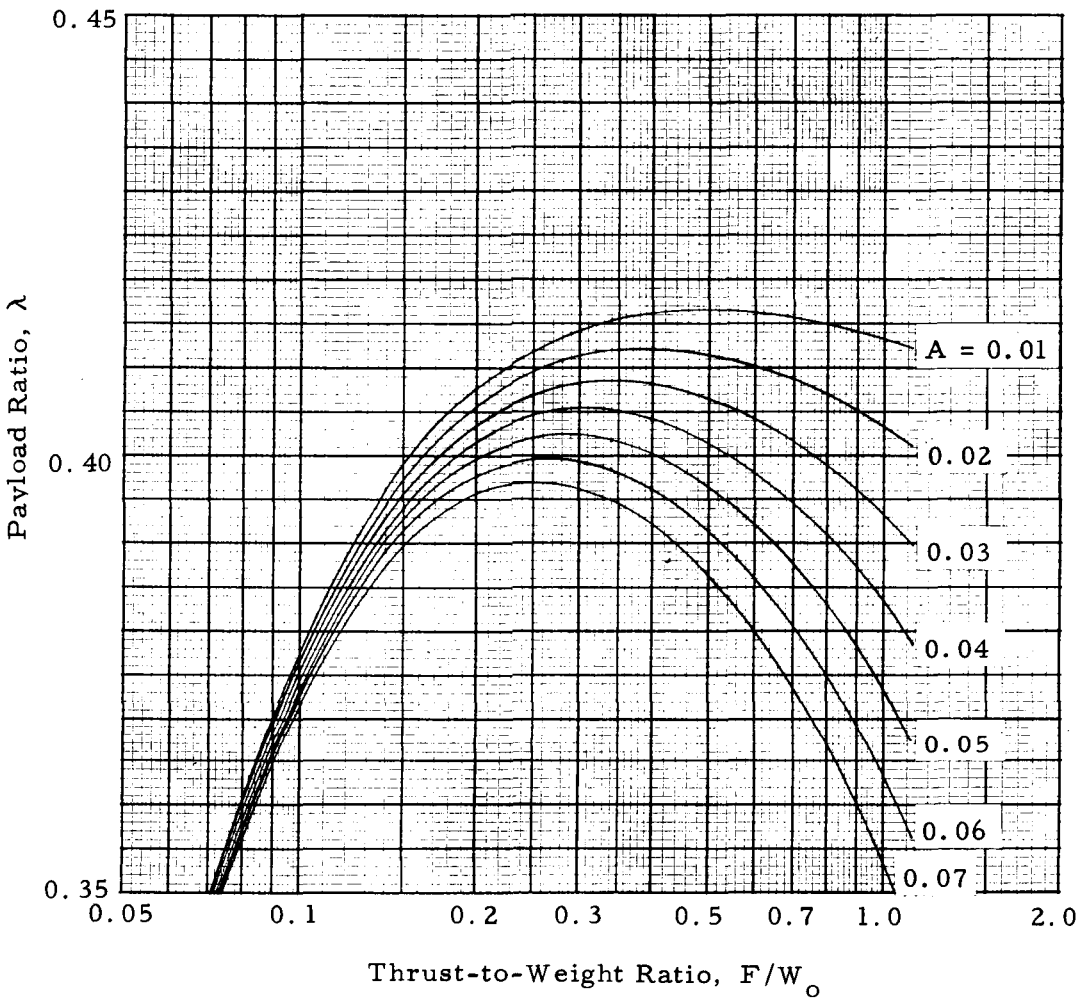

FIGURE 4. PAYLOAD RATIO AT ESCAPE

I_{sp} = 420 sec
β = 0°
h_o = 185.2 km (100 N. M.)
B = 0.09

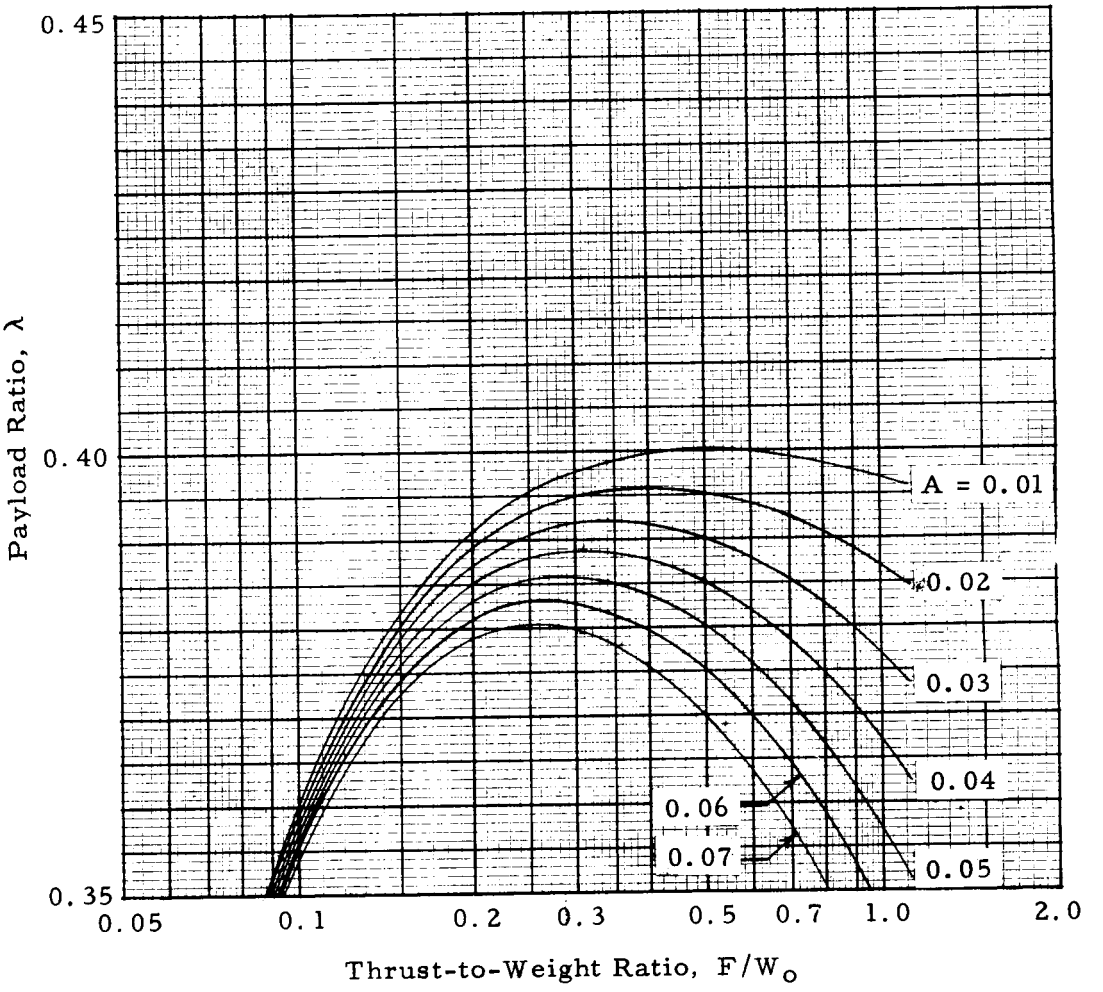

FIGURE 5. PAYLOAD RATIO AT ESCAPE

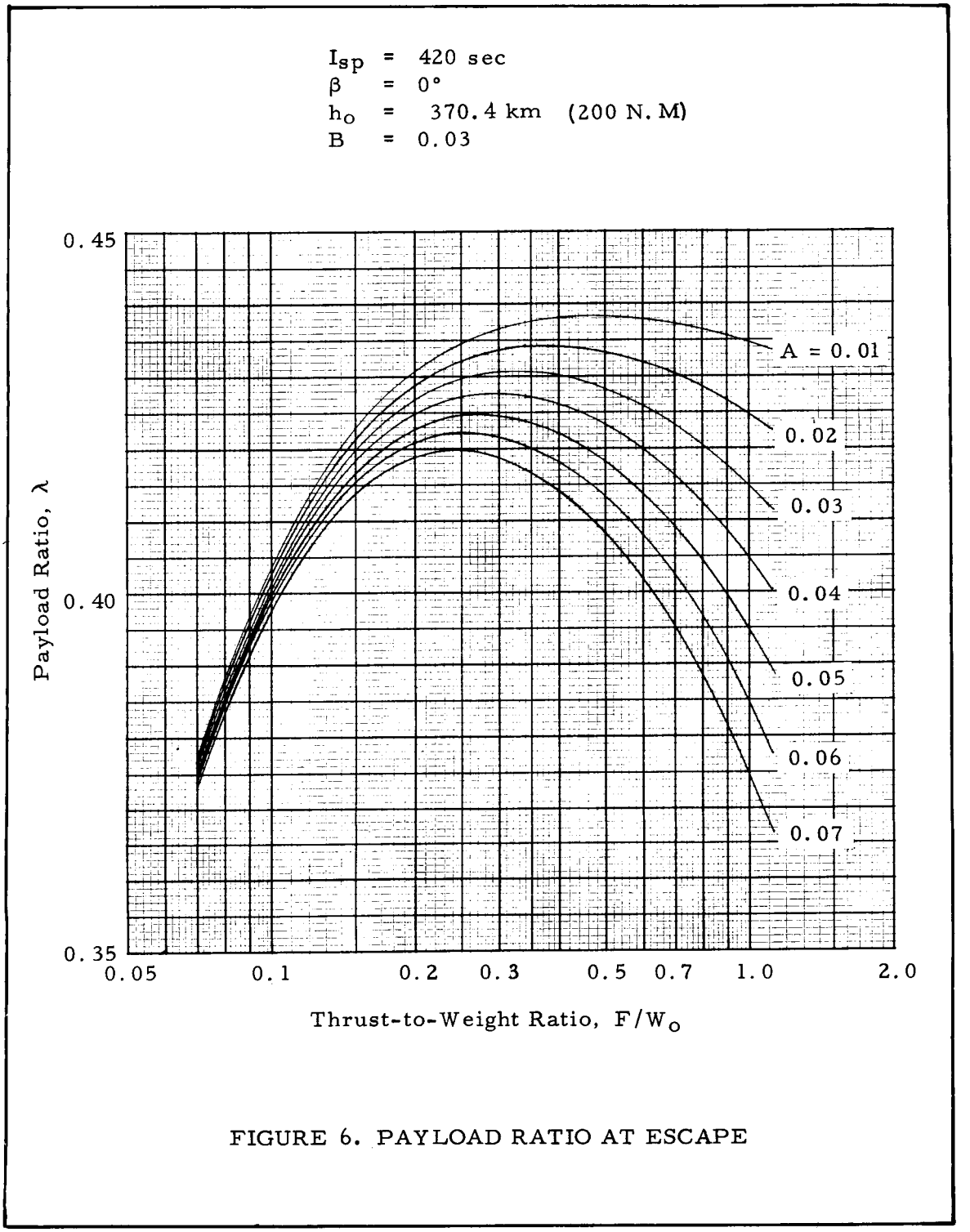

FIGURE 6. PAYLOAD RATIO AT ESCAPE

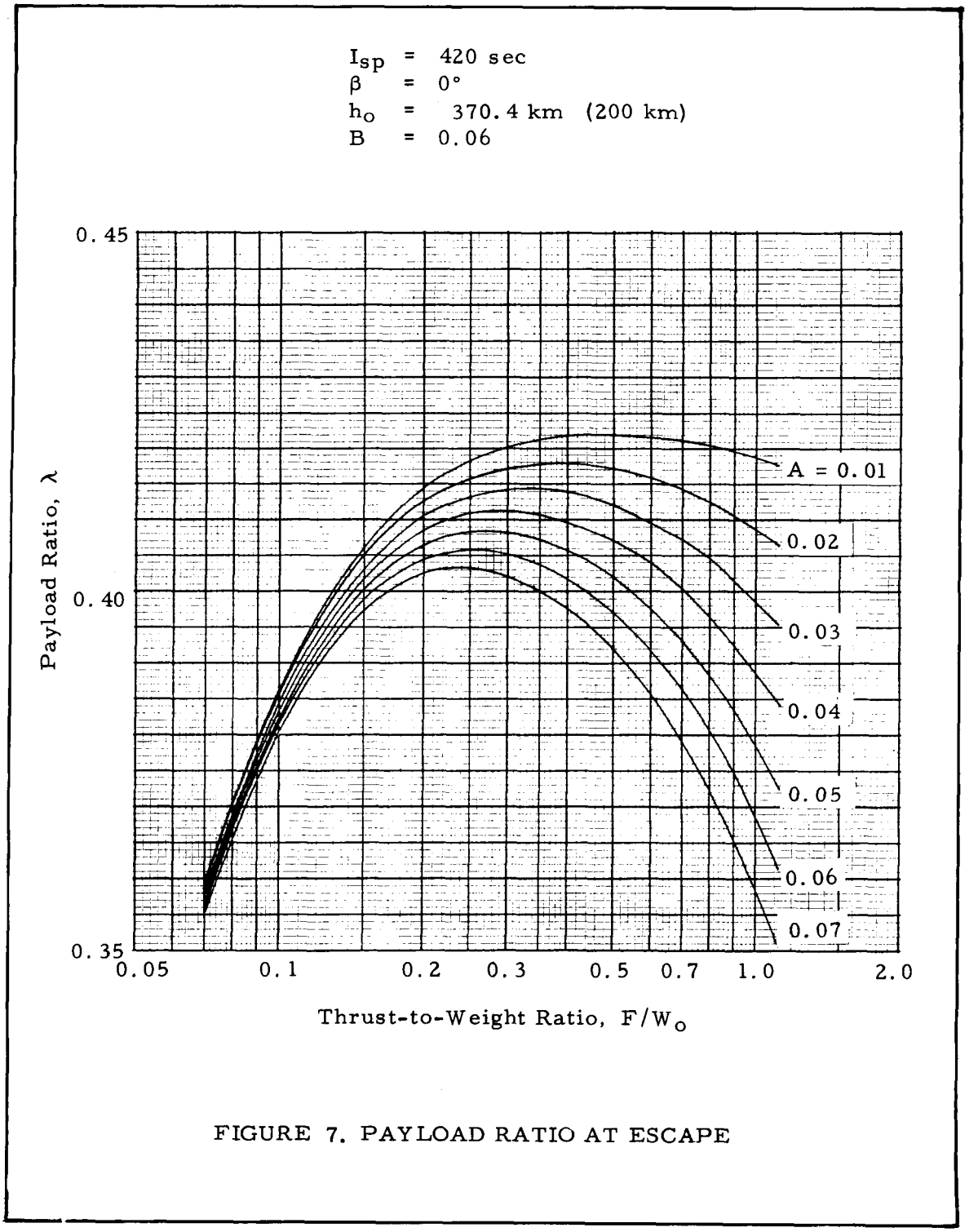

FIGURE 7. PAYLOAD RATIO AT ESCAPE

I_{sp} = 420 sec
β = 0°
h_o = 370.4 km (200 N.M)
B = 0.09

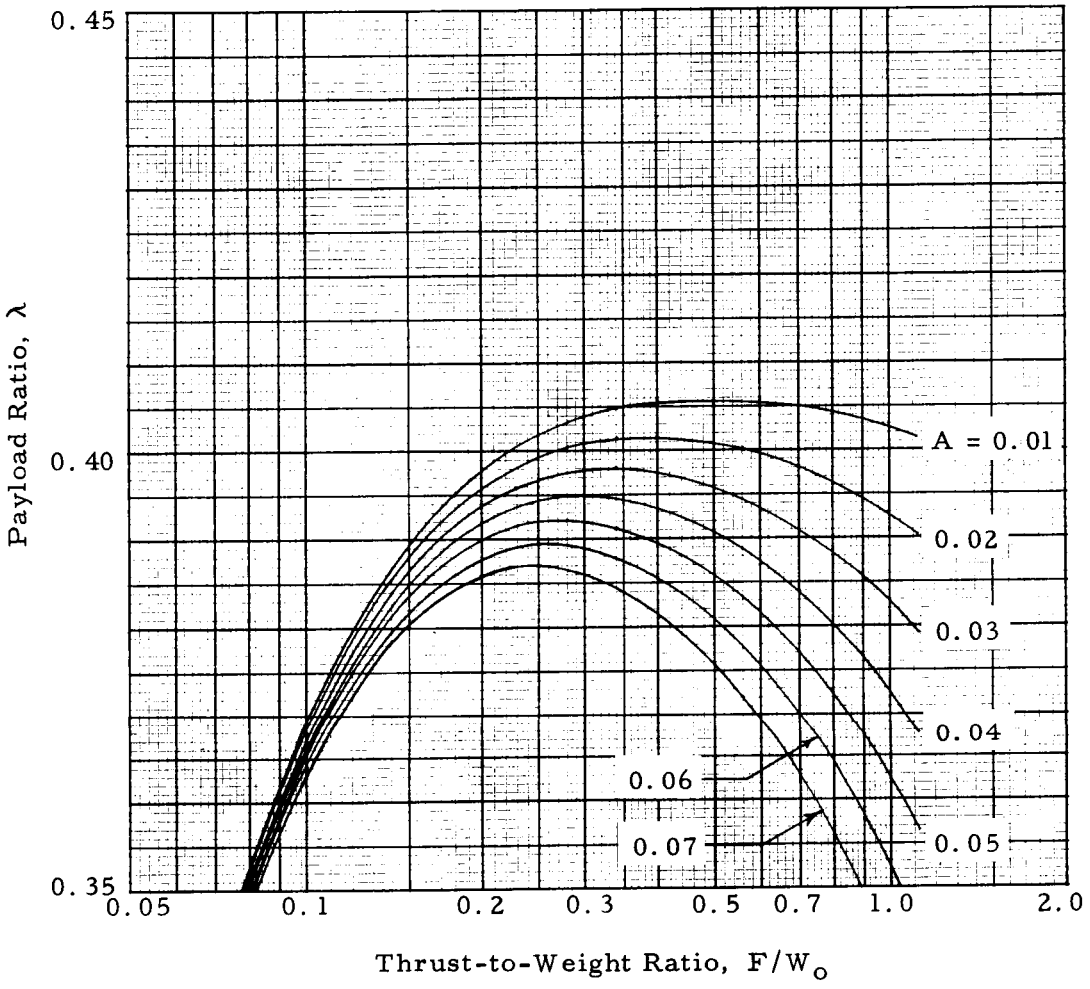

FIGURE 8. PAYLOAD RATIO AT ESCAPE

I_{sp} = 420 sec
β = 0°
h_o = 555.6 km (300 N.M.)
B = 0.03

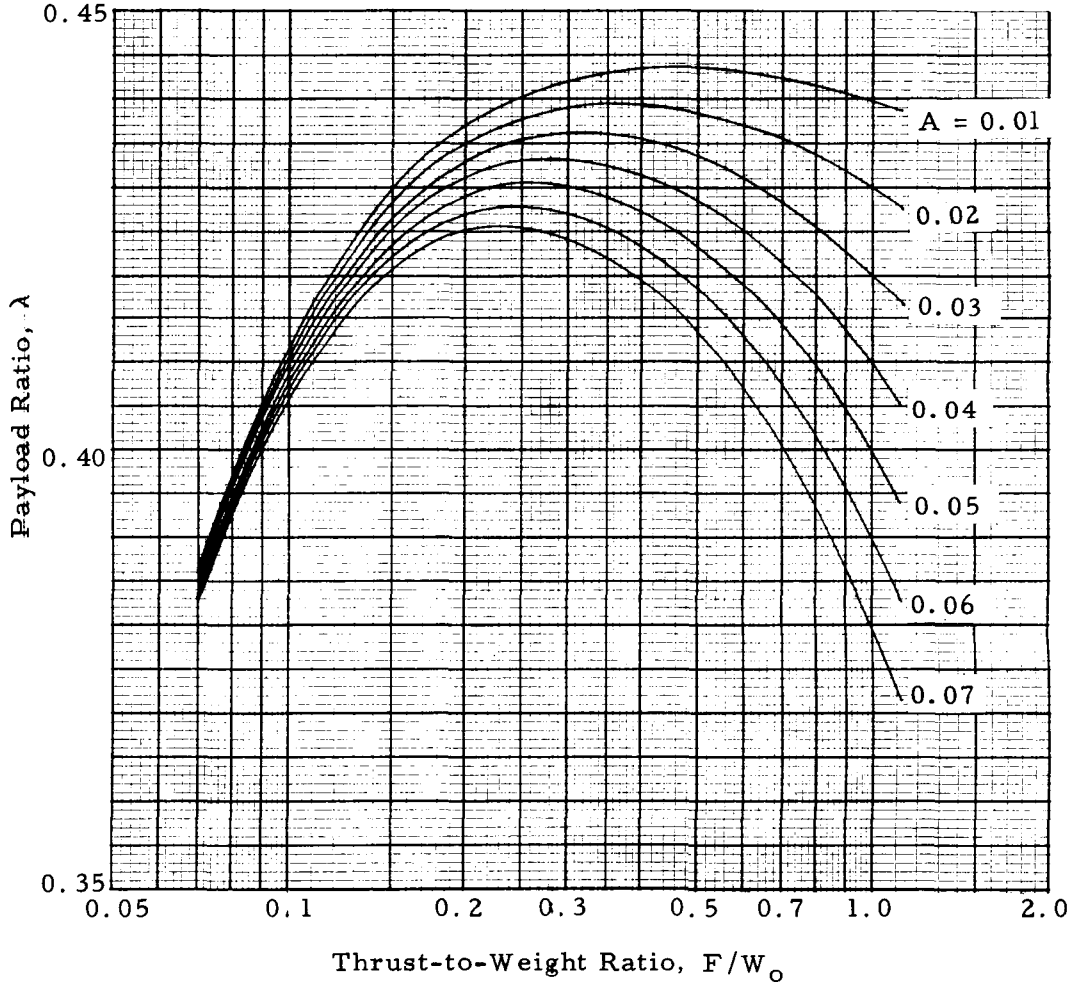

FIGURE 9. PAYLOAD RATIO AT ESCAPE

I_{sp} = 420 sec
β = 0°
h_o = 555.6 km (300 N. M)
B = 0.06

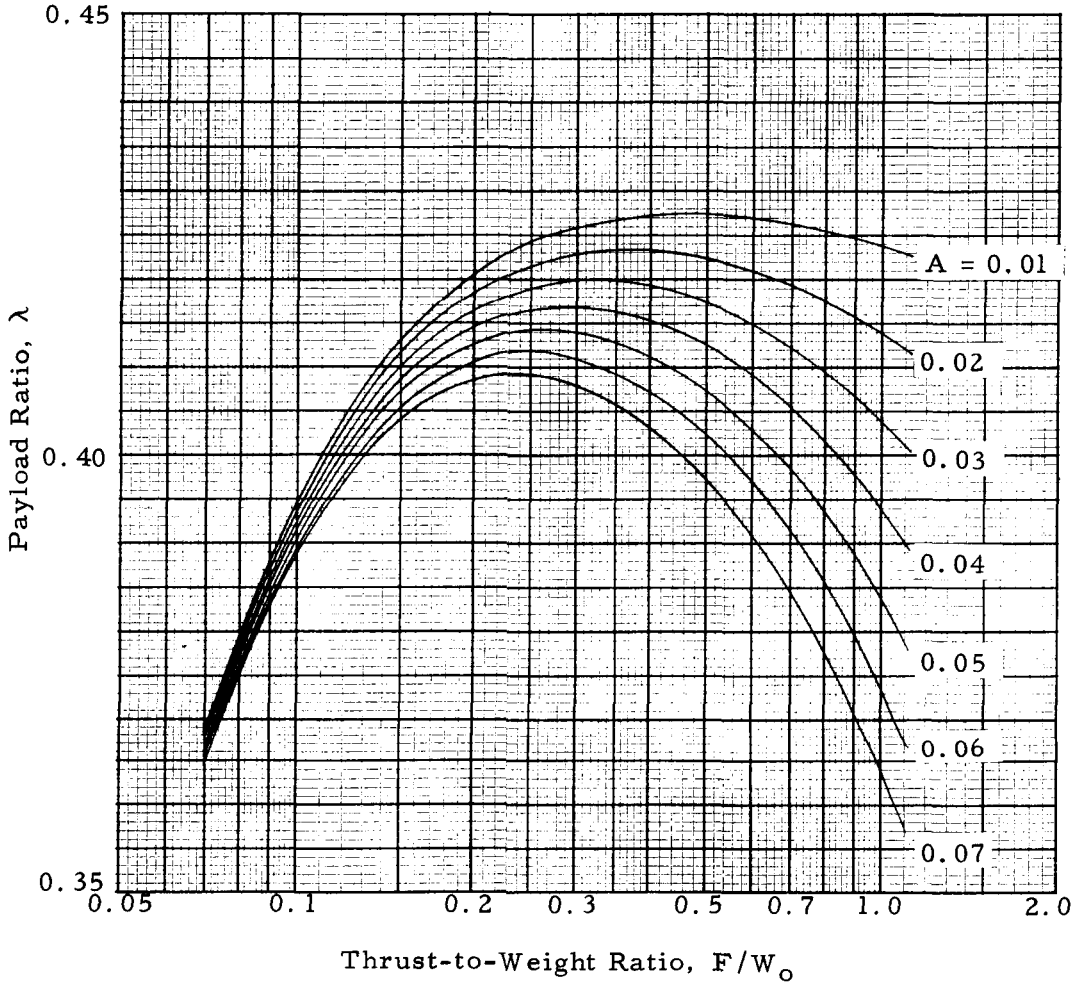

FIGURE 10. PAYLOAD RATIO AT ESCAPE

I_{sp} = 420 sec
β = 0°
h_o = 555.6 km (300 N. M.)
B = 0.09

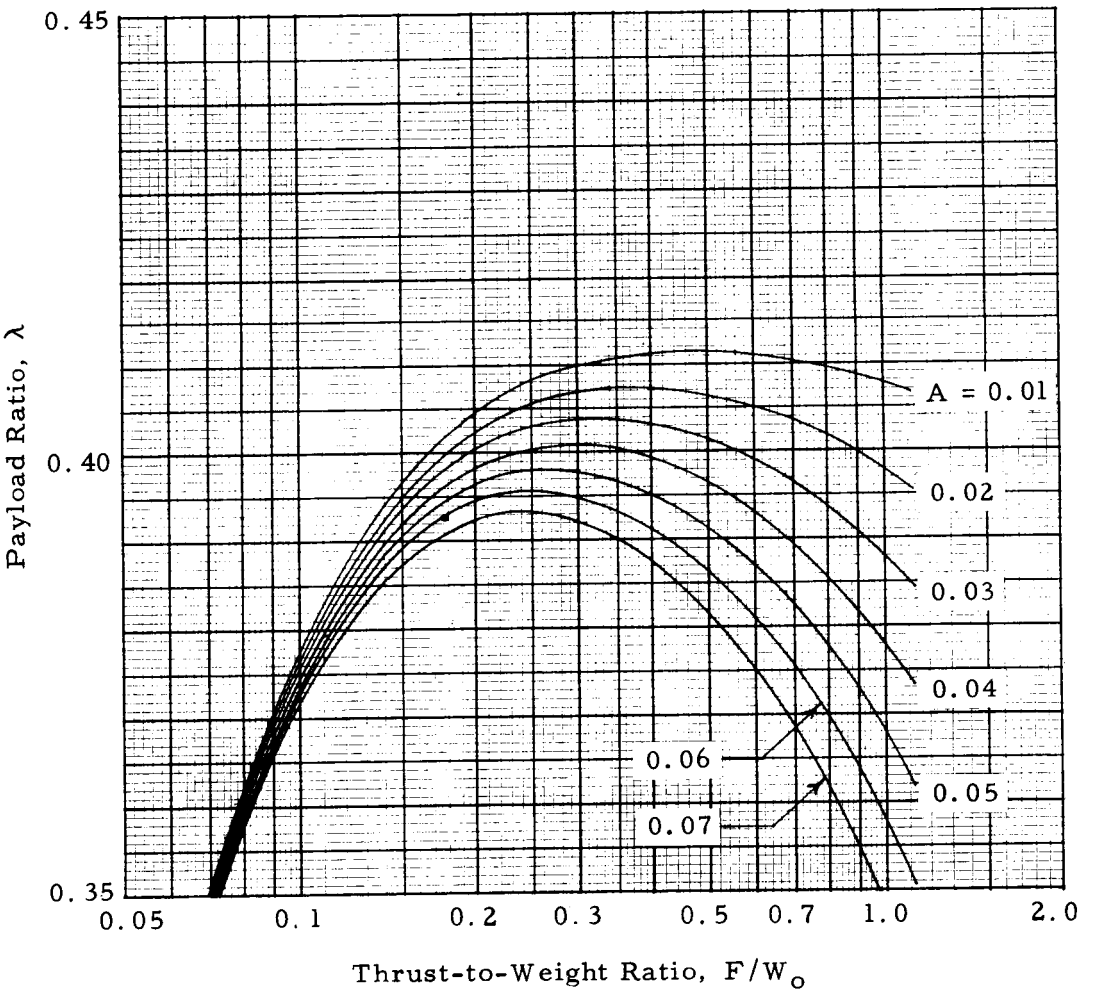

FIGURE 11. PAYLOAD RATIO AT ESCAPE

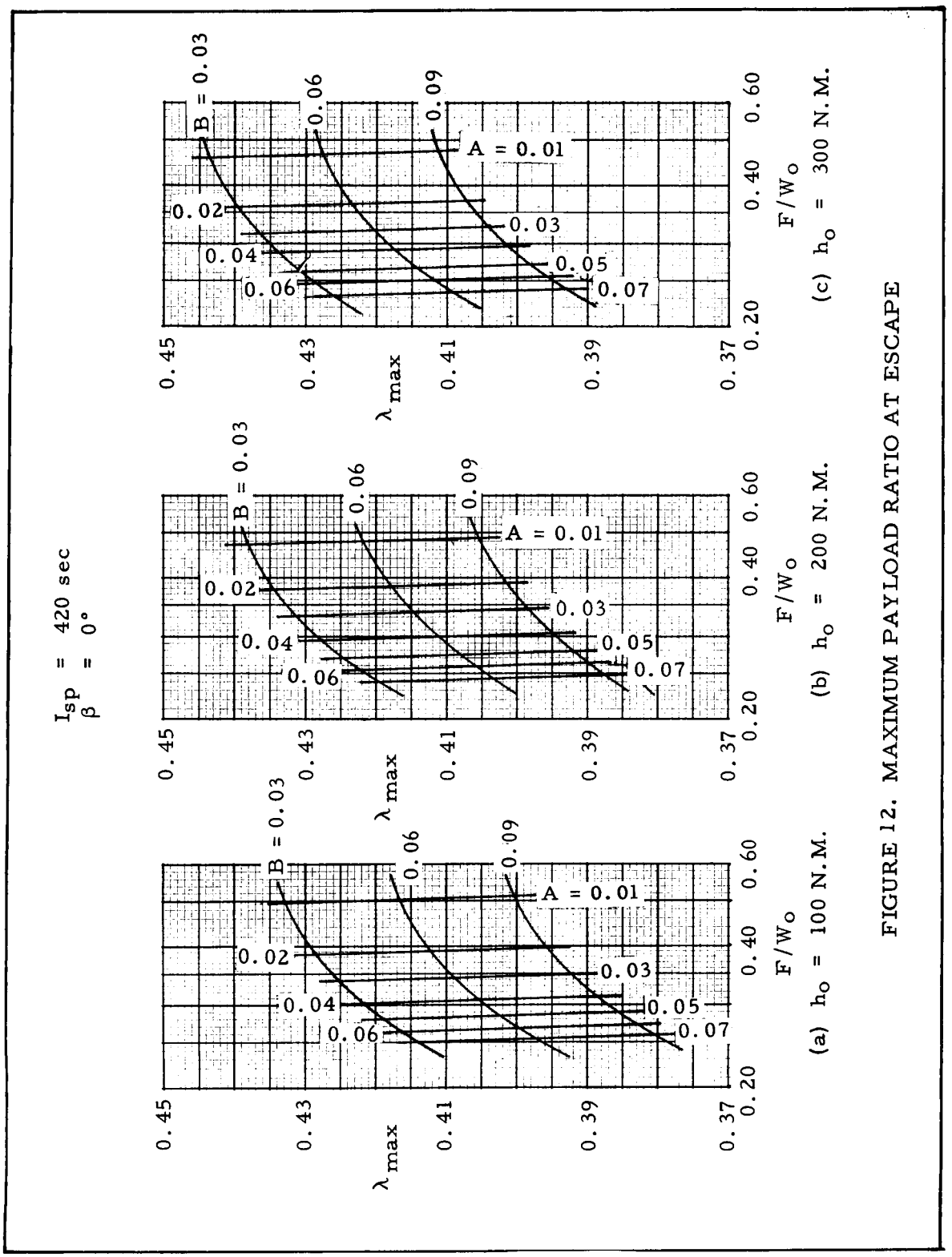

FIGURE 12. MAXIMUM PAYLOAD RATIO AT ESCAPE

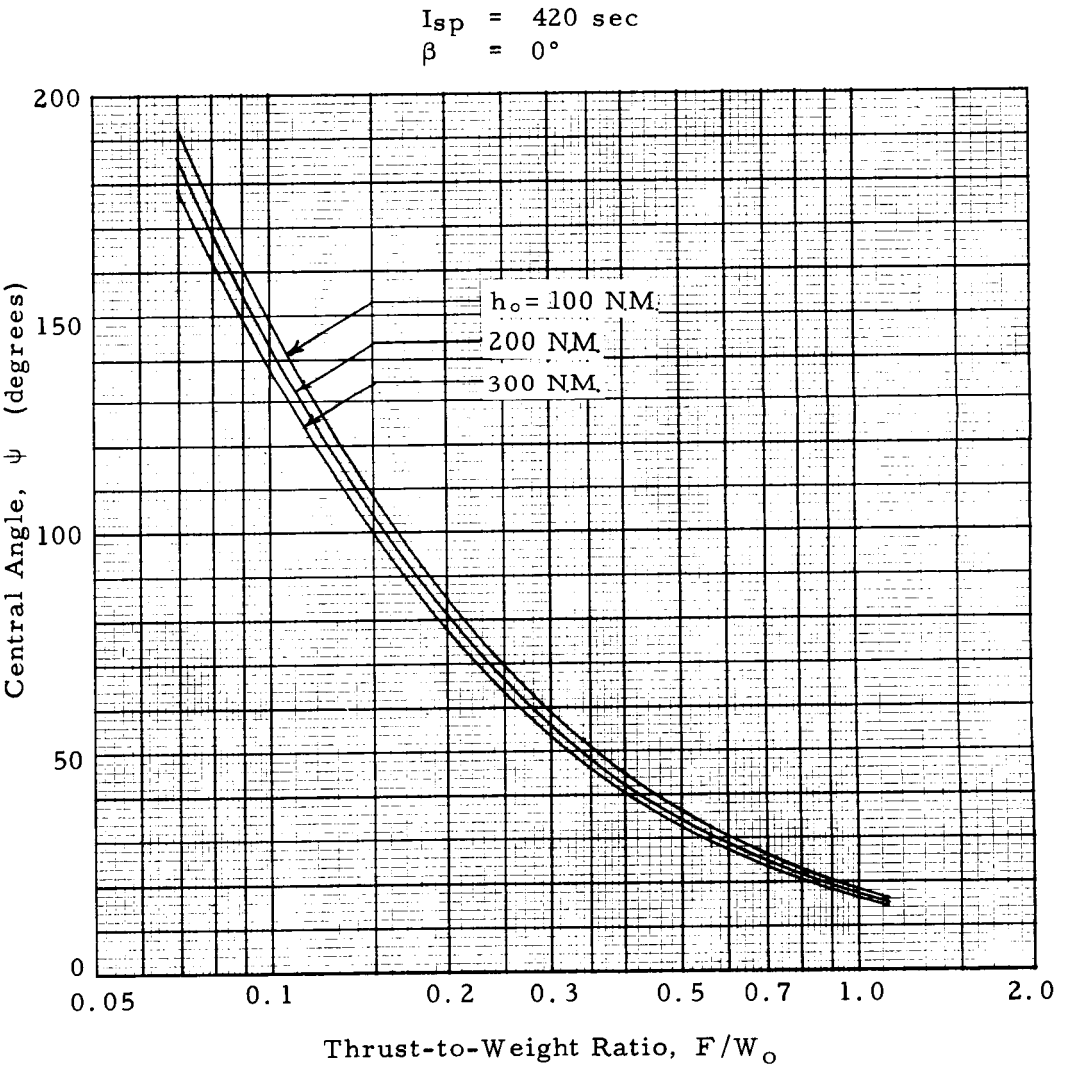

FIGURE 13. CENTRAL ANGLE AT ESCAPE

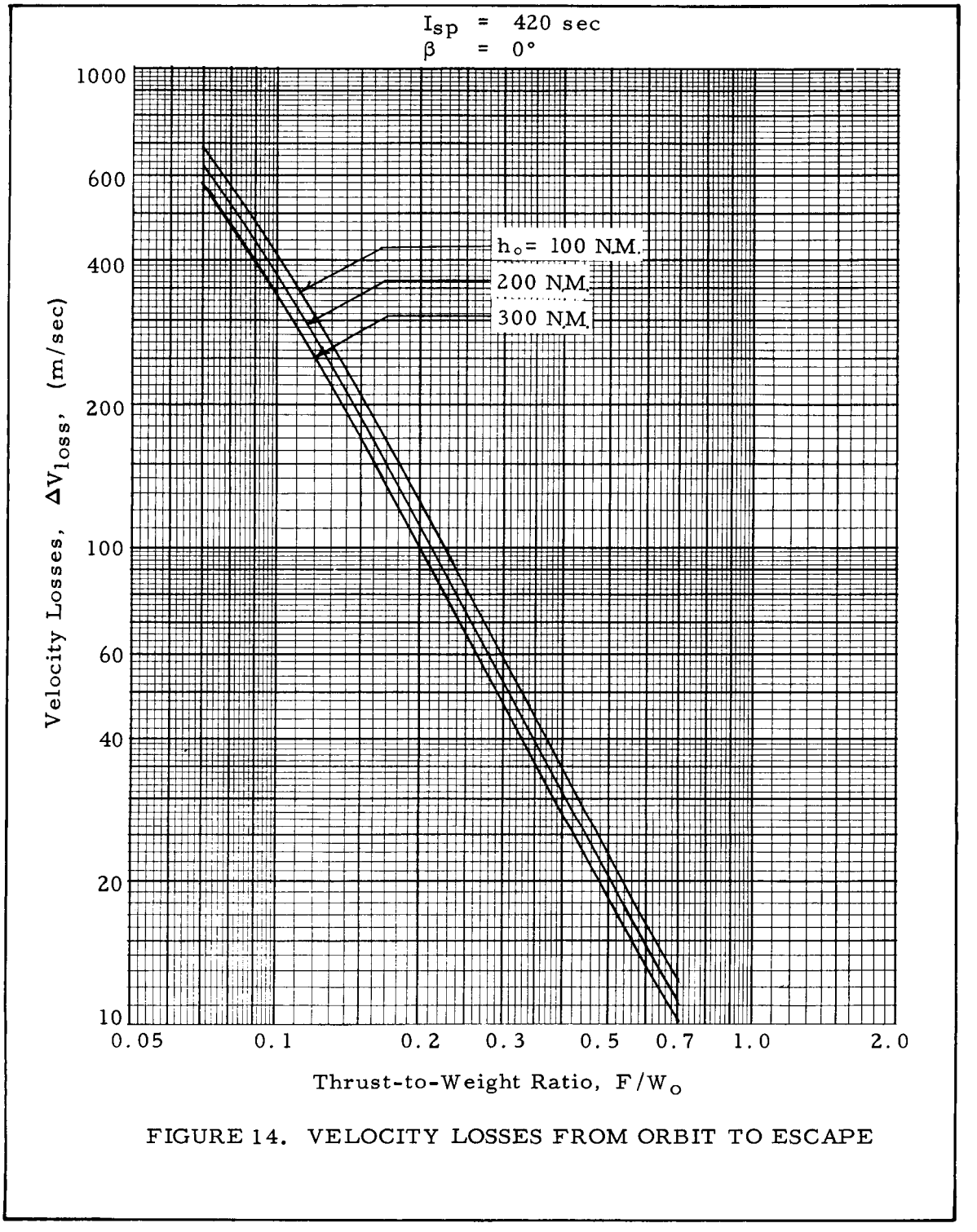

FIGURE 14. VELOCITY LOSSES FROM ORBIT TO ESCAPE

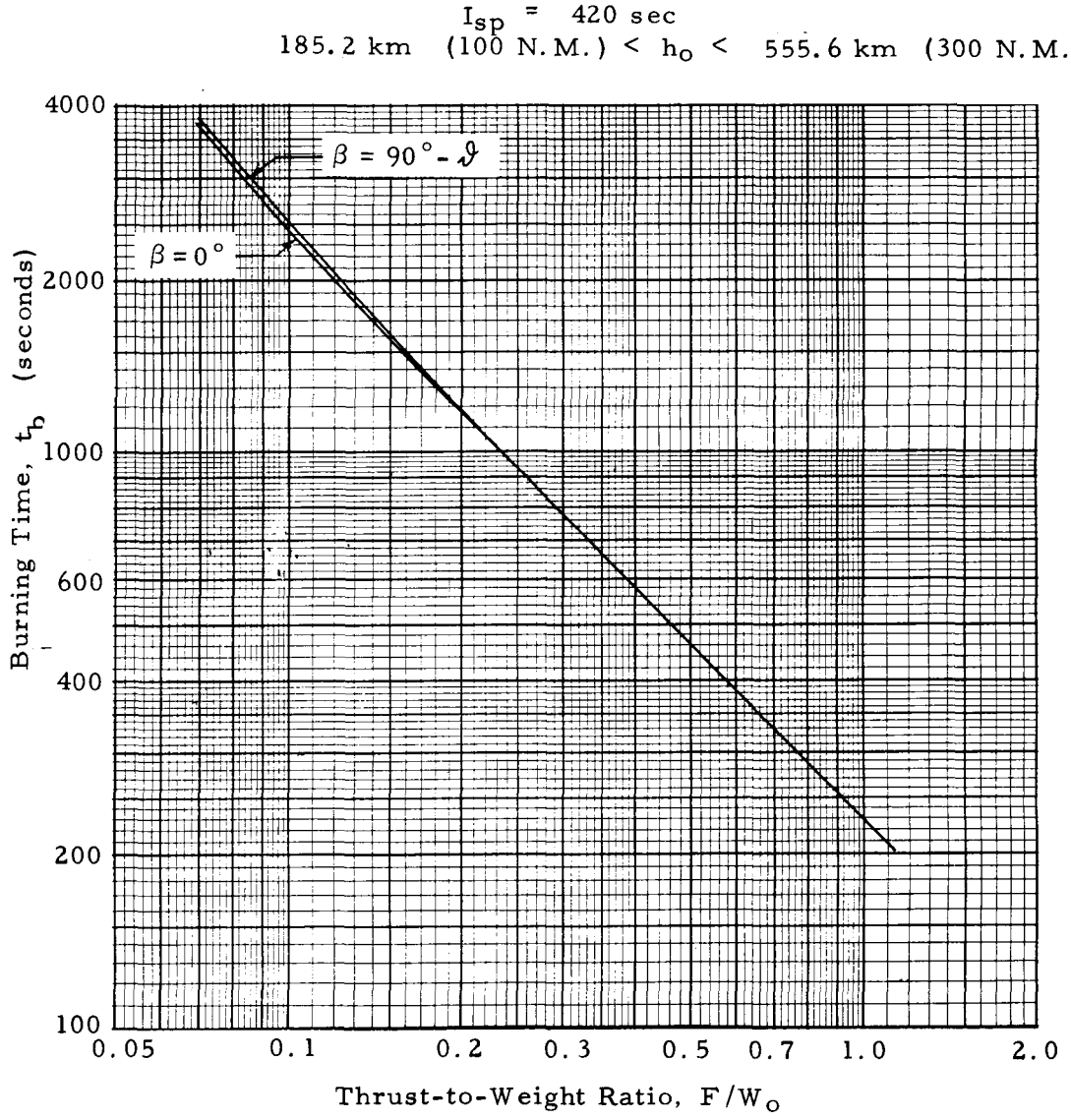

FIGURE 15. BURNING TIME TO ESCAPE

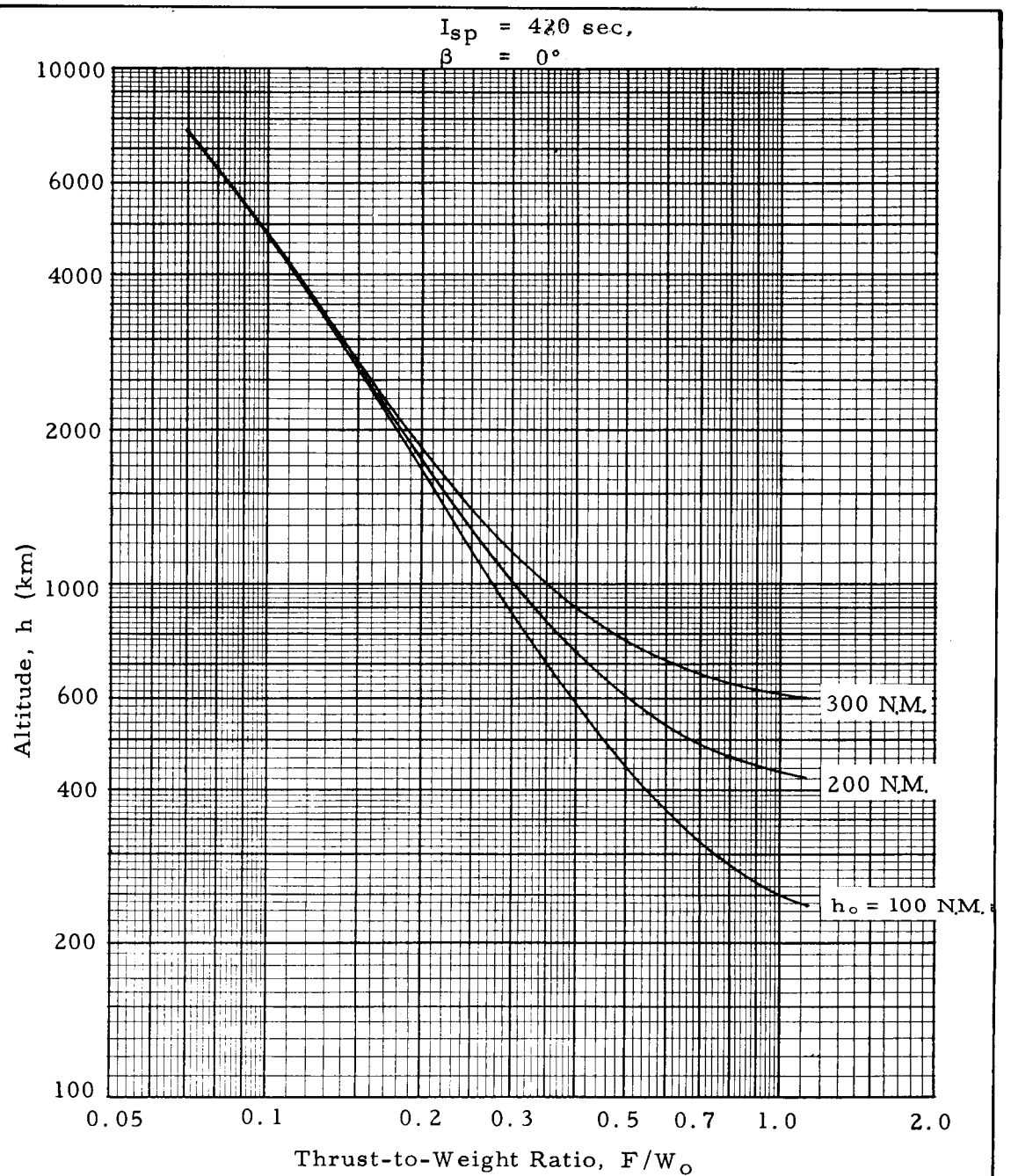

FIGURE 16. ALTITUDE AT ESCAPE

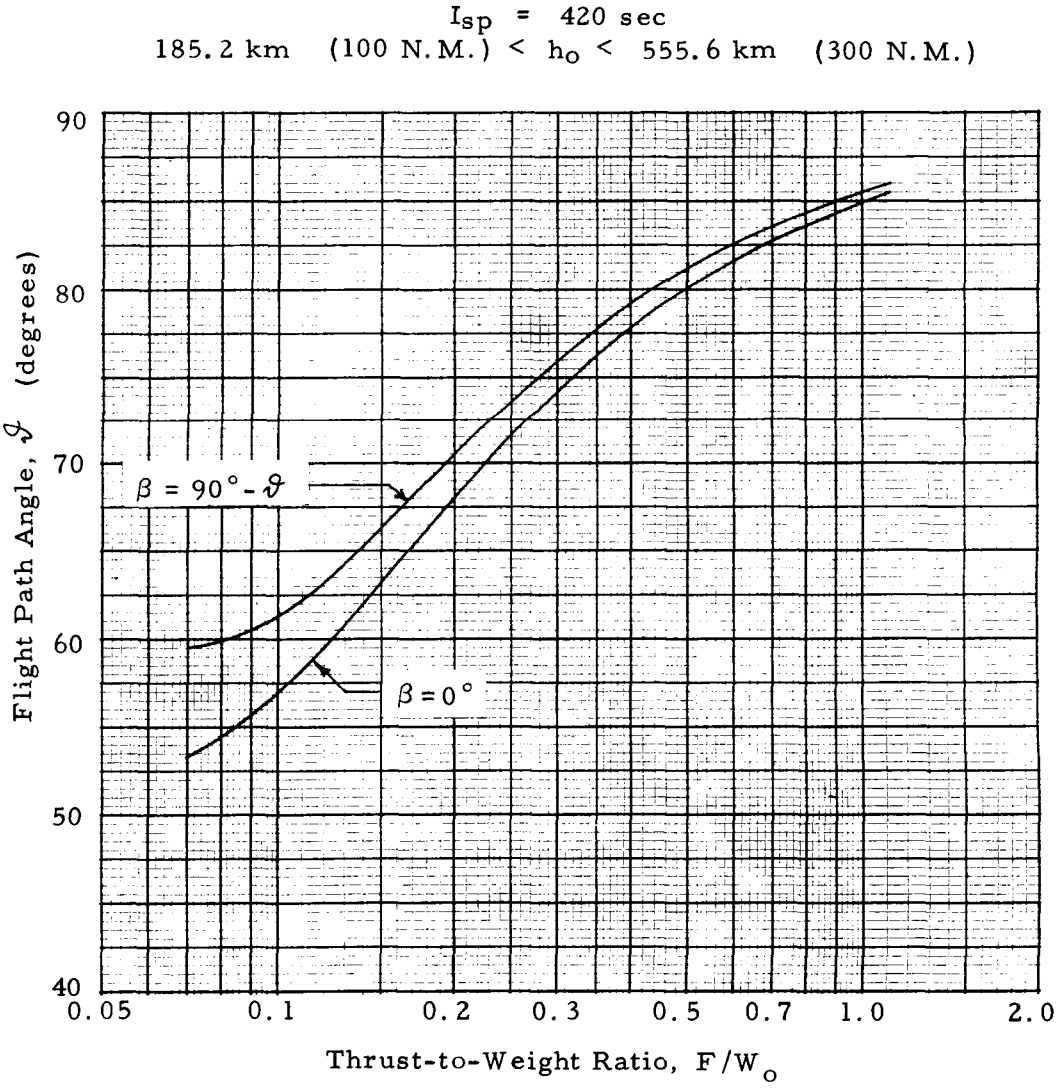

FIGURE 17. FLIGHT PATH ANGLE AT ESCAPE

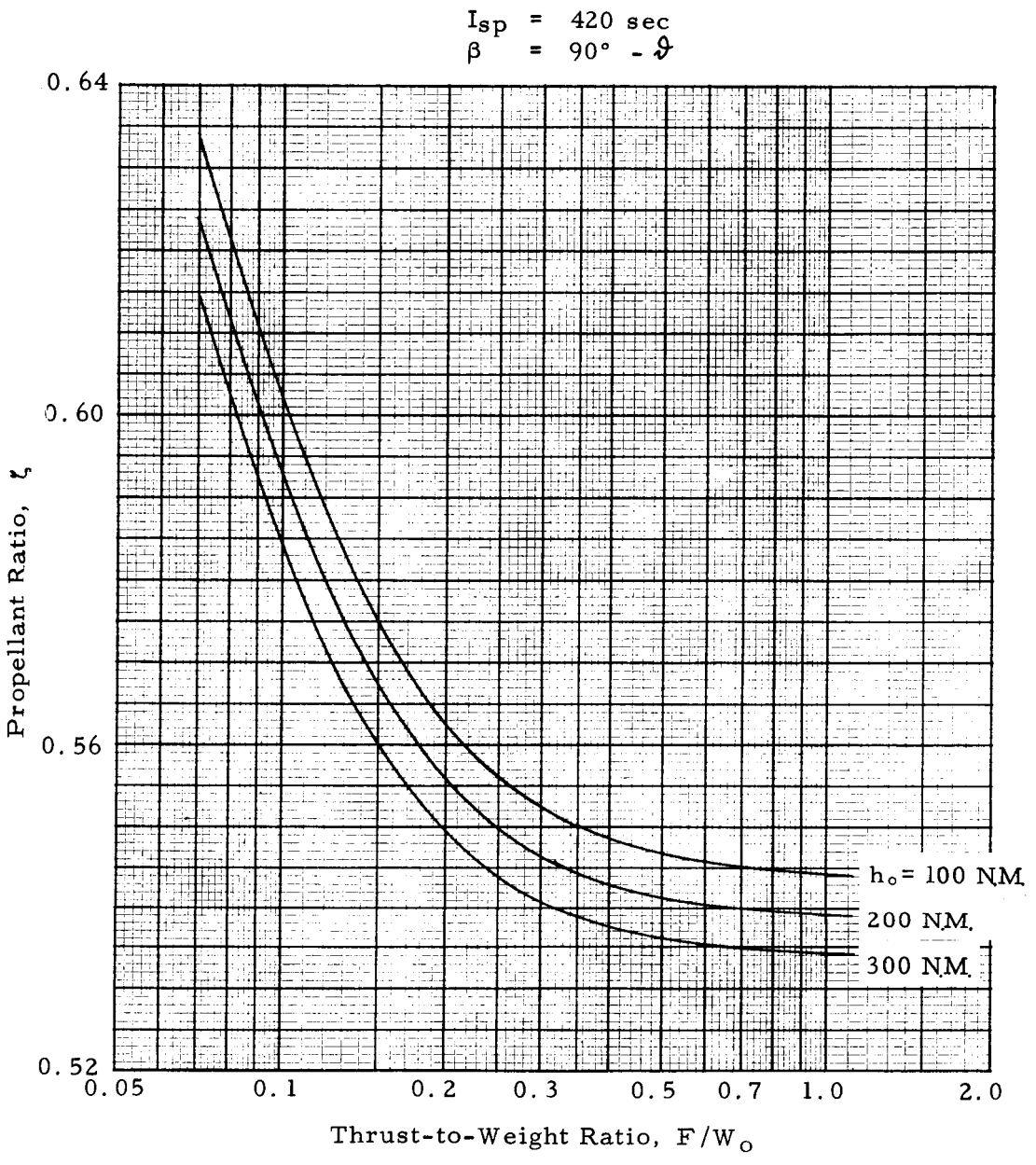

FIGURE 18. PROPELLANT CONSUMPTION REQUIRED FOR ESCAPE

I_{sp} = 420 sec
β = 90^{o} - ϑ
h_o = 185.2 km (100 N.M.)
B = 0.03

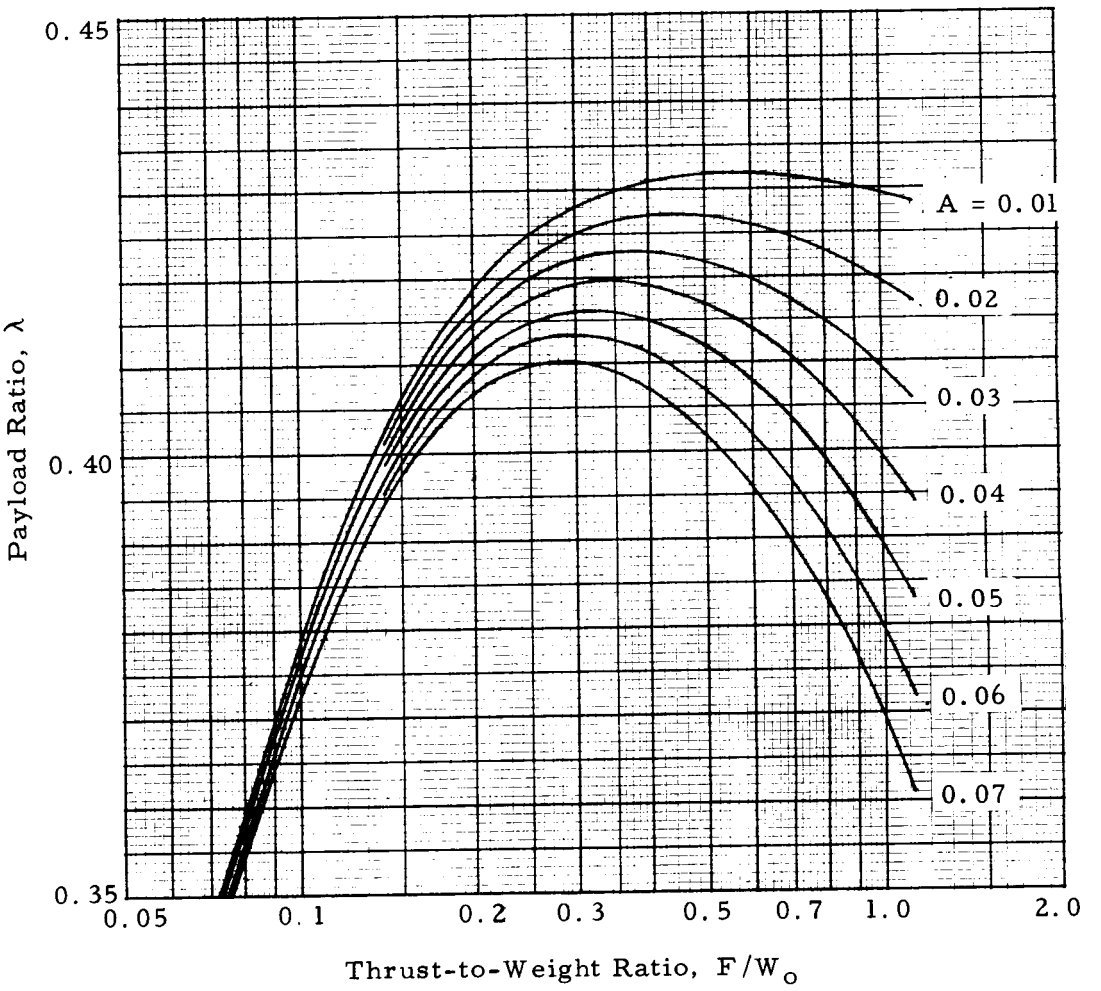

FIGURE 19. PAYLOAD RATIO AT ESCAPE

I_{sp} = 420 sec
β = 90° - ϑ
h_o = 185.2 km (100 N.M.)
B = 0.06

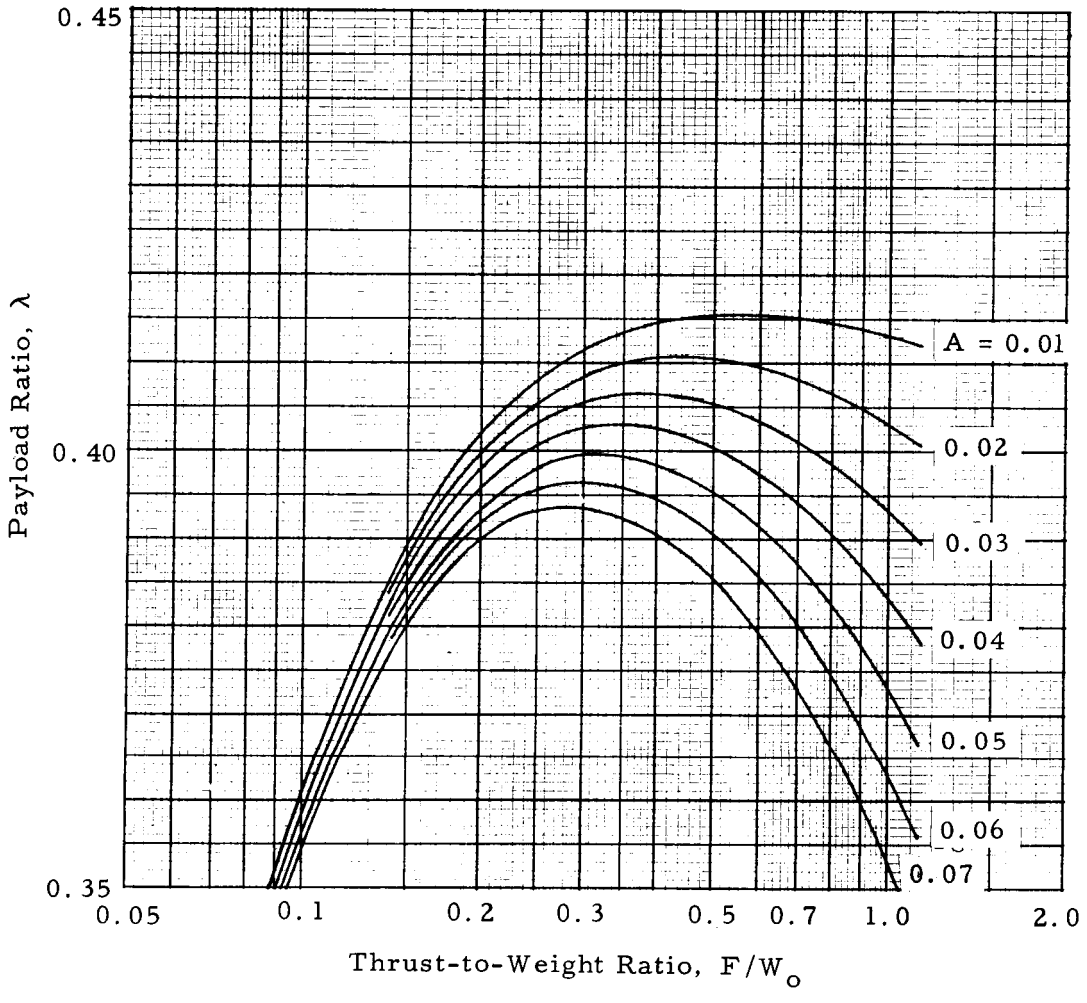

FIGURE 20. PAYLOAD RATIO AT ESCAPE

I_{sp} = 420 sec
β = 90° - ϑ
h_o = 185.2 km (100 N.M.)
B = 0.09

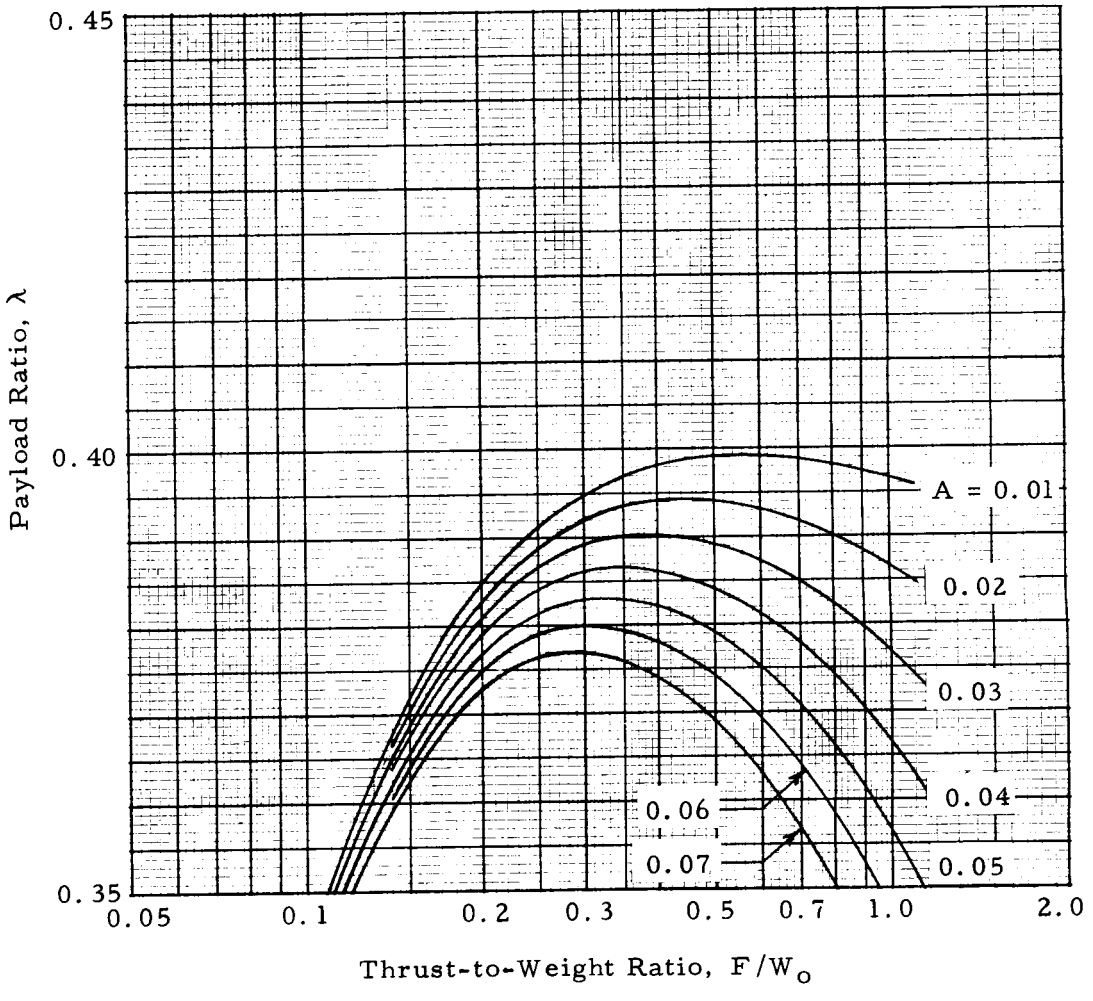

FIGURE 21. PAYLOAD RATIO AT ESCAPE

I_{sp} = 420 sec
β = 90° - ϑ
h_o = 370.4 km (200 N.M.)
B = 0.03

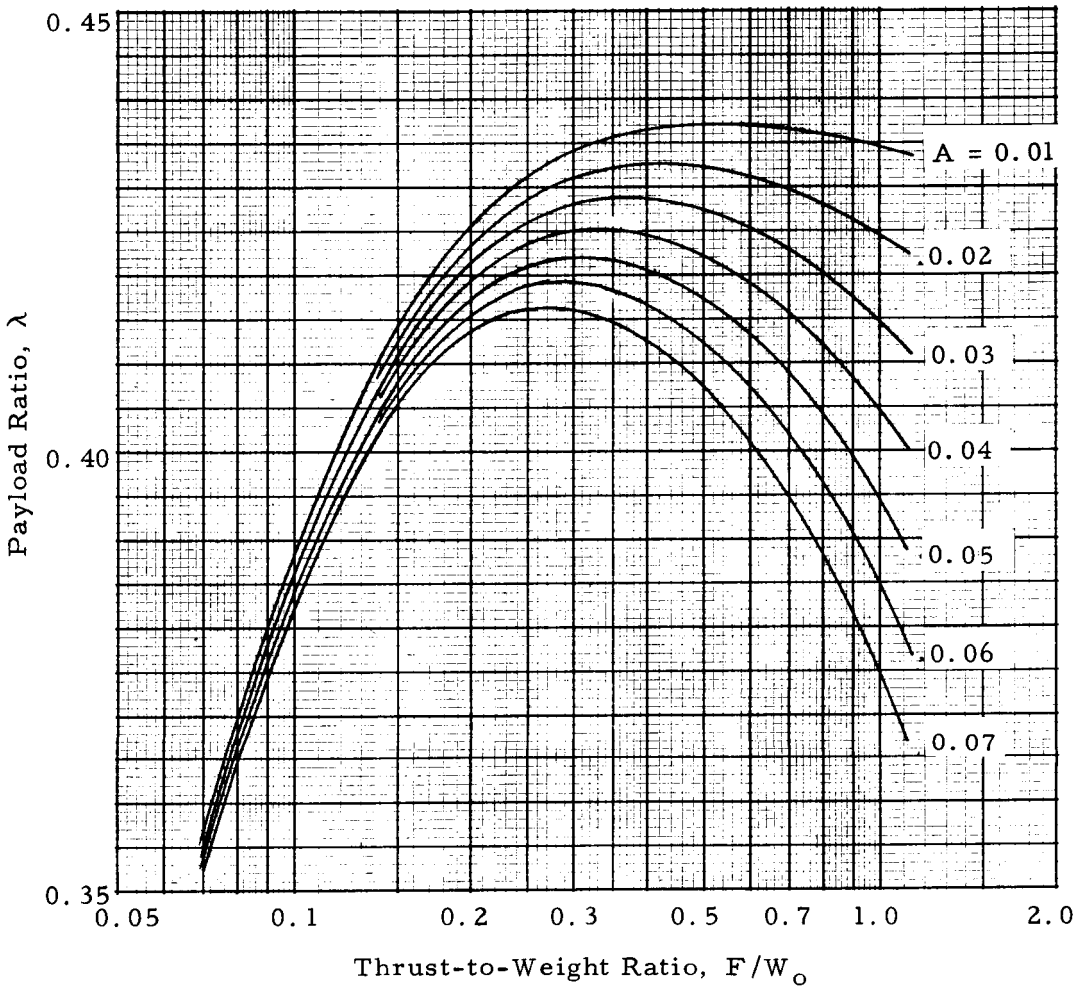

FIGURE 22. PAYLOAD RATIO AT ESCAPE

I_{sp} = 420 sec
β = 90° - ϑ
h_o = 370.4 km (200 N.M.)
B = 0.06

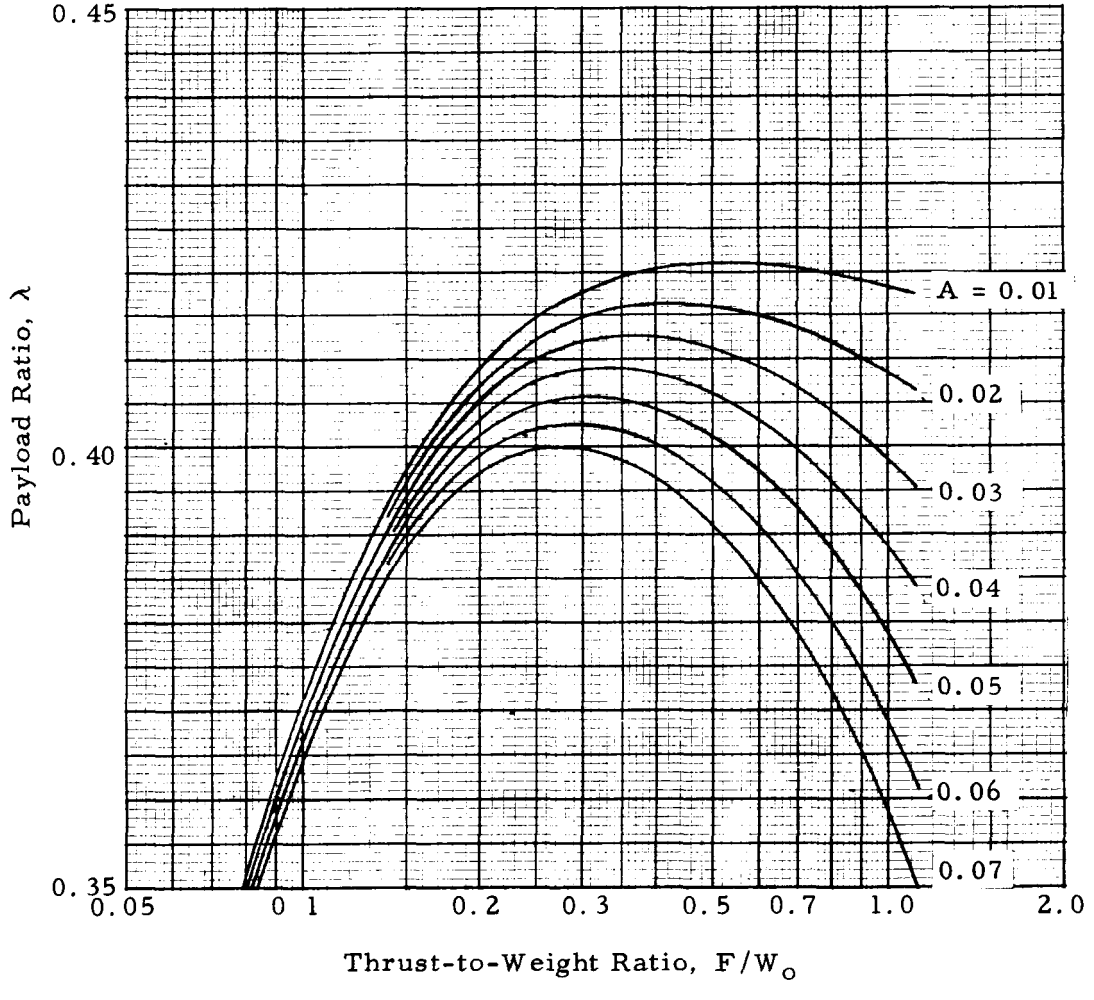

FIGURE 23. PAYLOAD RATIO AT ESCAPE

I_{sp} = 420 sec
β = 90° - ϑ
h_o = 370.4 km (200 N.M.)
B = 0.09

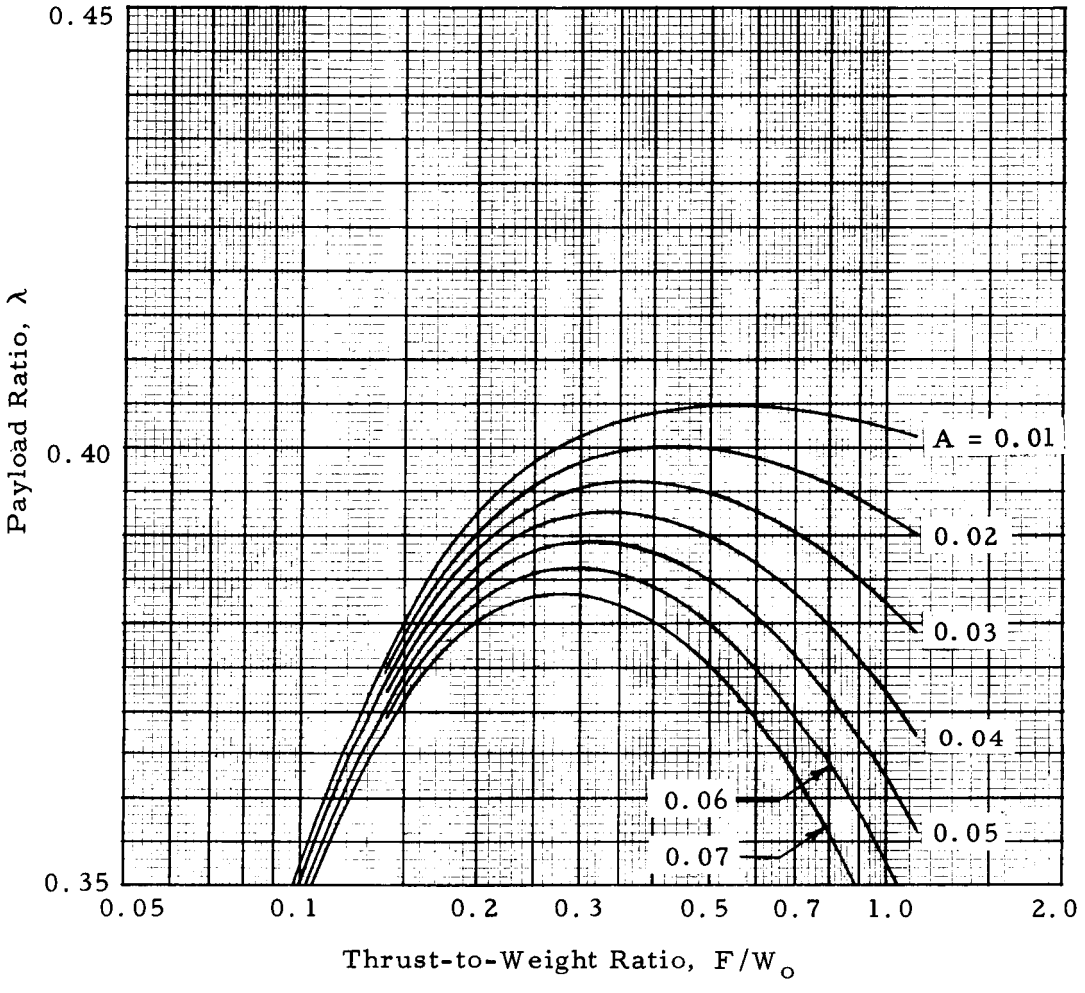

FIGURE 24. PAYLOAD RATIO AT ESCAPE

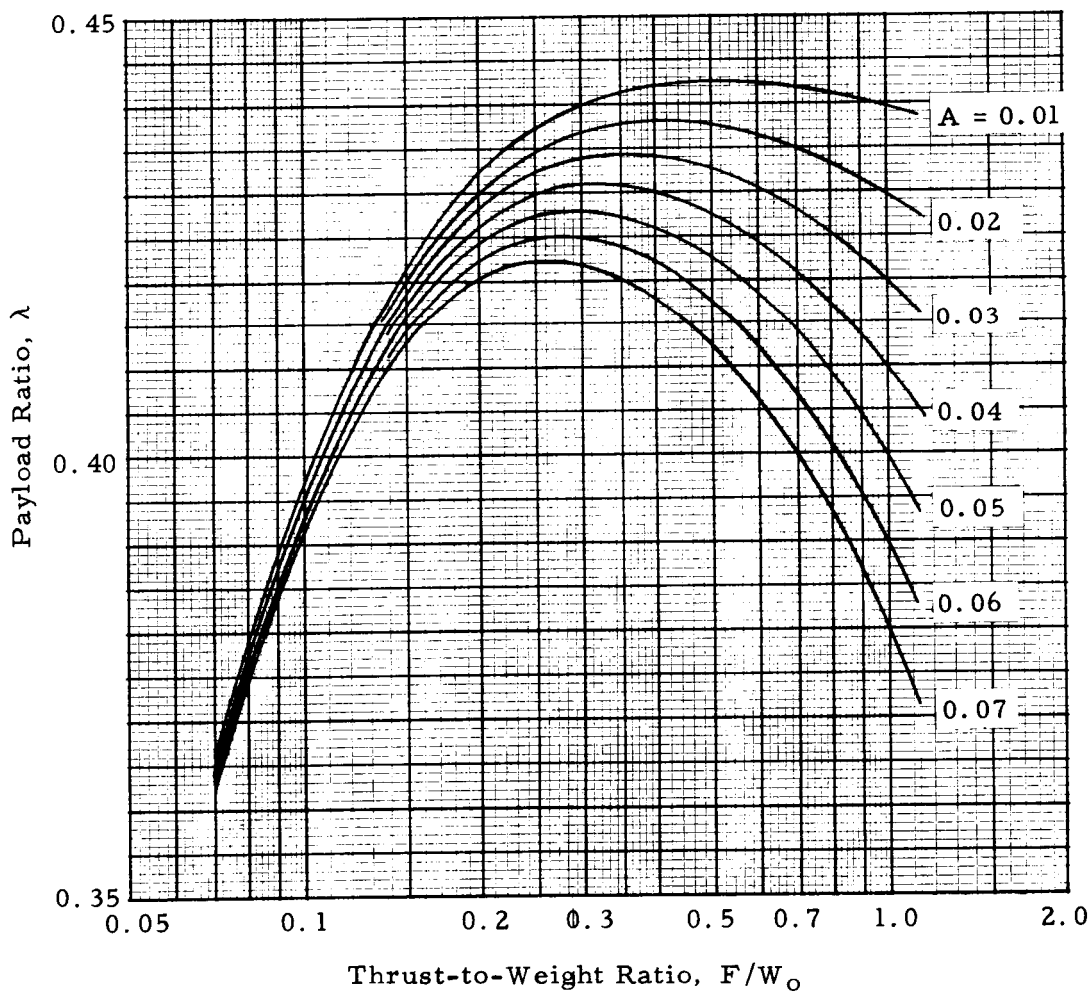

FIGURE 25. PAYLOAD RATIO AT ESCAPE

I_{sp} = 420 sec
β = 90° - ϑ
h_o = 555.6 km (300 N.M.)
B = 0.06

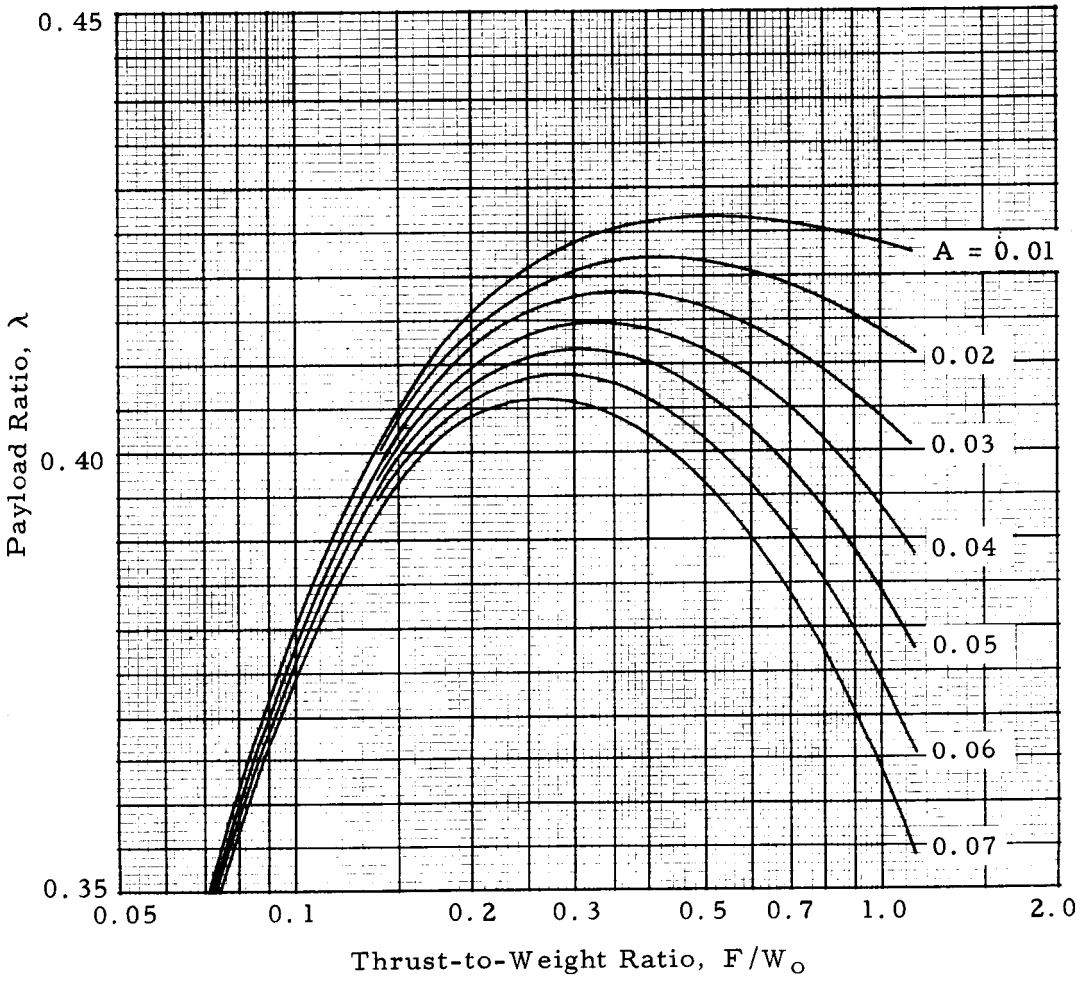

FIGURE 26. PAYLOAD RATIO AT ESCAPE

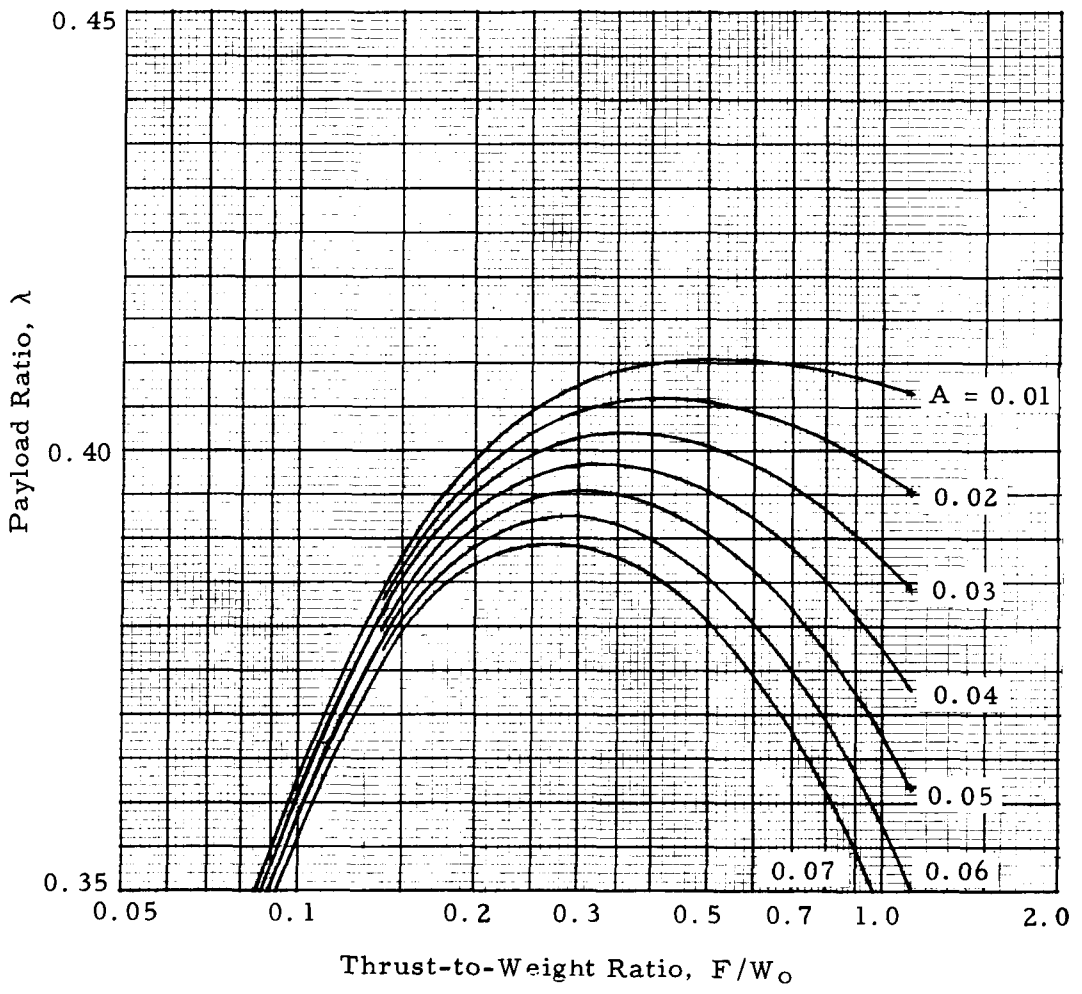

FIGURE 27. PAYLOAD RATIO AT ESCAPE

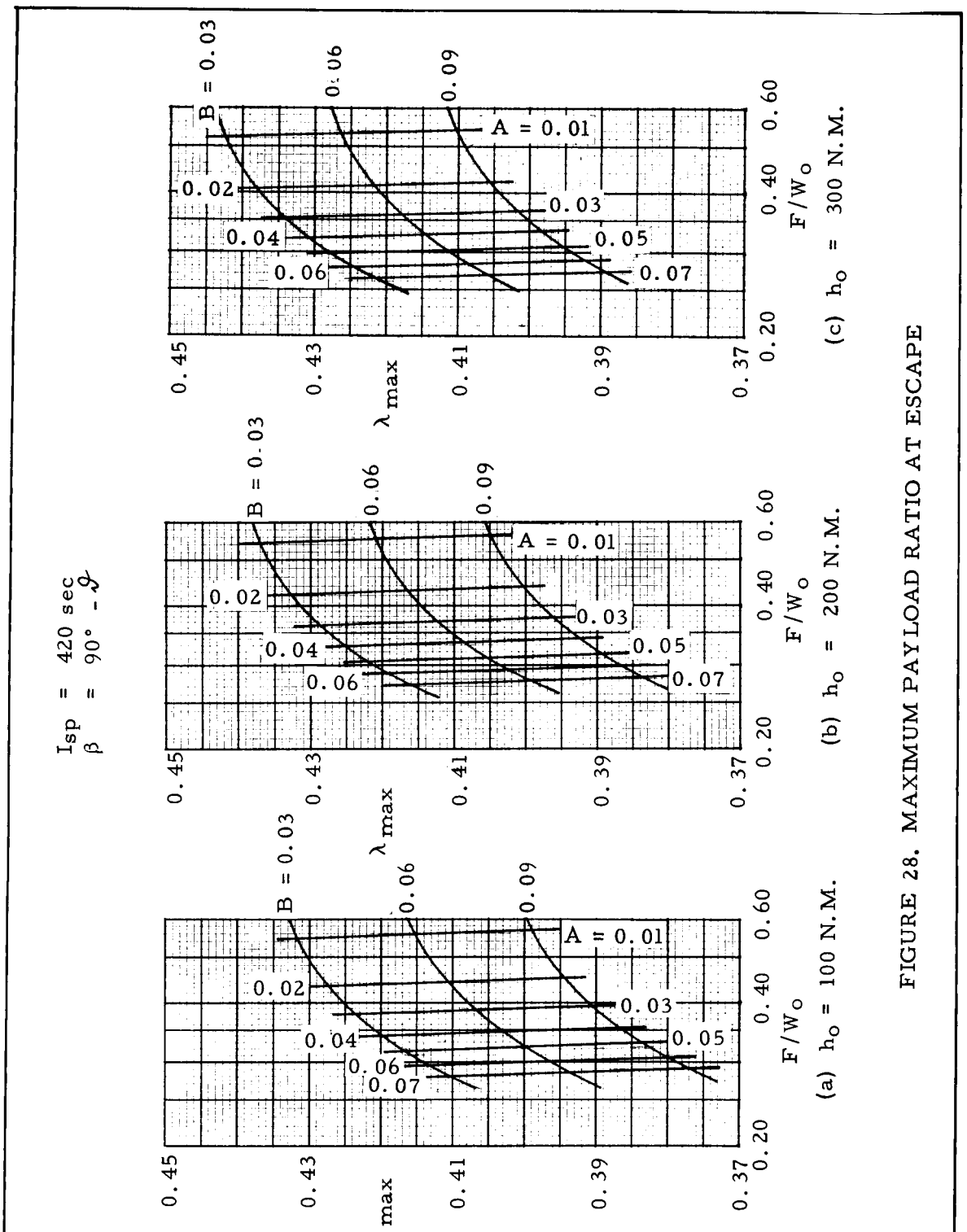

FIGURE 28. MAXIMUM PAYLOAD RATIO AT ESCAPE

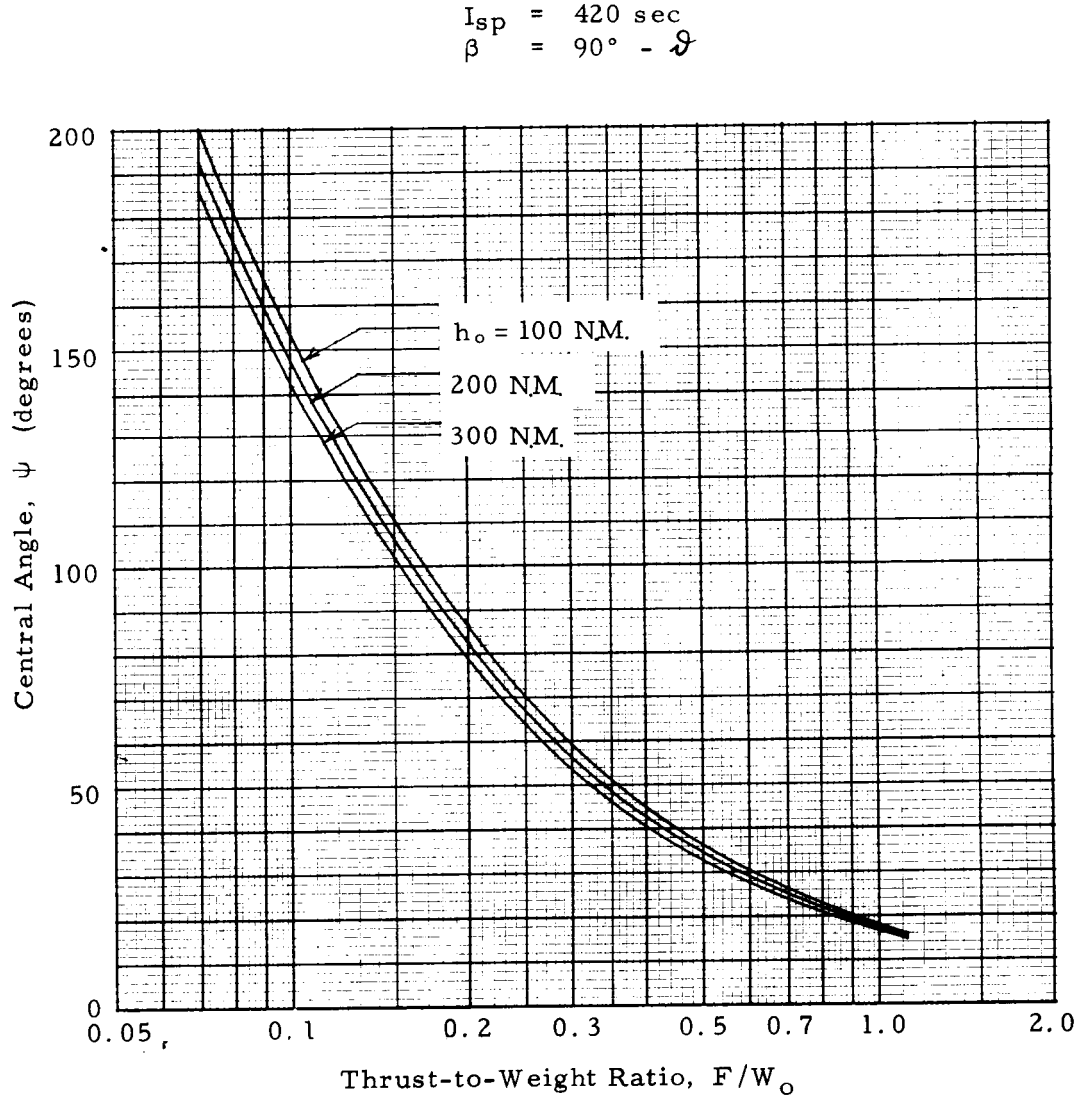

FIGURE 29. CENTRAL ANGLE AT ESCAPE

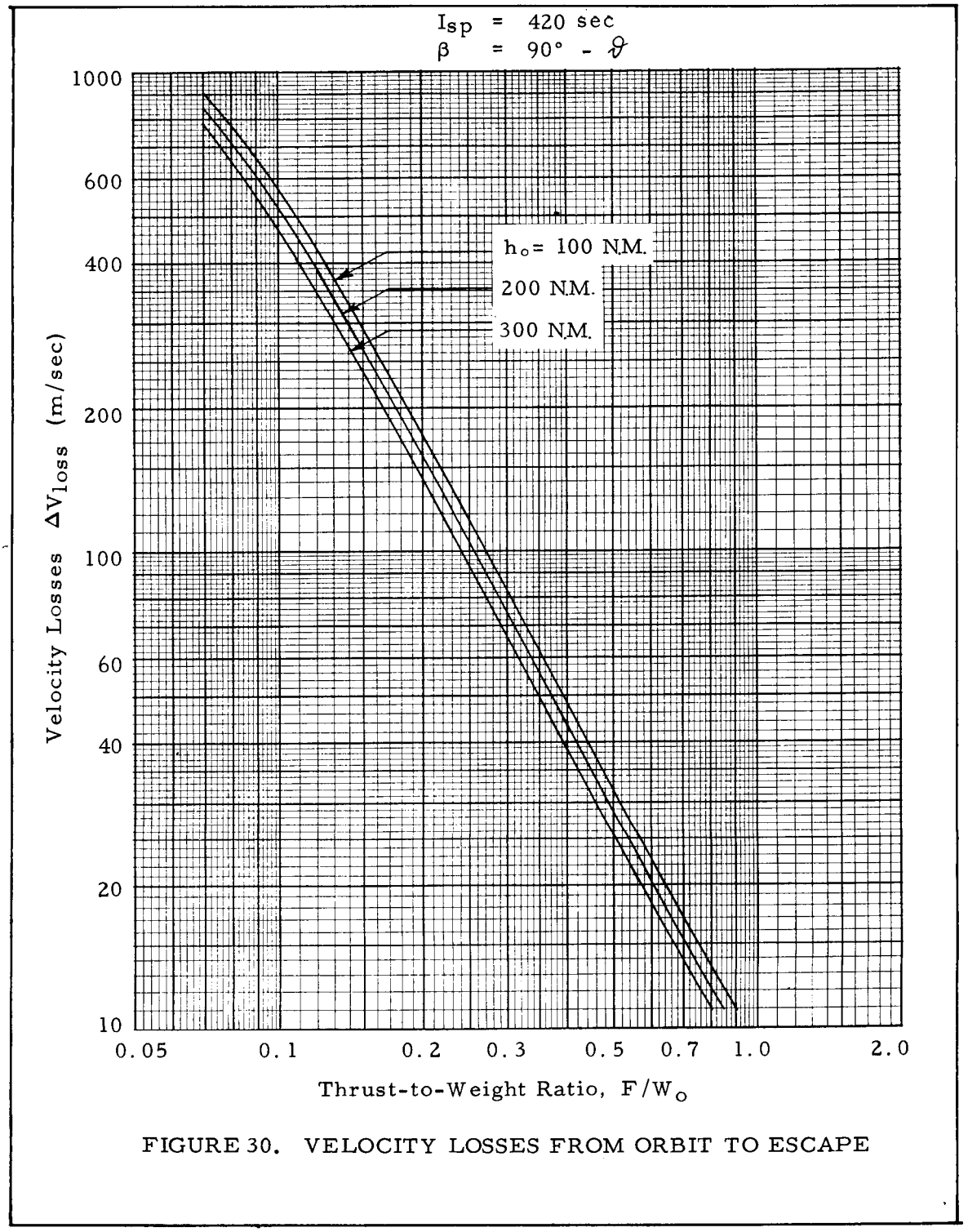

FIGURE 30. VELOCITY LOSSES FROM ORBIT TO ESCAPE

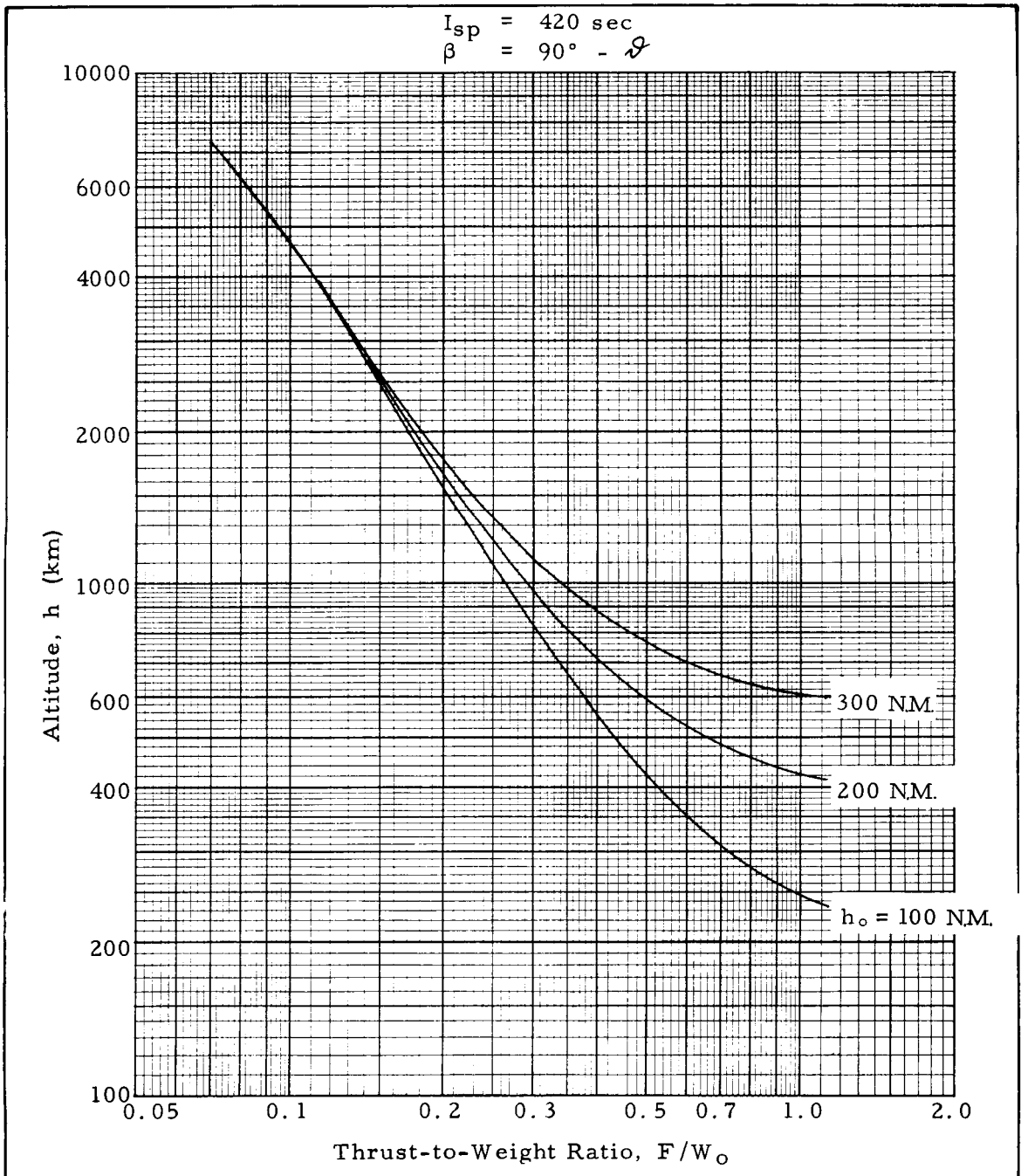

FIGURE 31. ALTITUDE AT ESCAPE

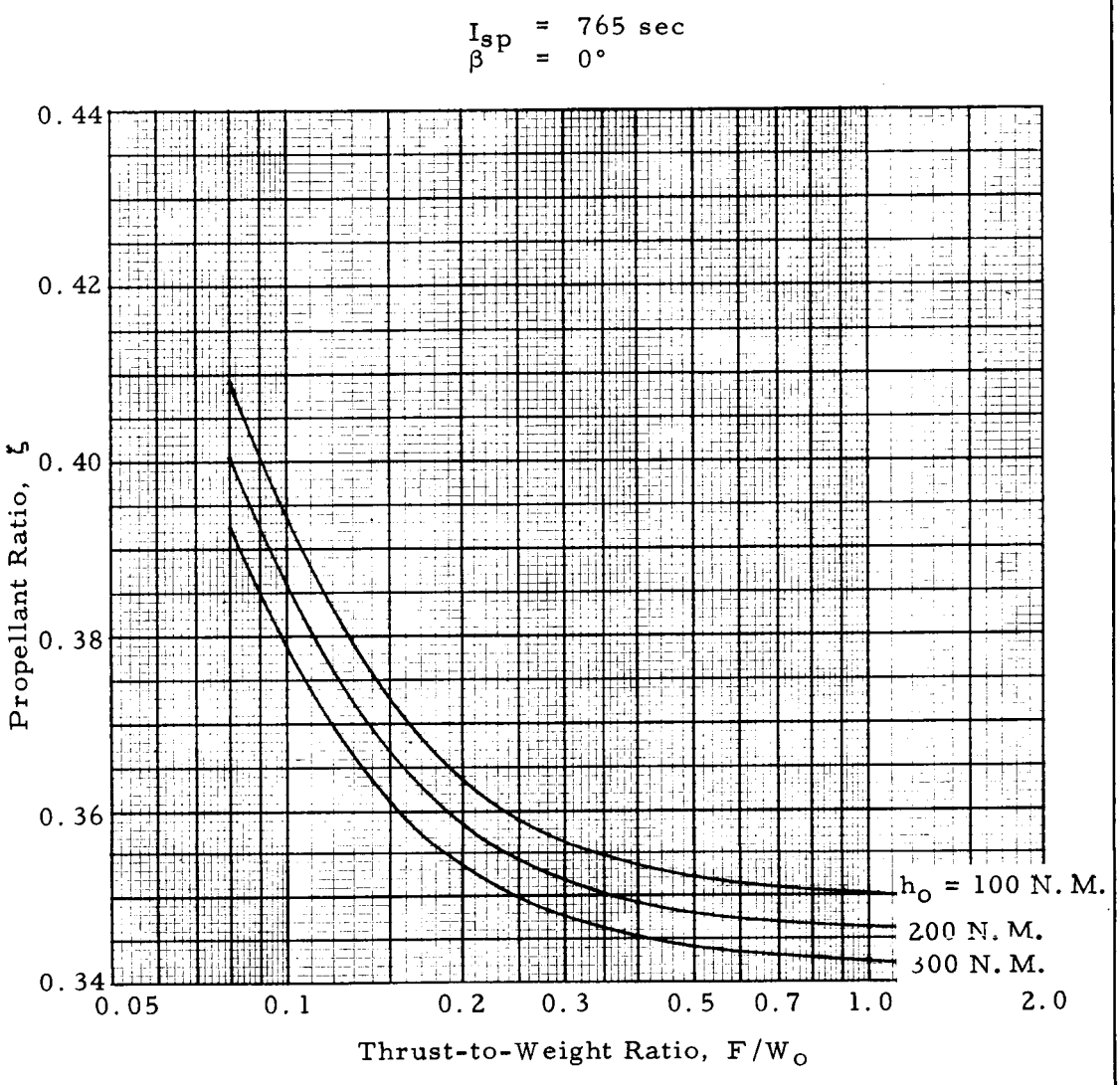

FIGURE 32. PROPELLANT CONSUMPTION REQUIRED FOR ESCAPE

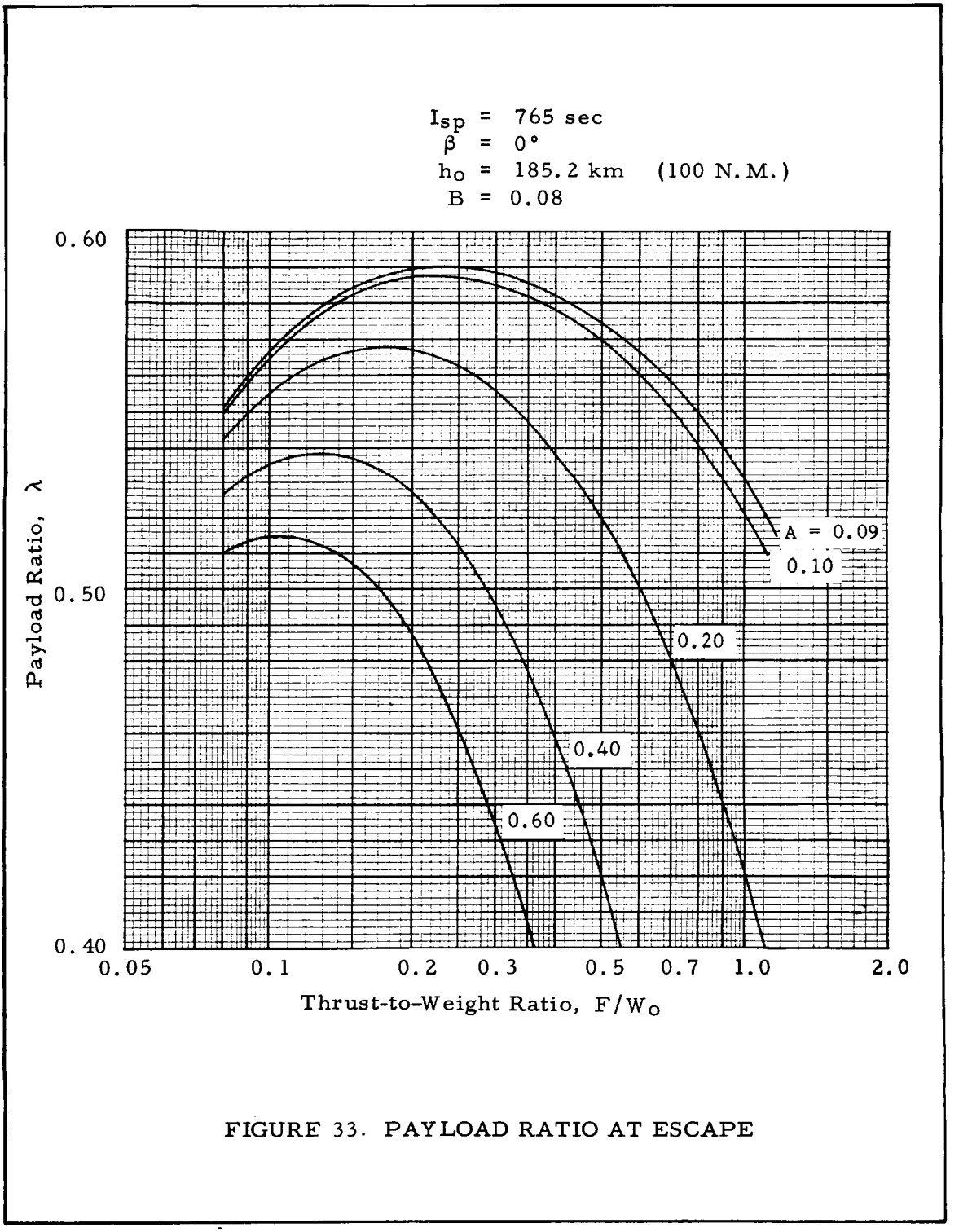

FIGURE 33. PAYLOAD RATIO AT ESCAPE

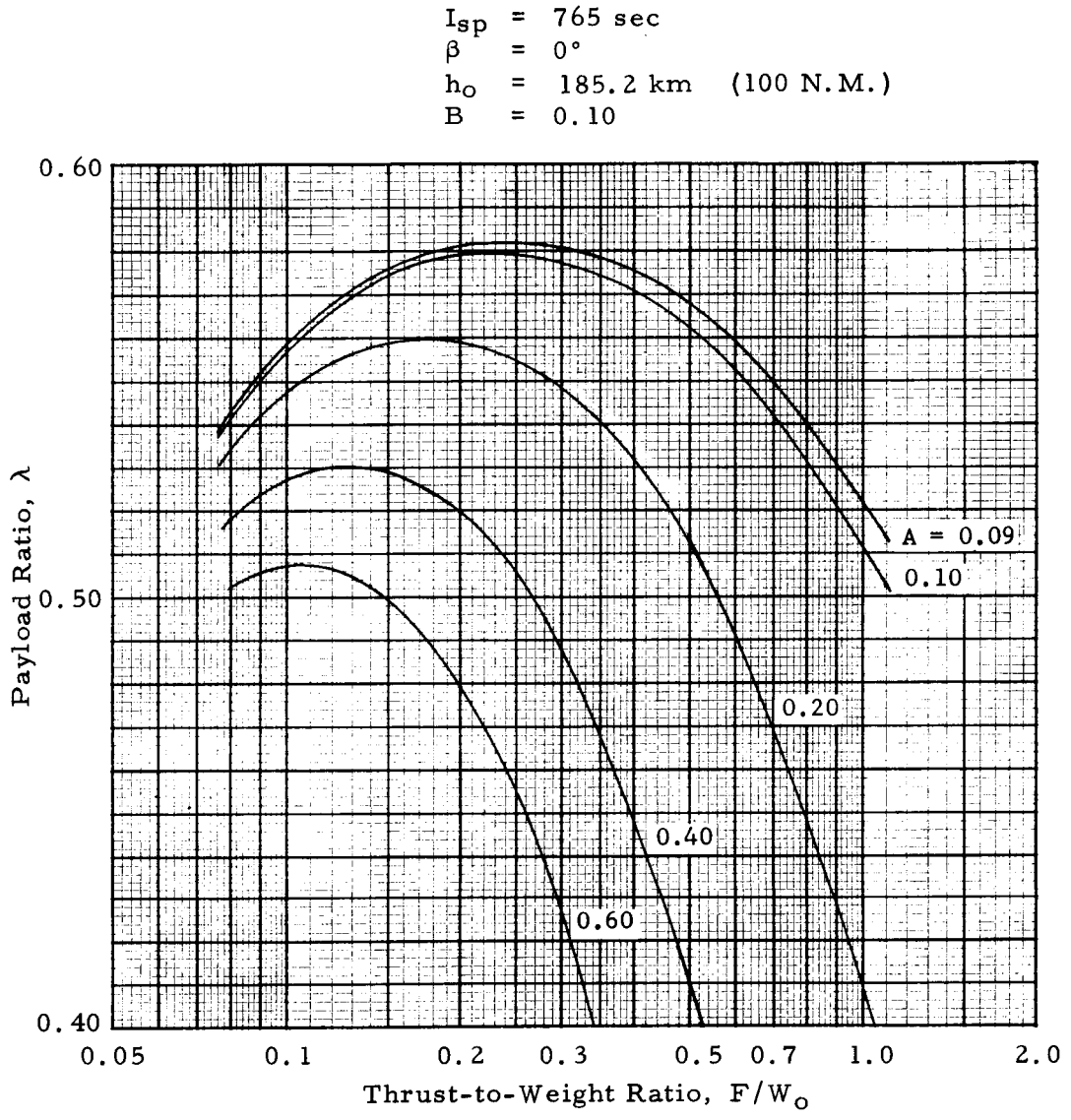

FIGURE 34. PAYLOAD RATIO AT ESCAPE

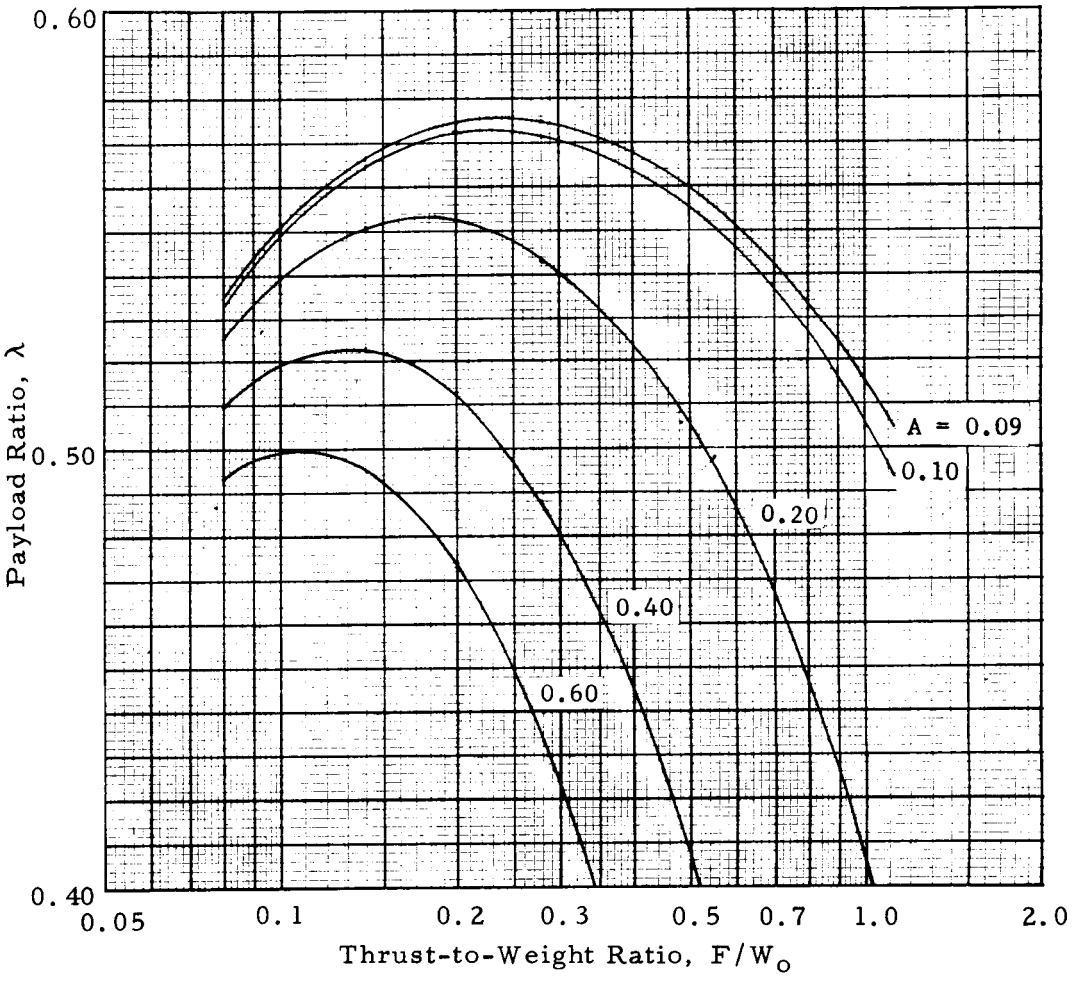

FIGURE 35. PAYLOAD RATIO AT ESCAPE

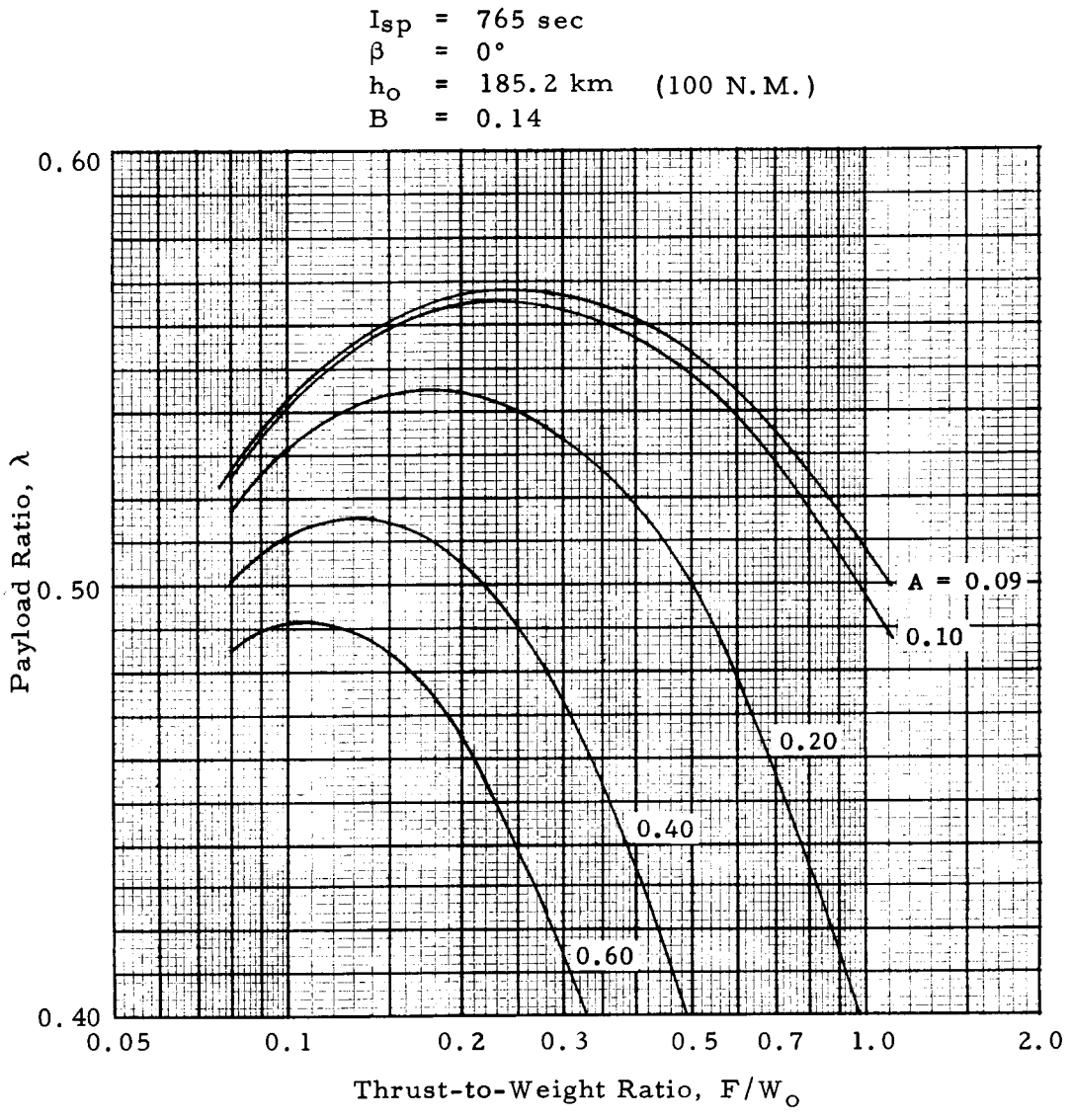

FIGURE 36. PAYLOAD RATIO AT ESCAPE

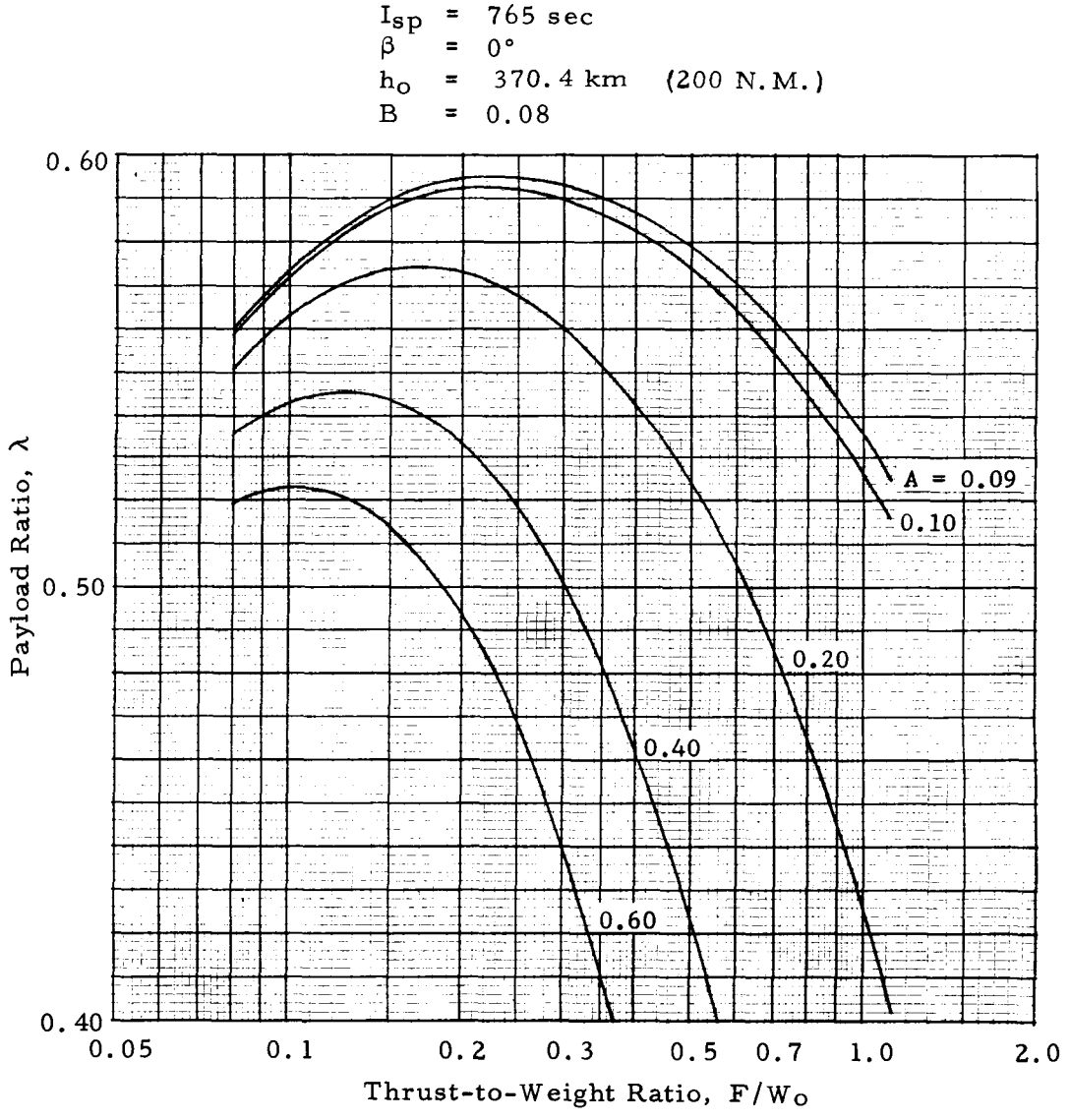

FIGURE 37. PAYLOAD RATIO AT ESCAPE

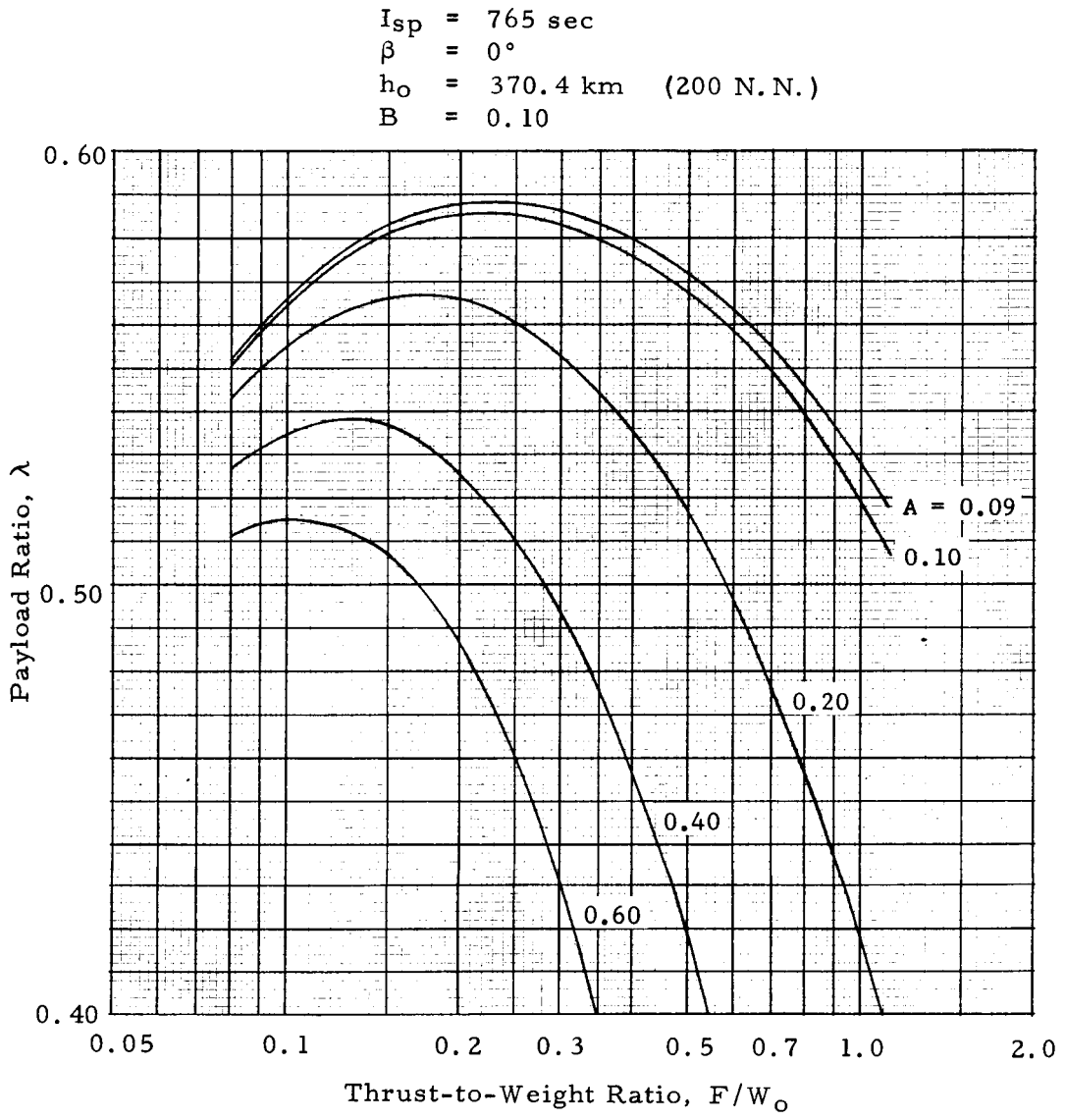

FIGURE 38. PAYLOAD RATIO AT ESCAPE

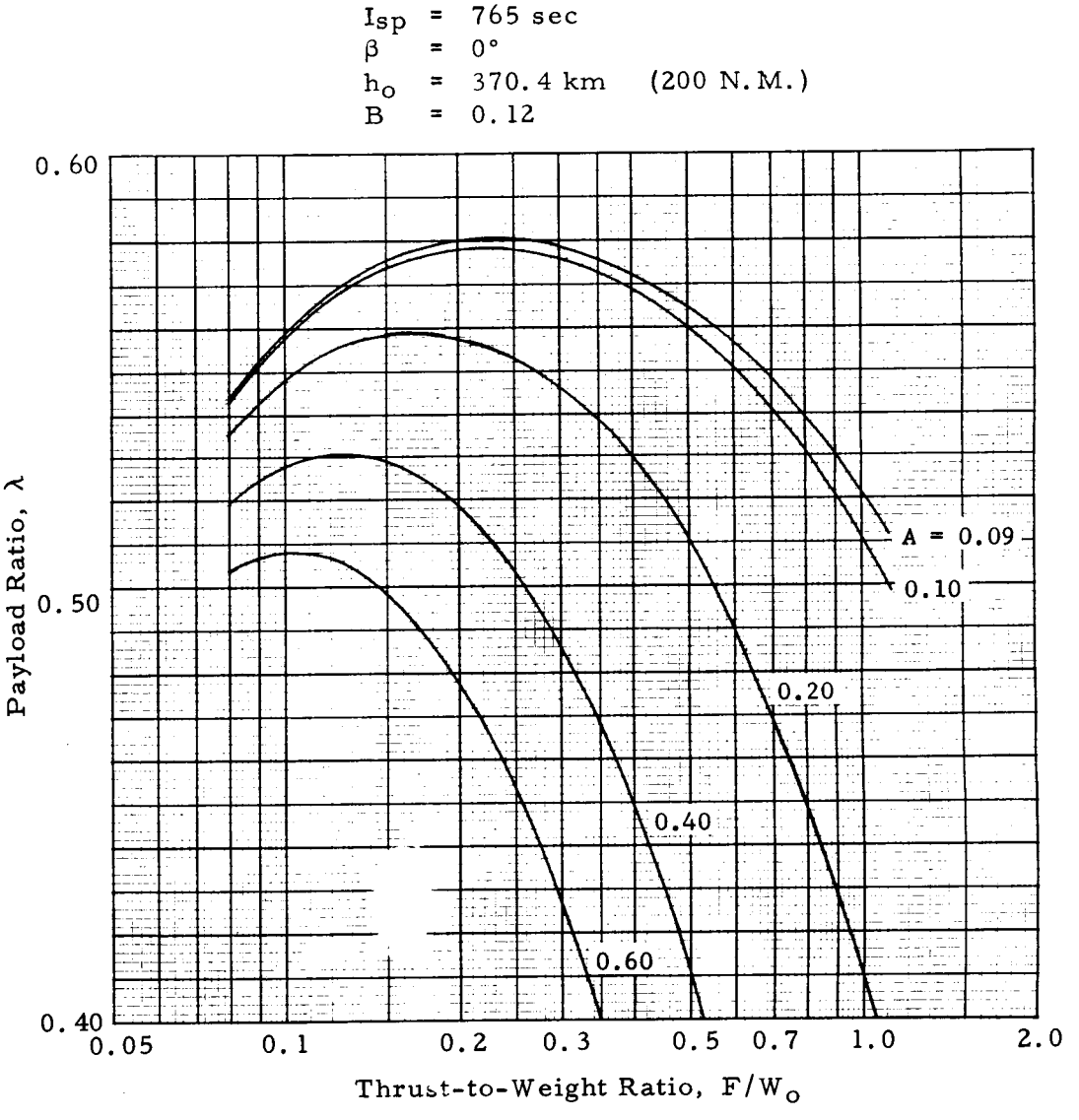

FIGURE 39. PAYLOAD RATIO AT ESCAPE

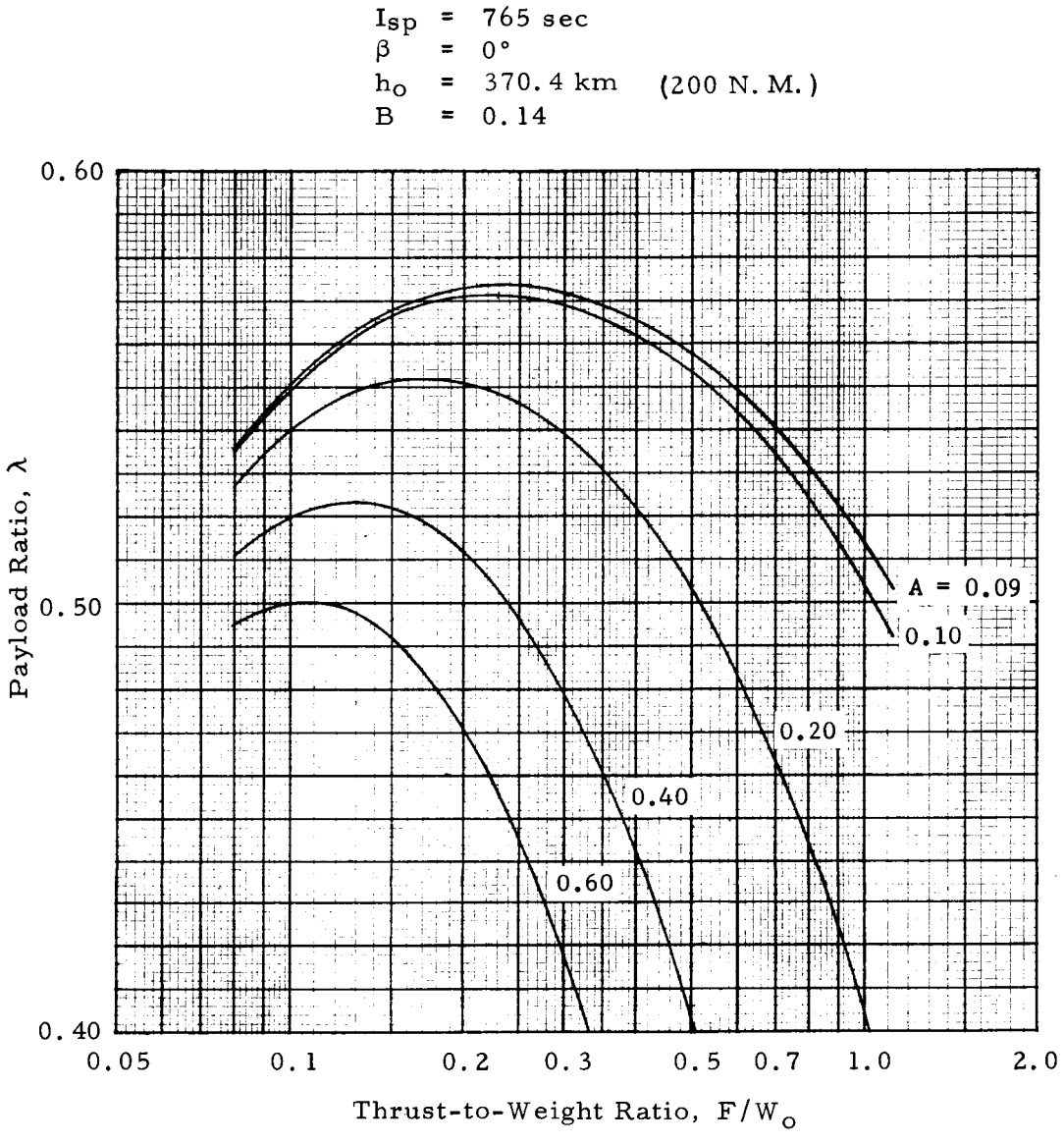

FIGURE 40. PAYLOAD RATIO AT ESCAPE

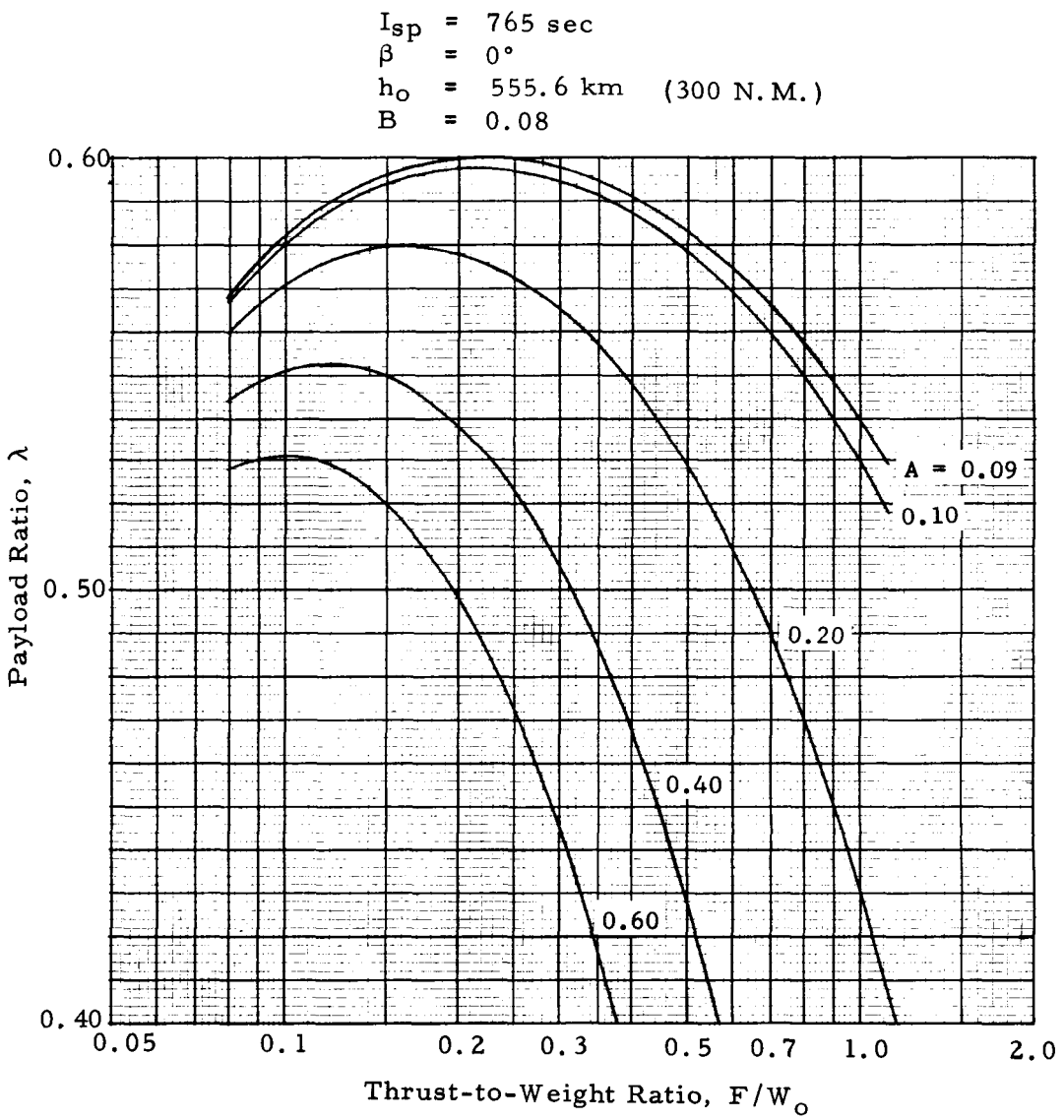

FIGURE 41. PAYLOAD RATIO AT ESCAPE

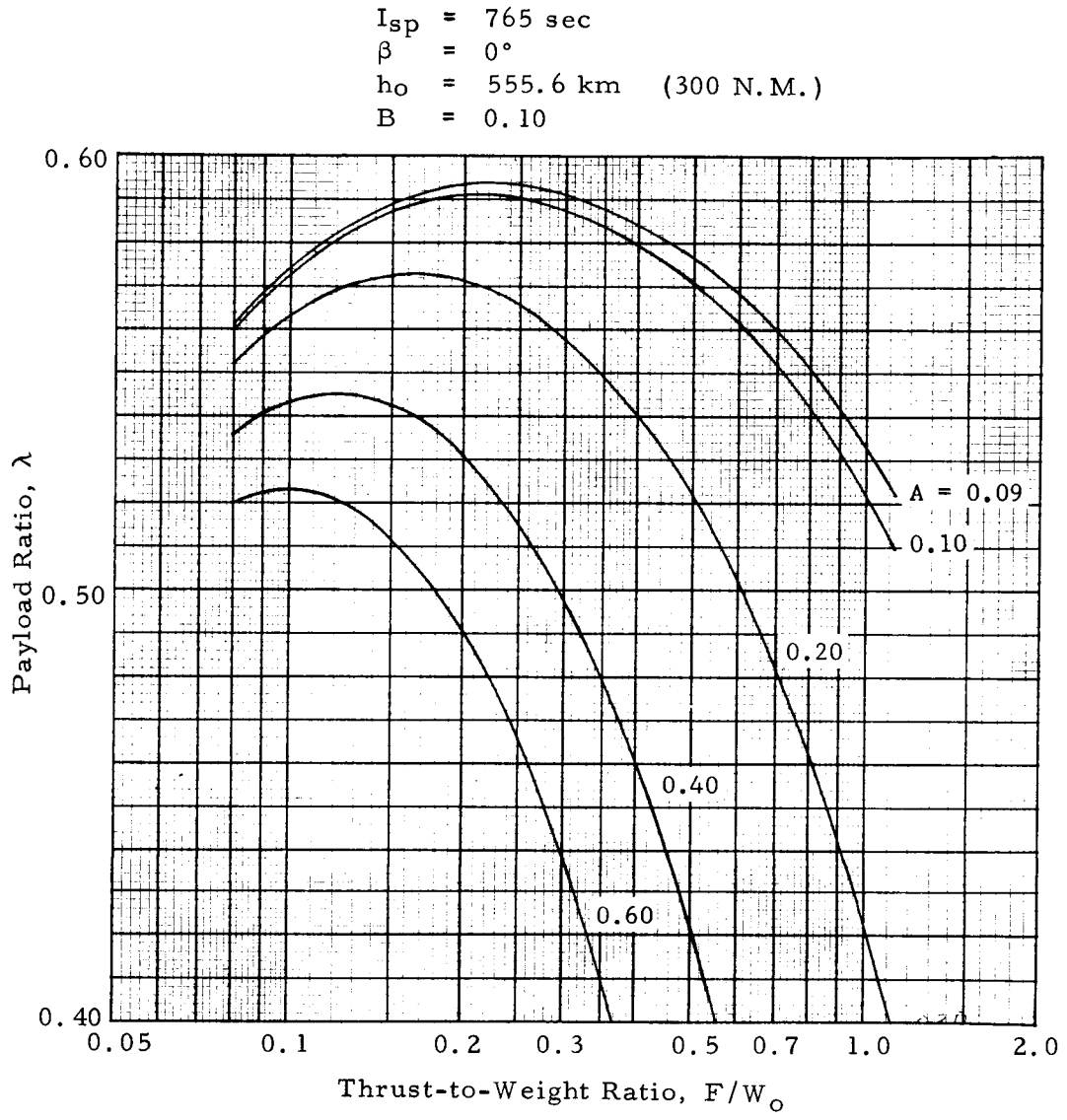

FIGURE 42. PAYLOAD RATIO AT ESCAPE

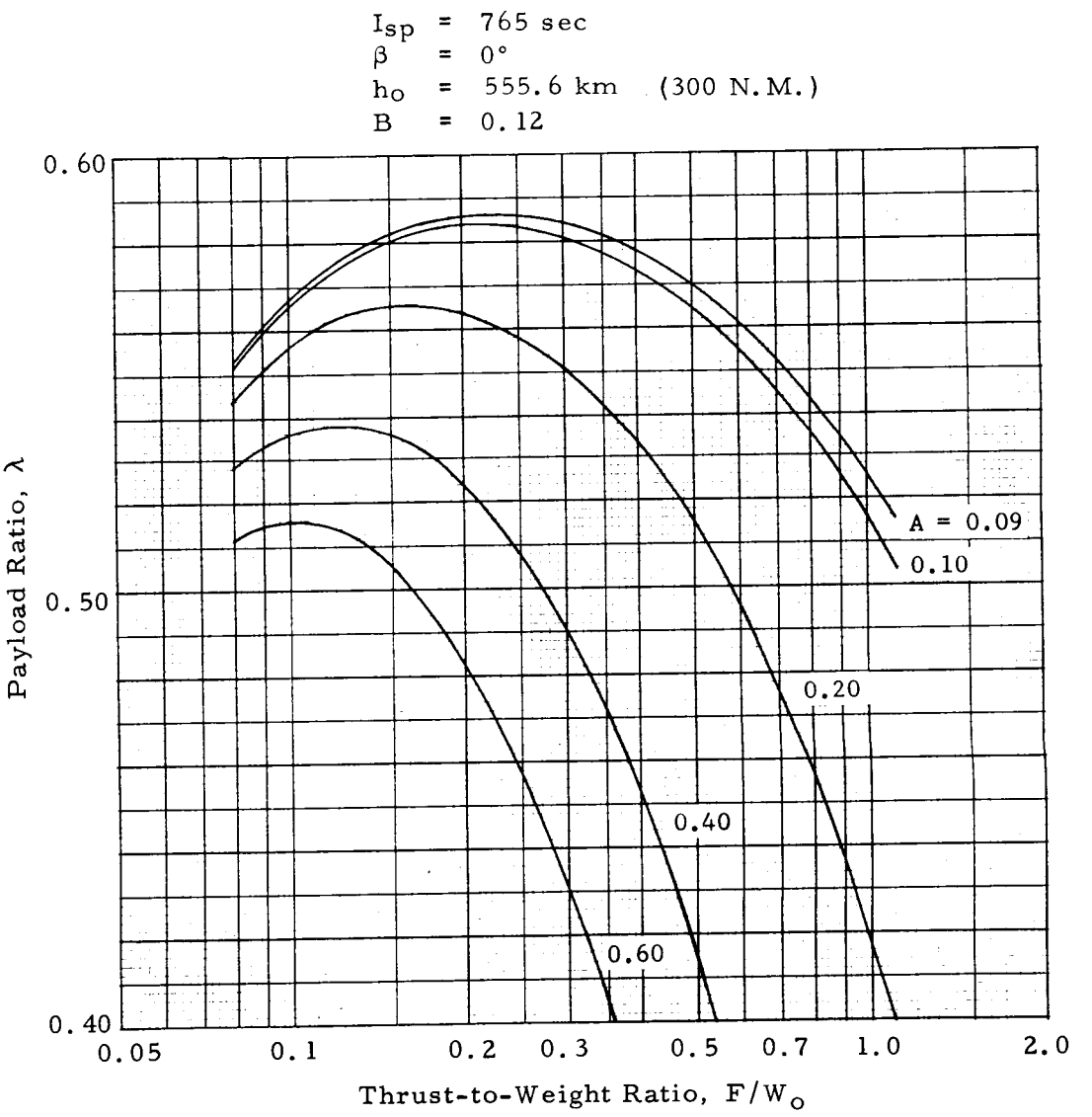

FIGURE 43. PAYLOAD RATIO AT ESCAPE

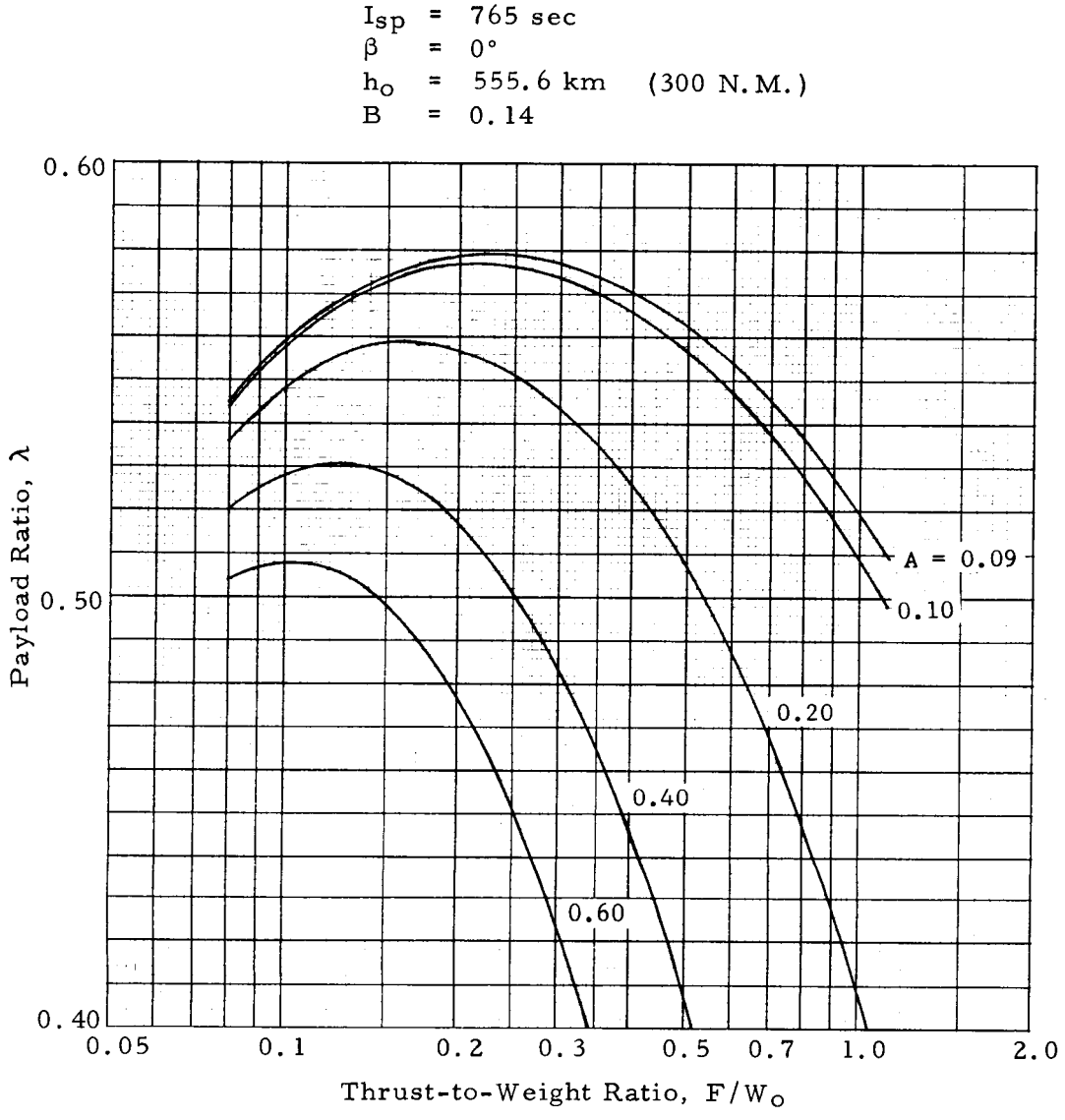

FIGURE 44. PAYLOAD RATIO AT ESCAPE

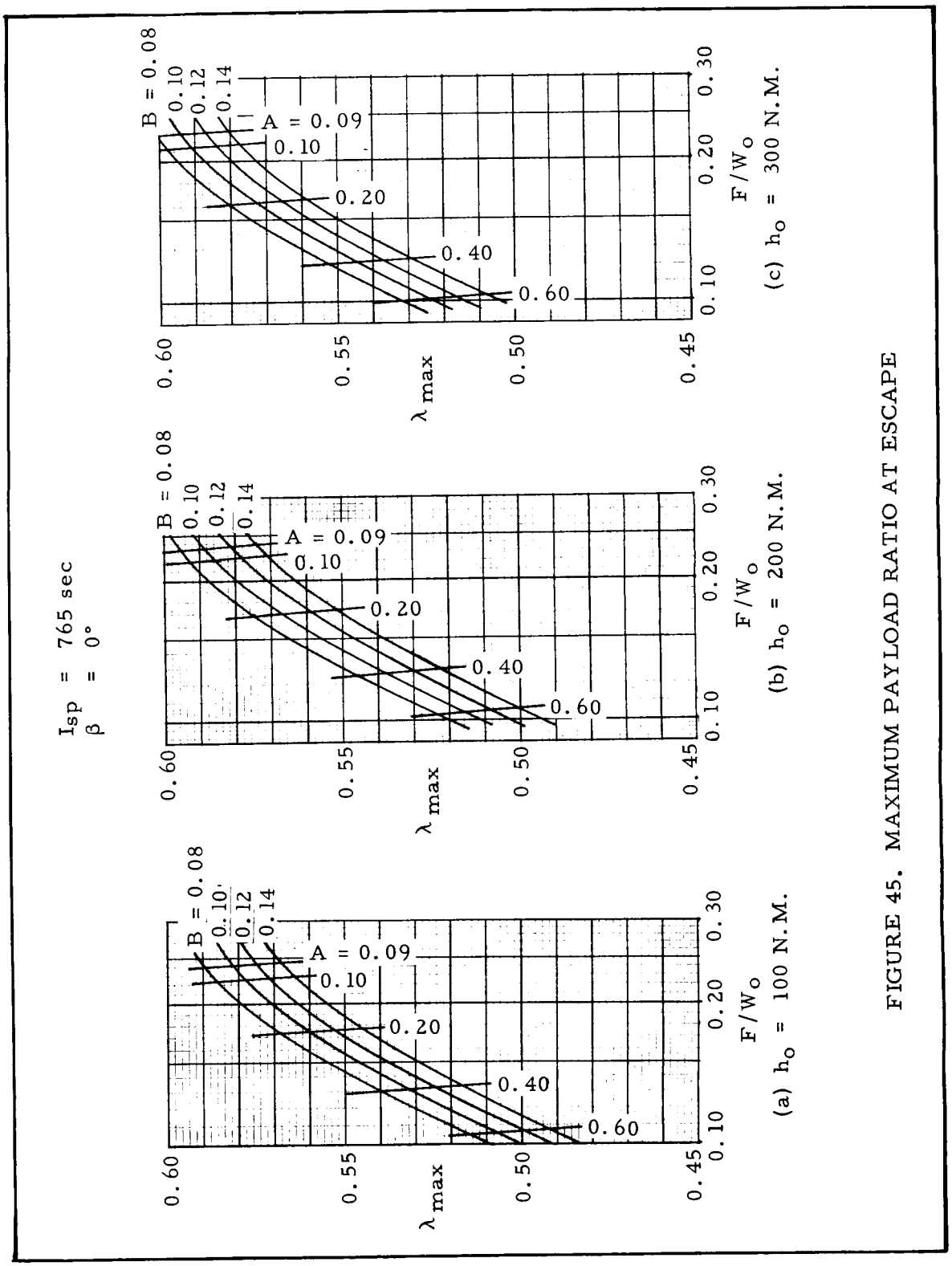

FIGURE 45. MAXIMUM PAYLOAD RATIO AT ESCAPE

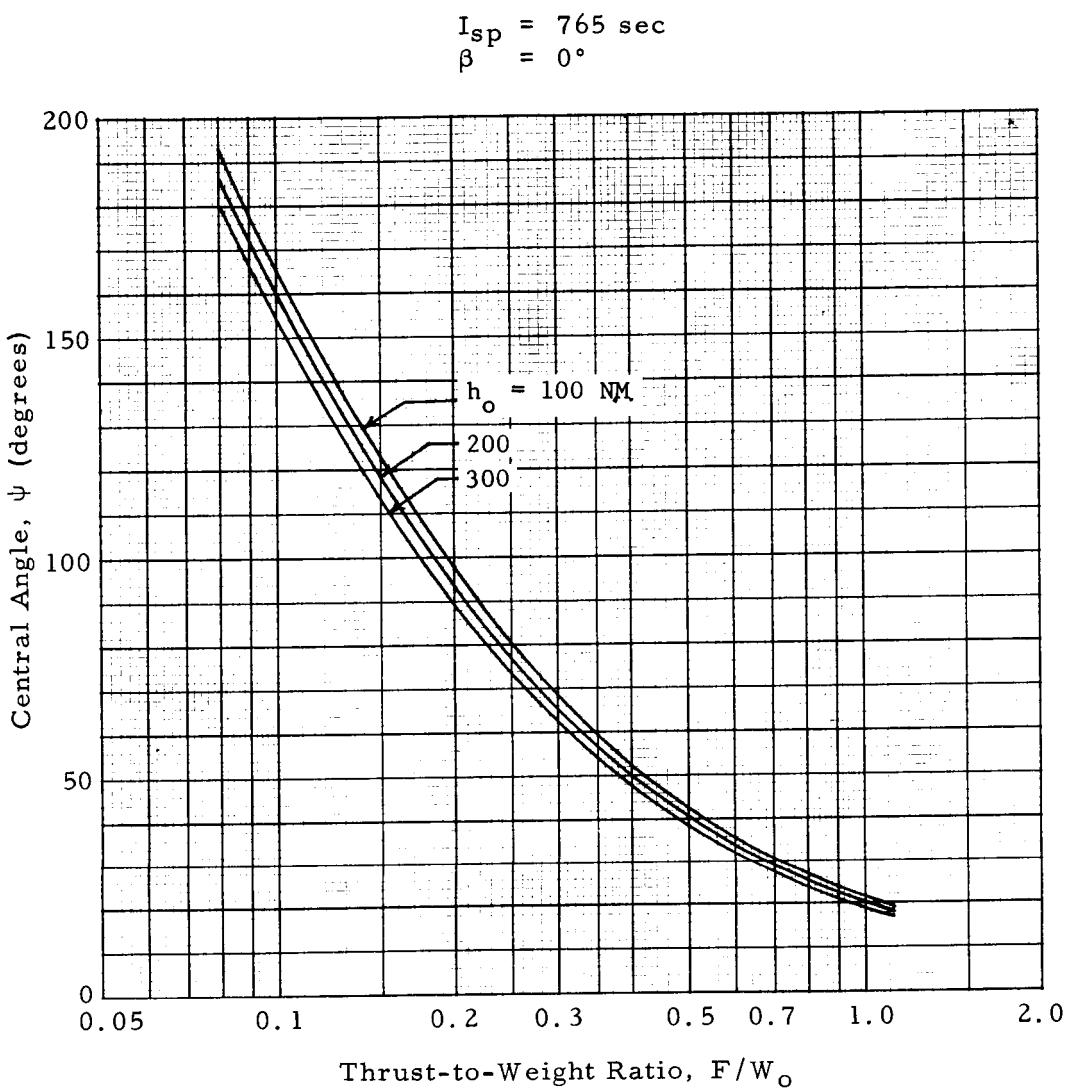

FIGURE 46. CENTRAL ANGLE AT ESCAPE

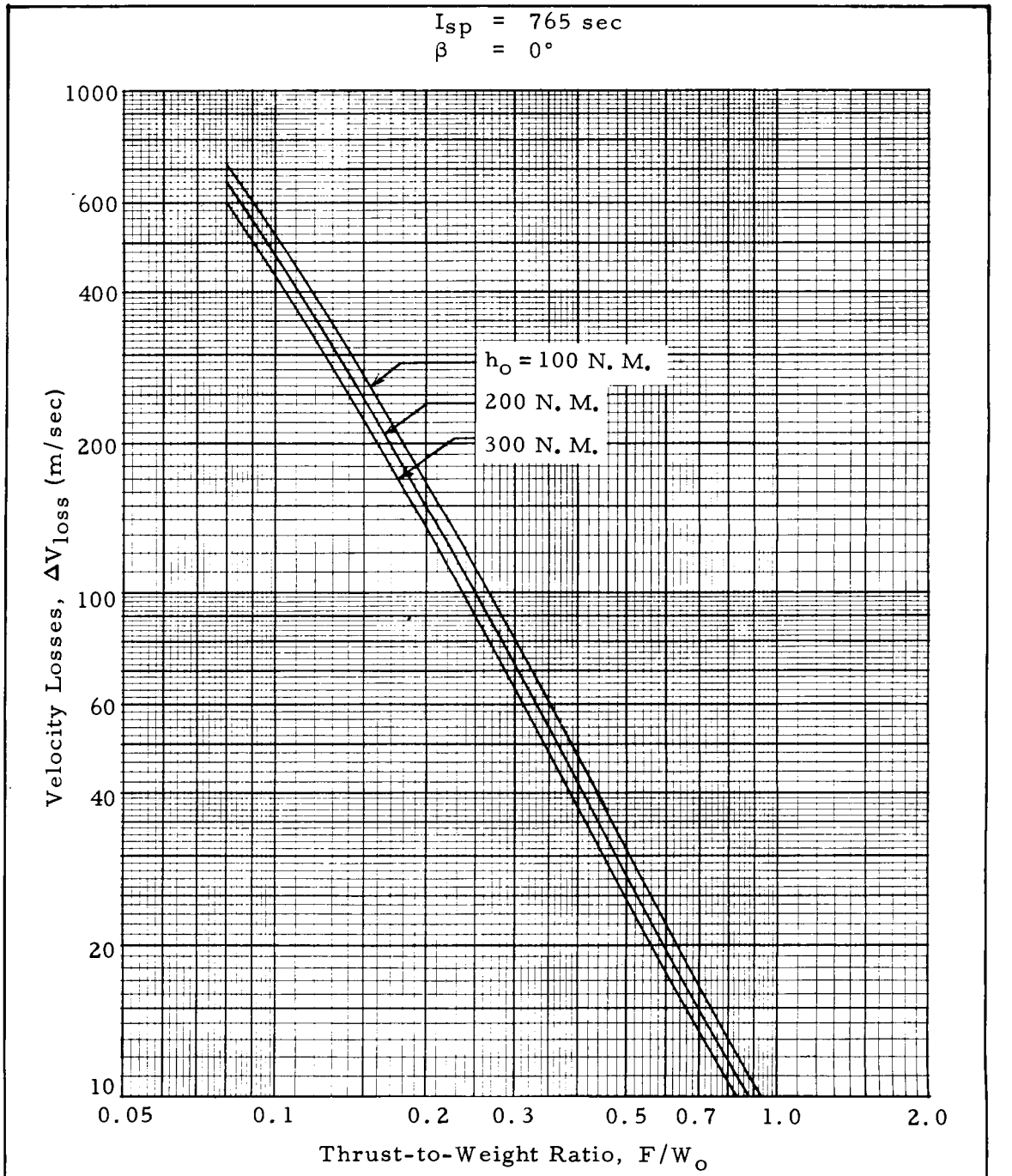

FIGURE 47. VELOCITY LOSSES FROM ORBIT TO ESCAPE

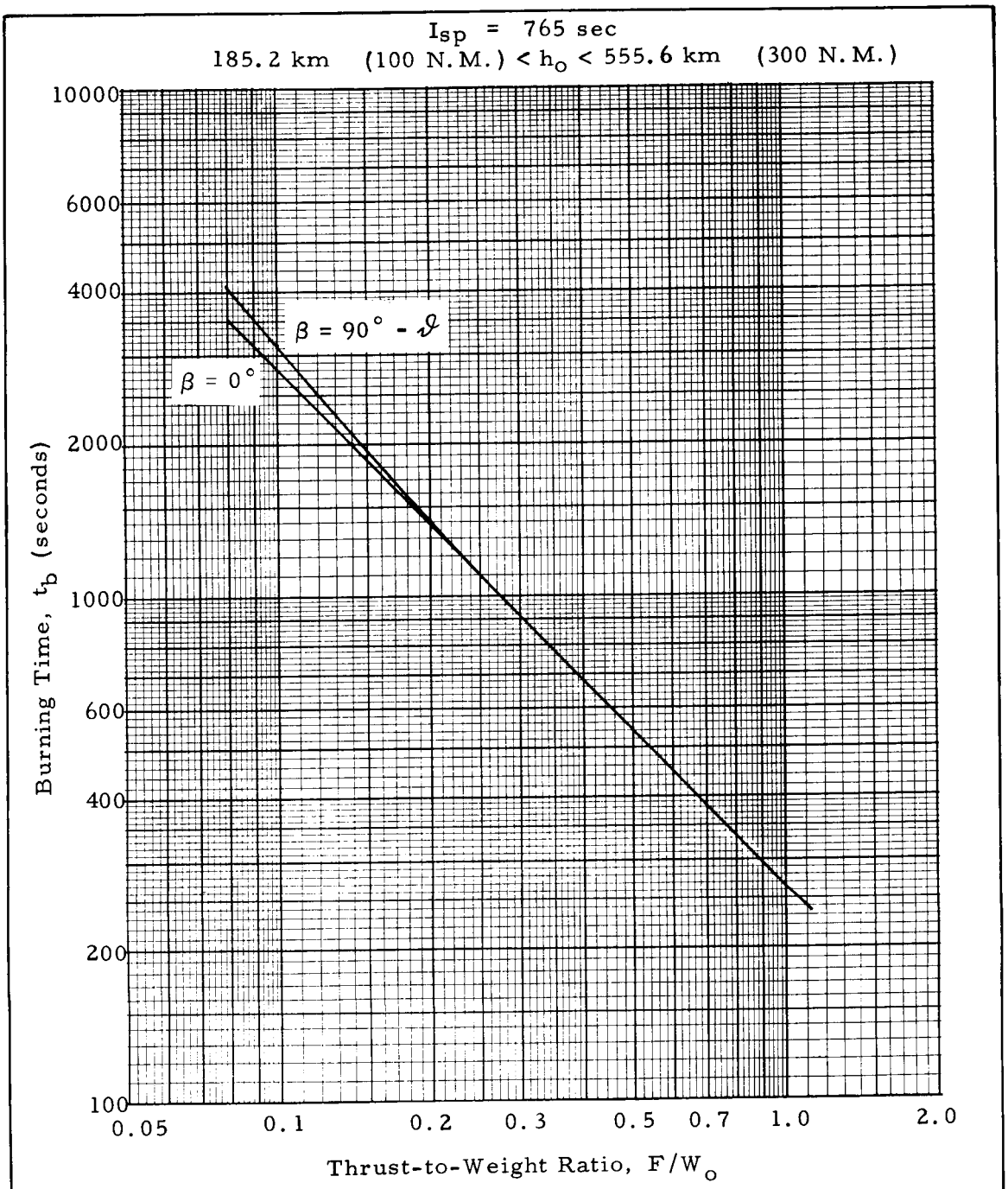

FIGURE 48. BURNING TIME TO ESCAPE

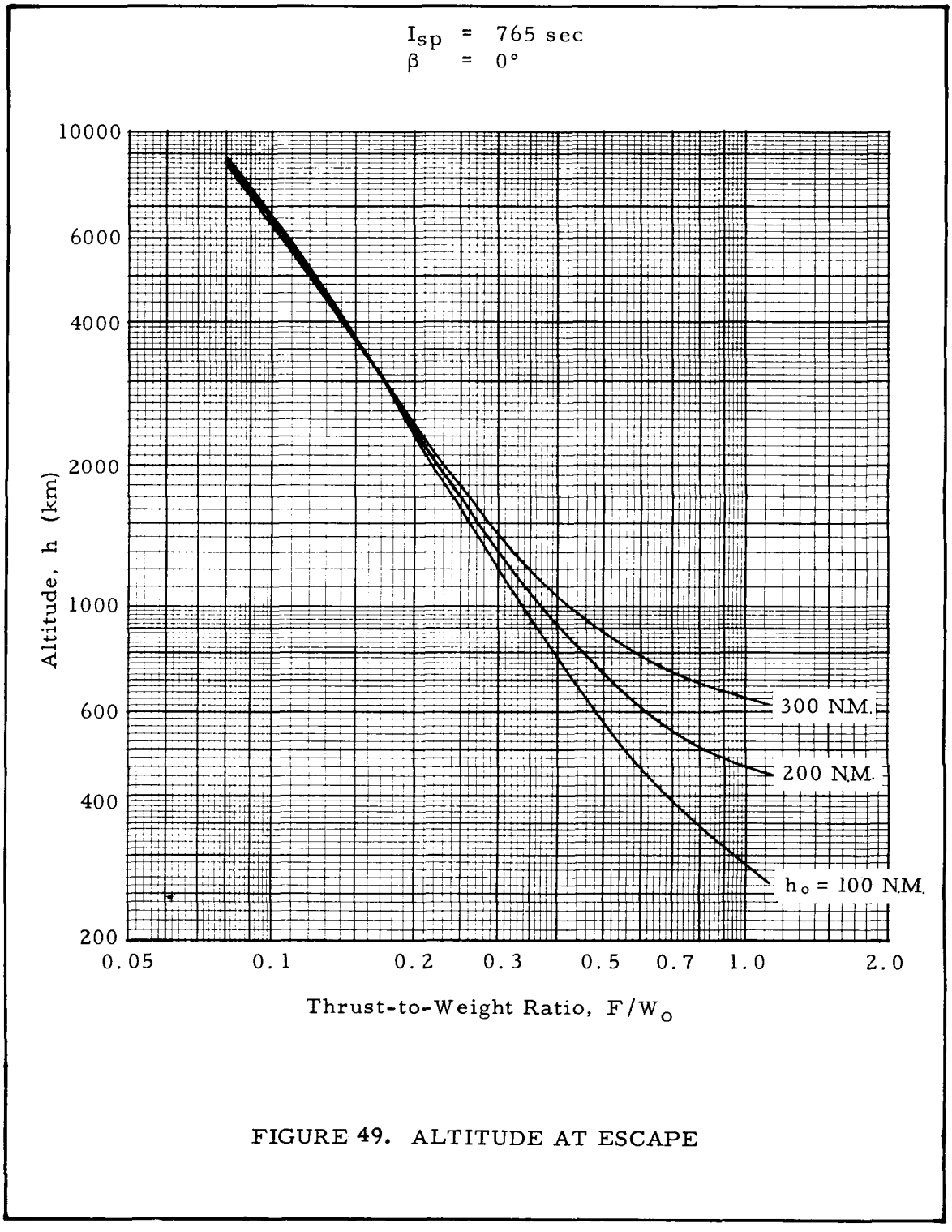

FIGURE 49. ALTITUDE AT ESCAPE

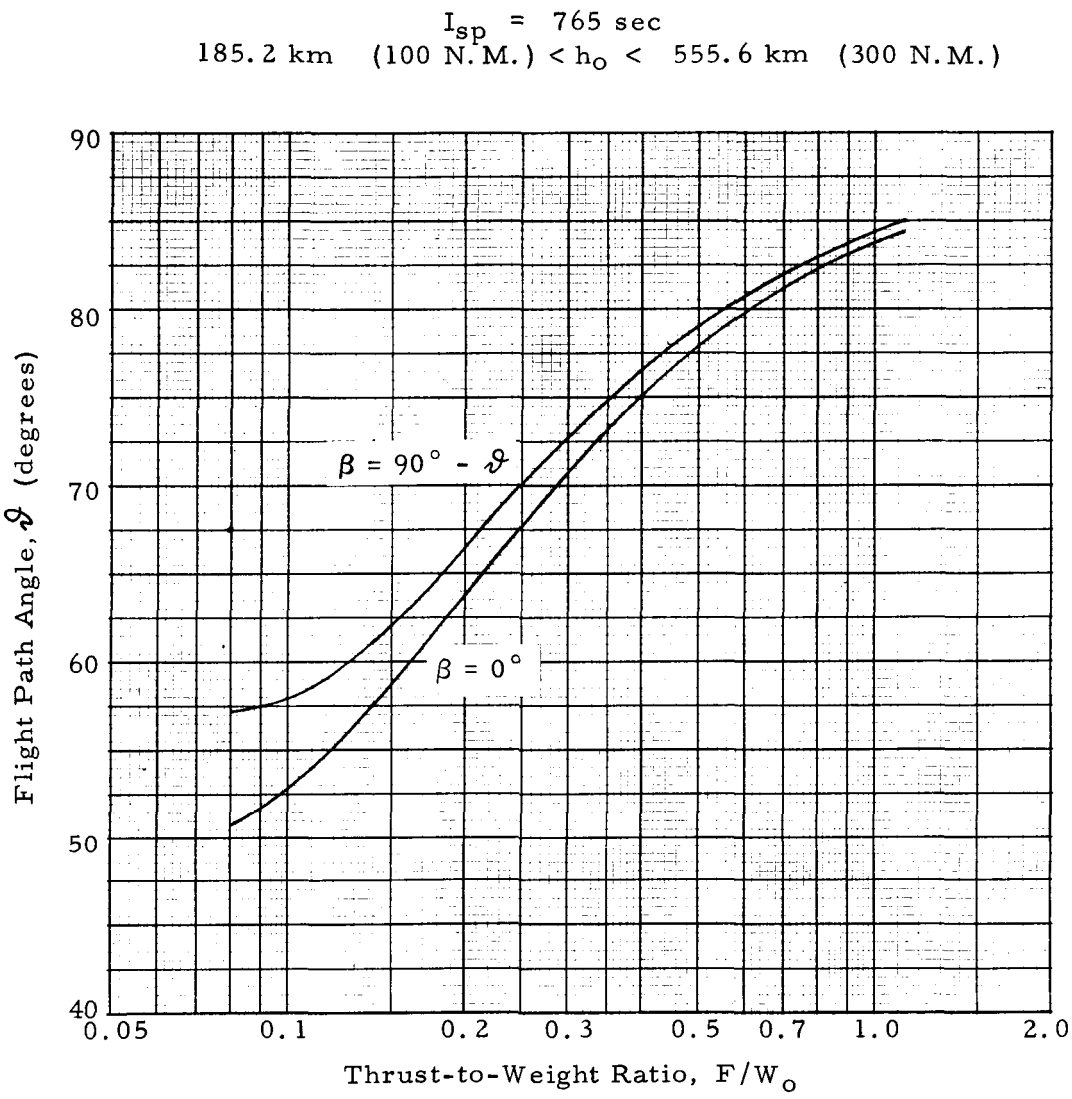

FIGURE 50. FLIGHT PATH ANGLE AT ESCAPE

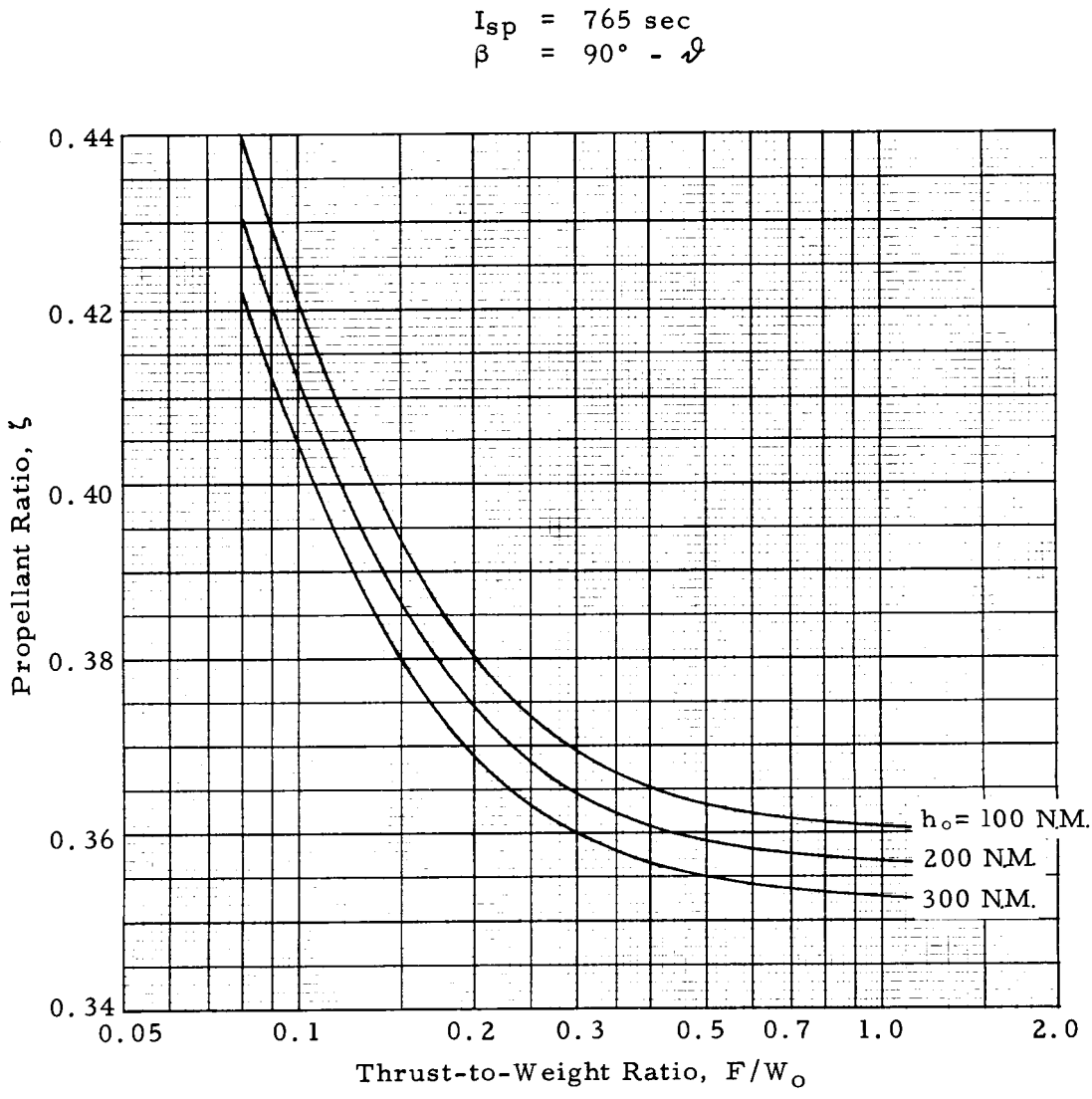

FIGURE 51. PROPELLANT CONSUMPTION REQUIRED FOR ESCAPE

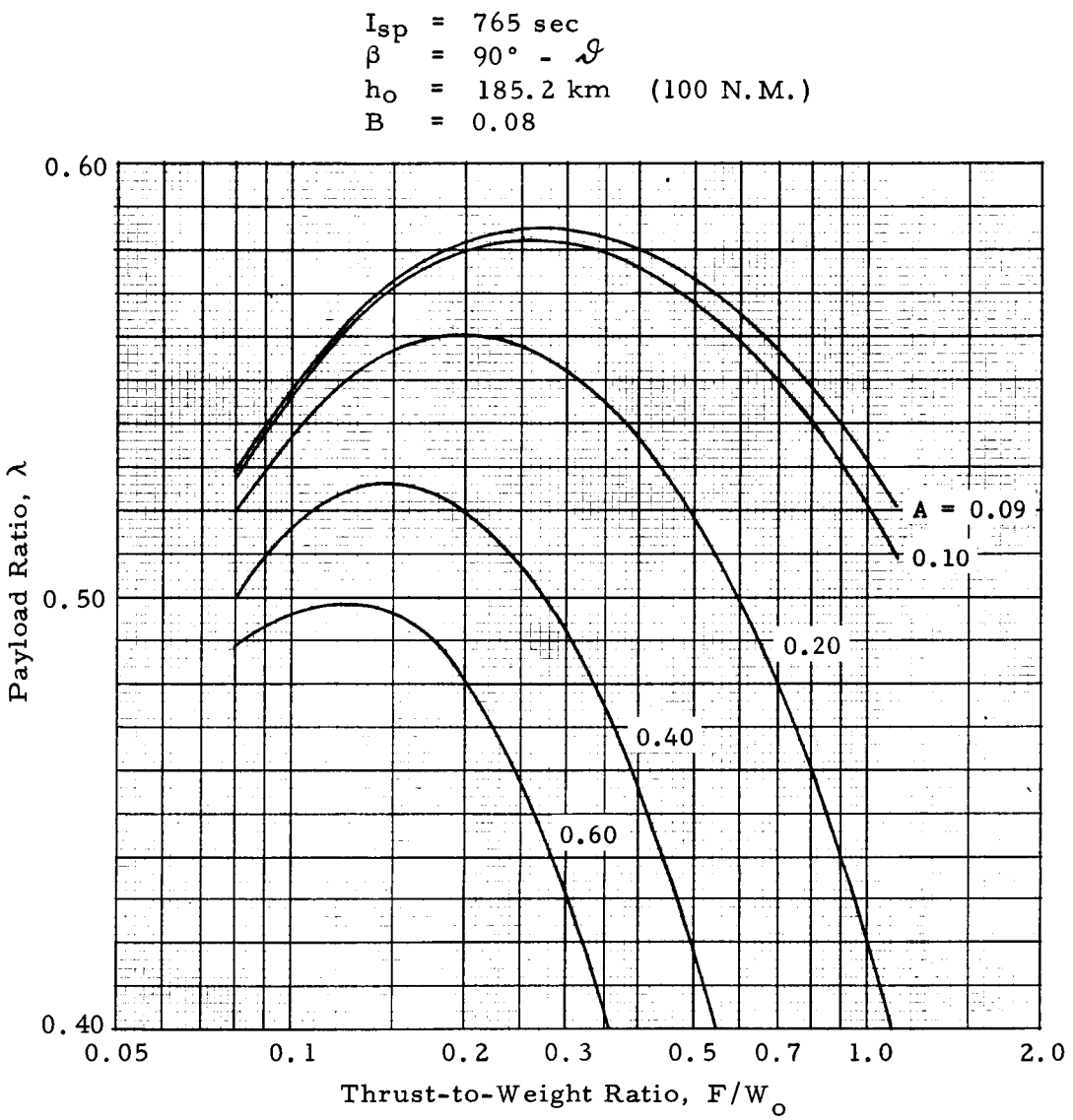

FIGURE 52. PAYLOAD RATIO AT ESCAPE

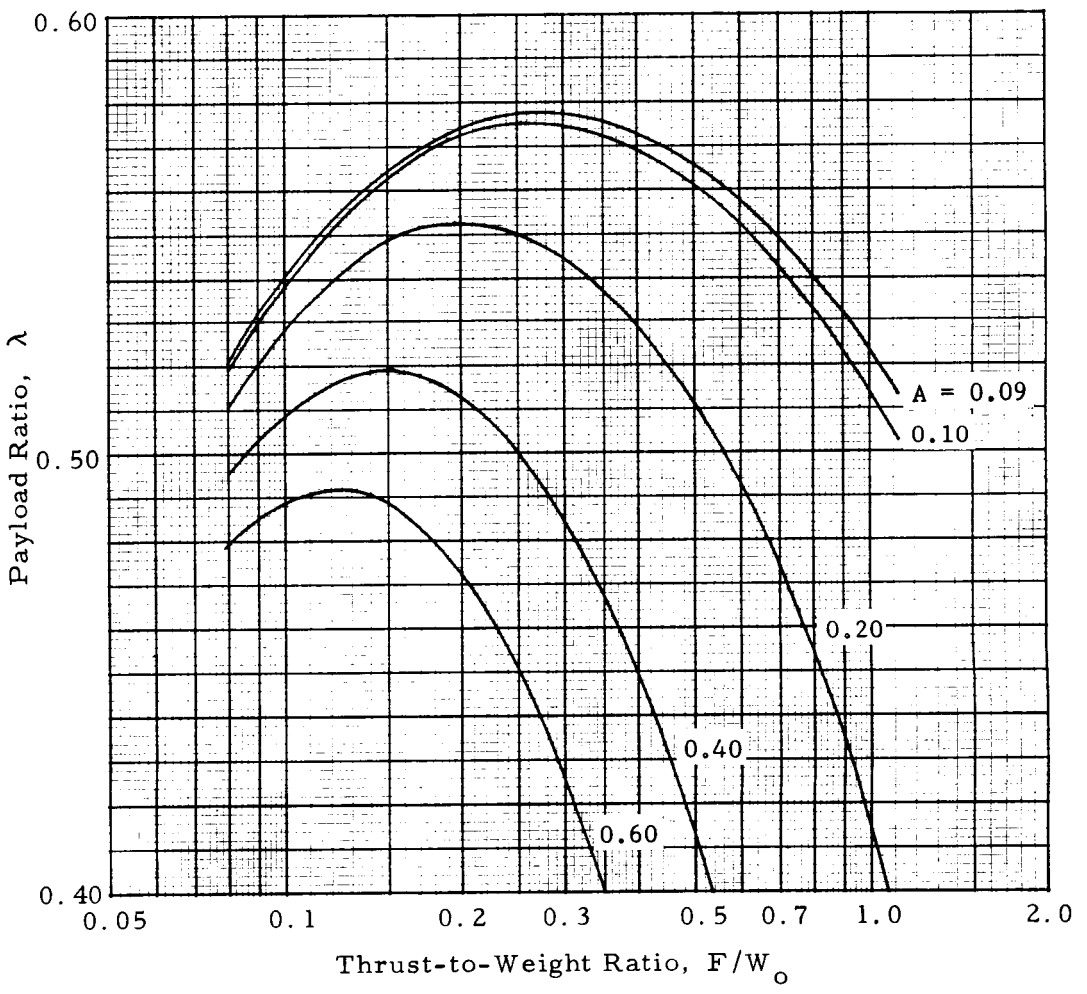

FIGURE 53. PAYLOAD RATIO AT ESCAPE

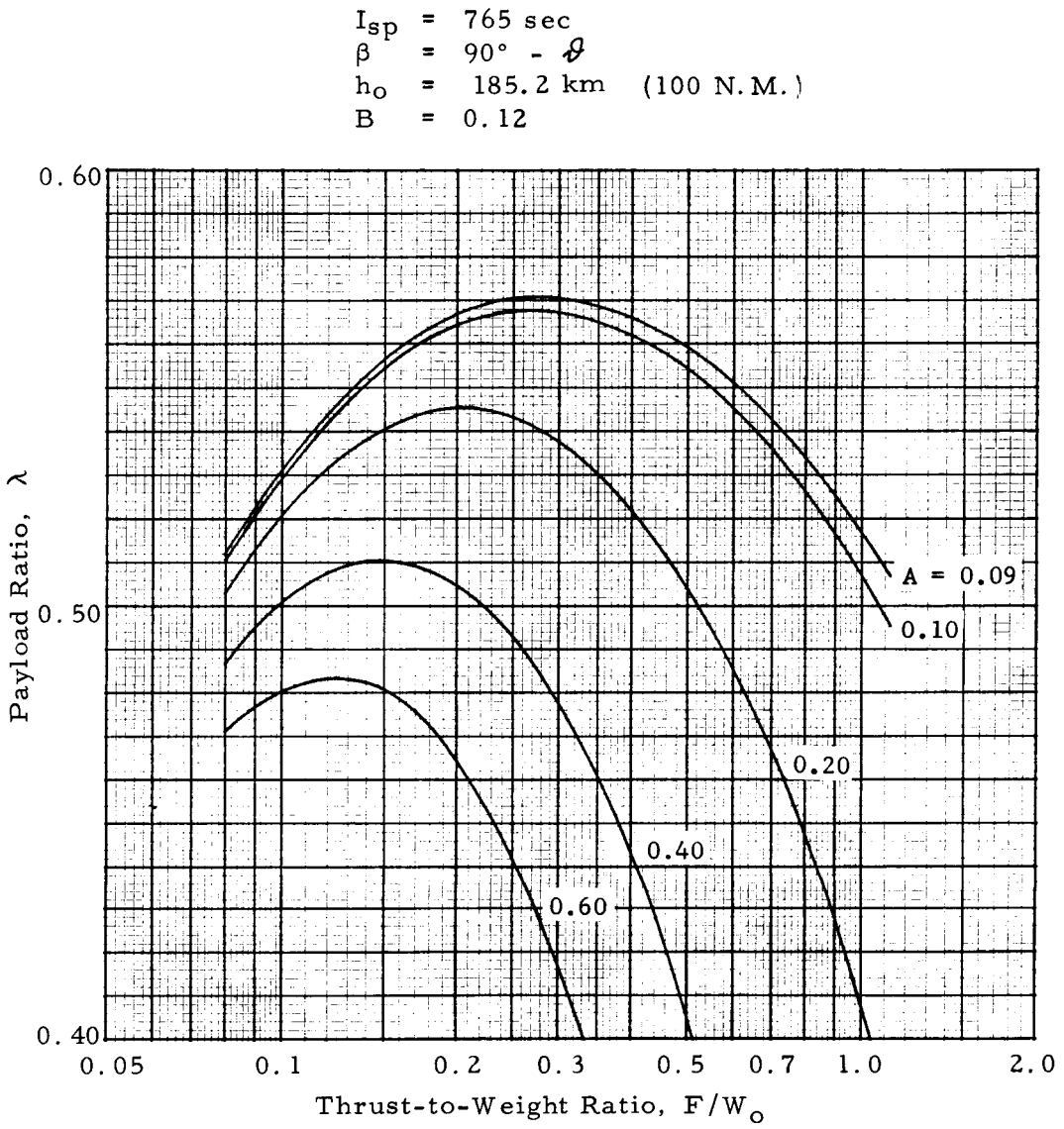

FIGURE 54. PAYLOAD RATIO AT ESCAPE

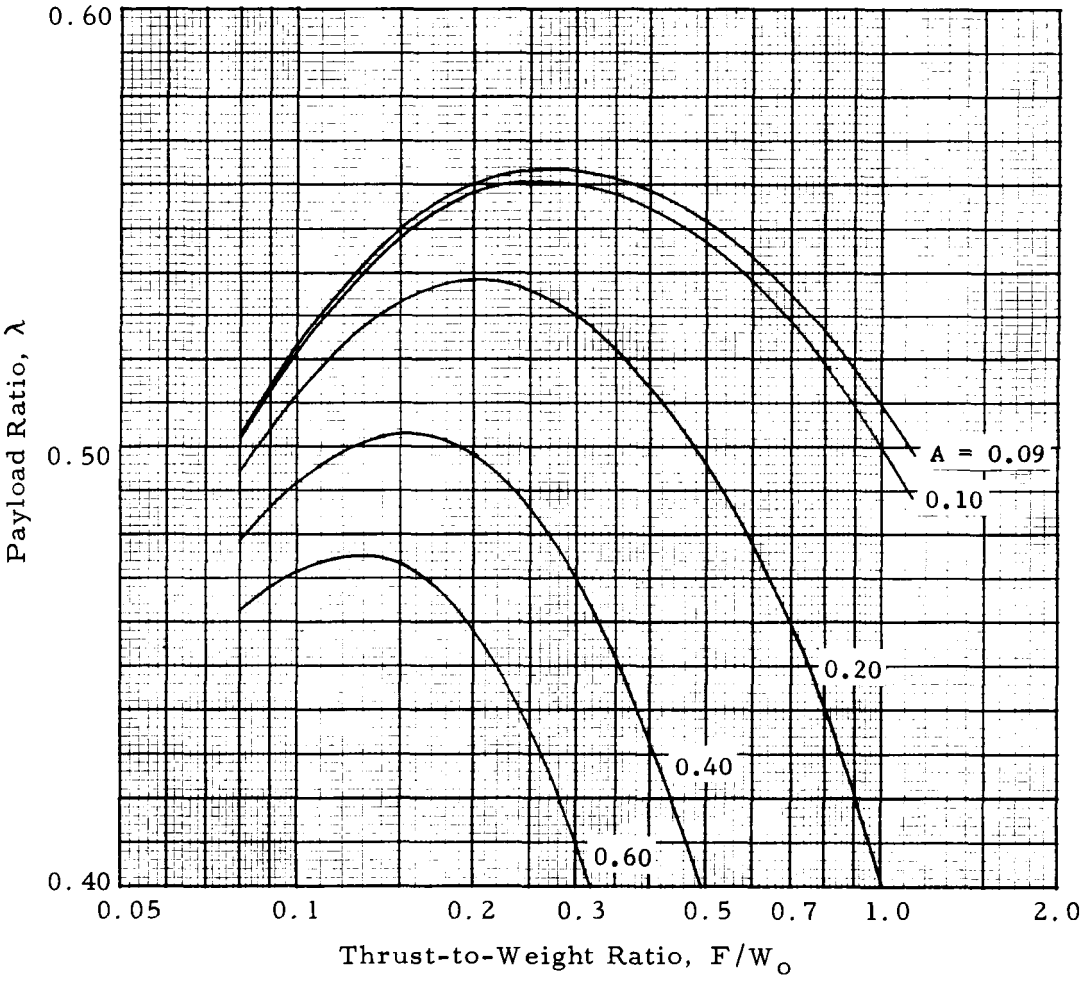

FIGURE 55. PAYLOAD RATIO AT ESCAPE

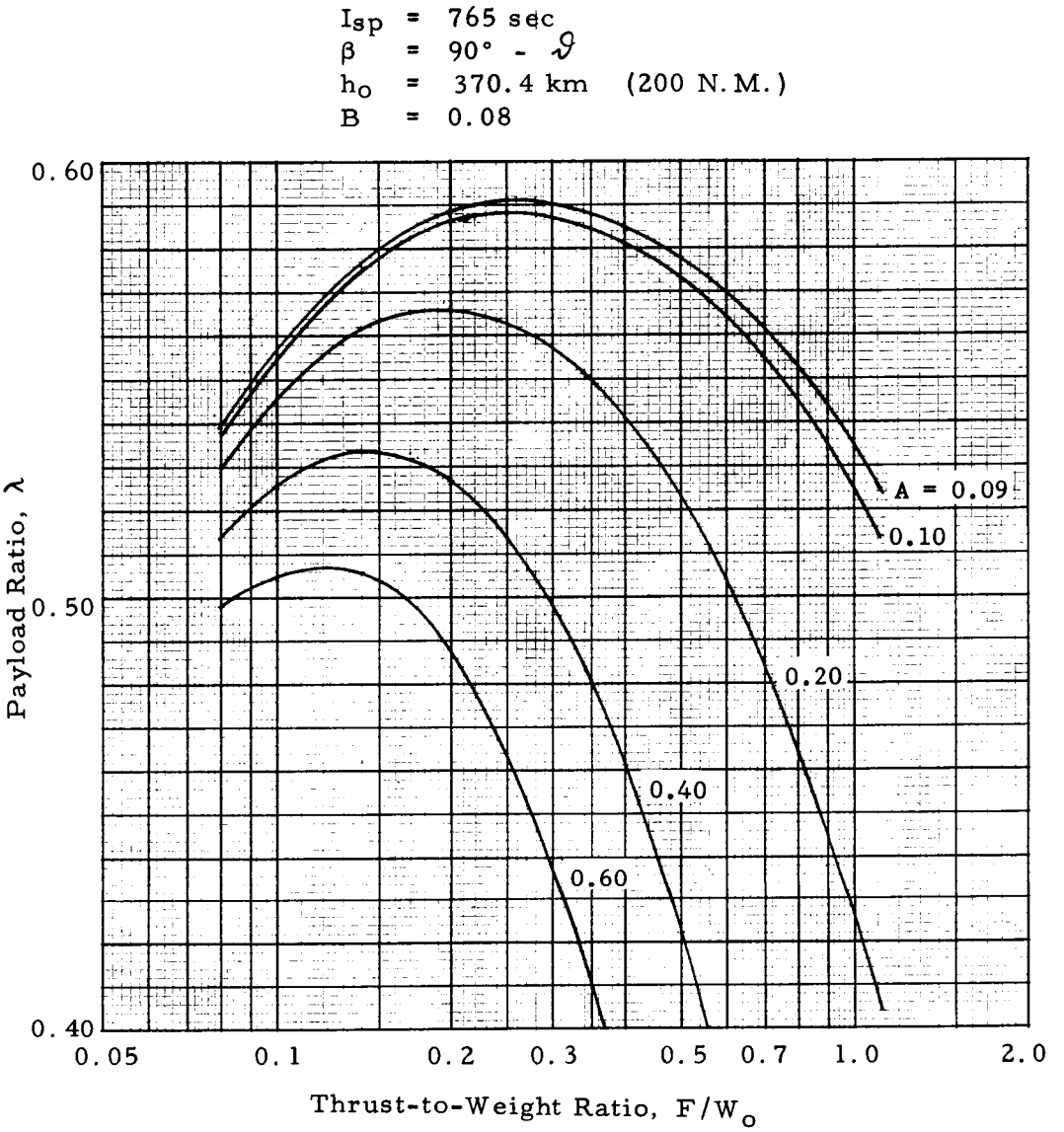

FIGURE 56. PAYLOAD RATIO AT ESCAPE

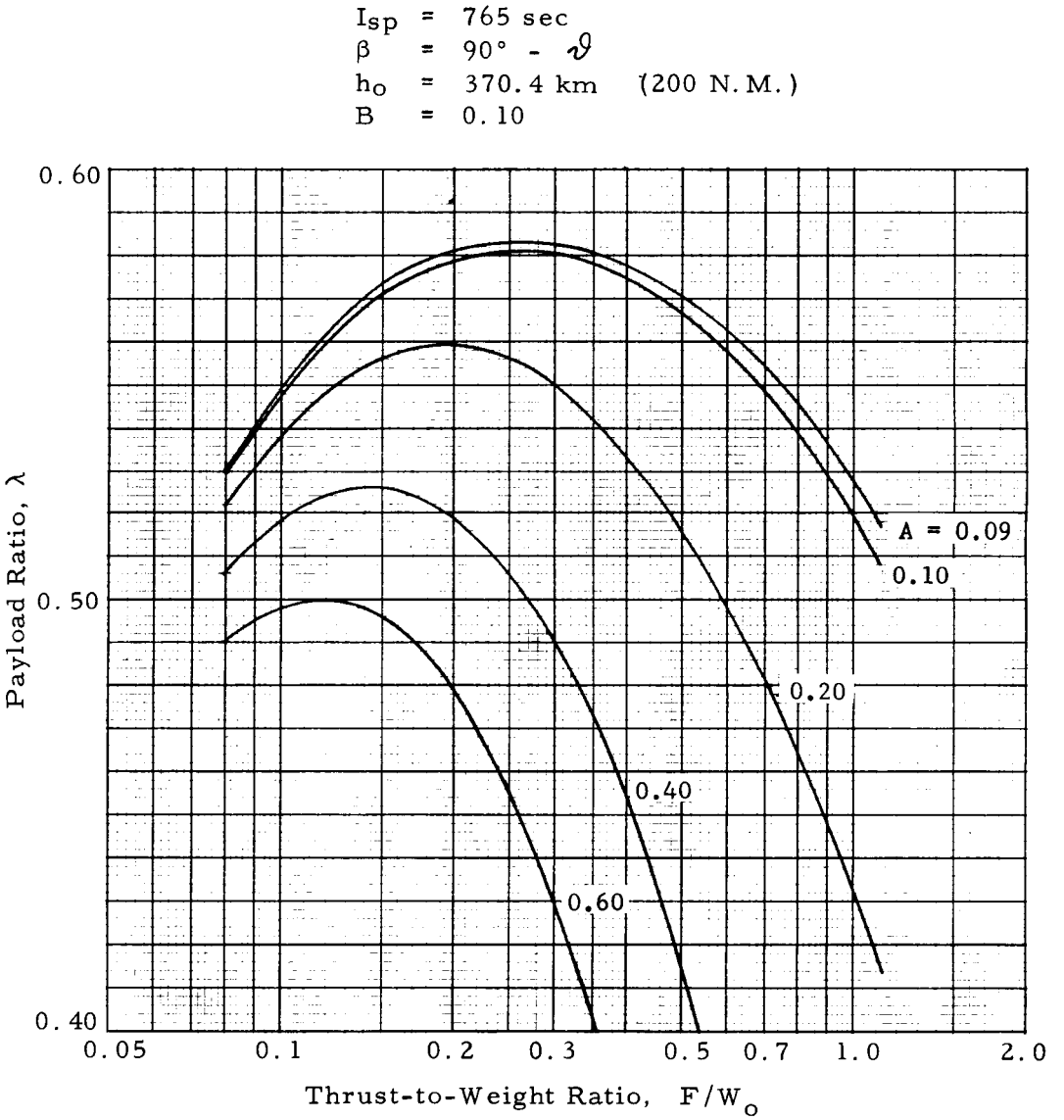

FIGURE 57. PAYLOAD RATIO AT ESCAPE

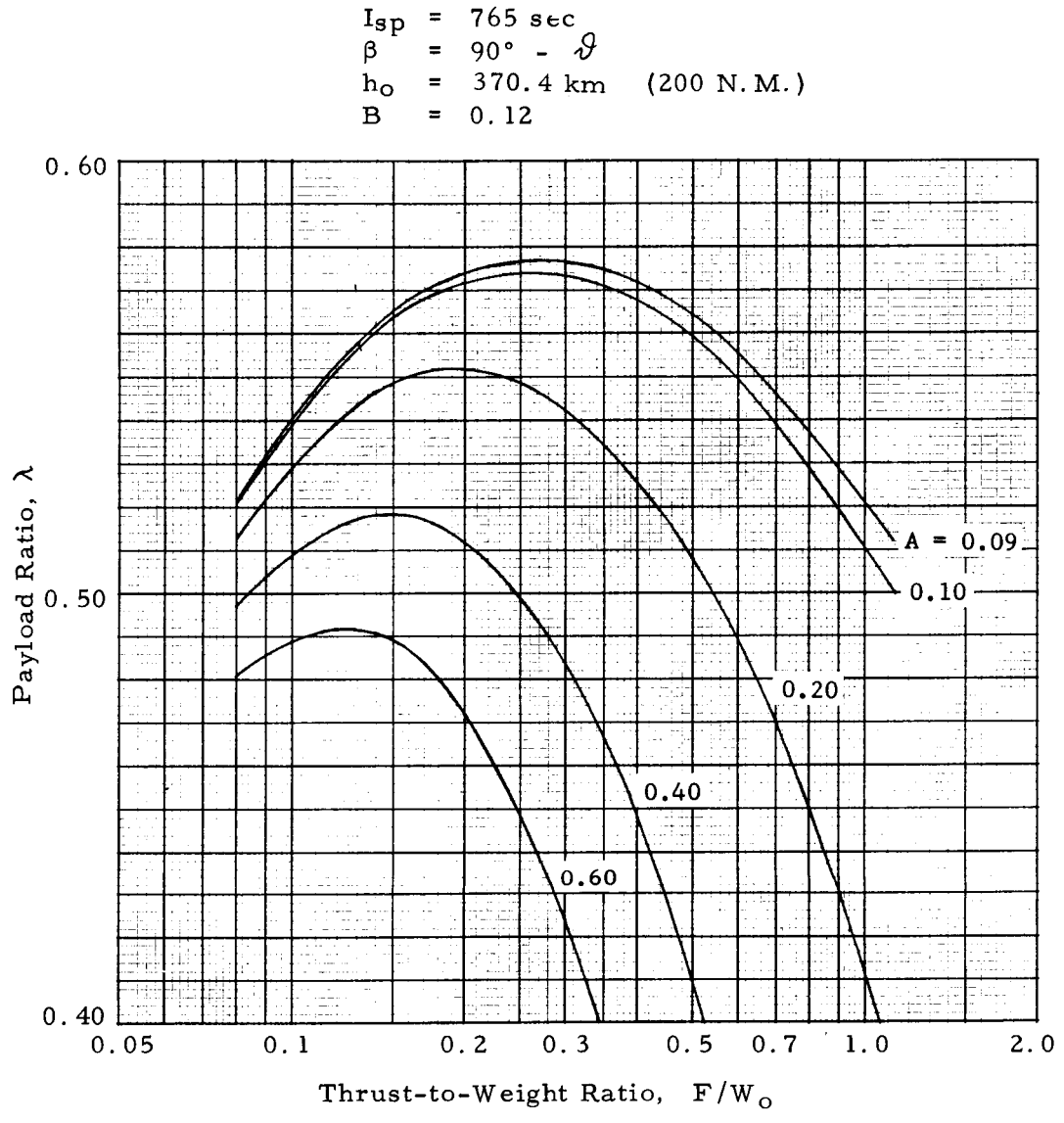

FIGURE 58. PAYLOAD RATIO AT ESCAPE

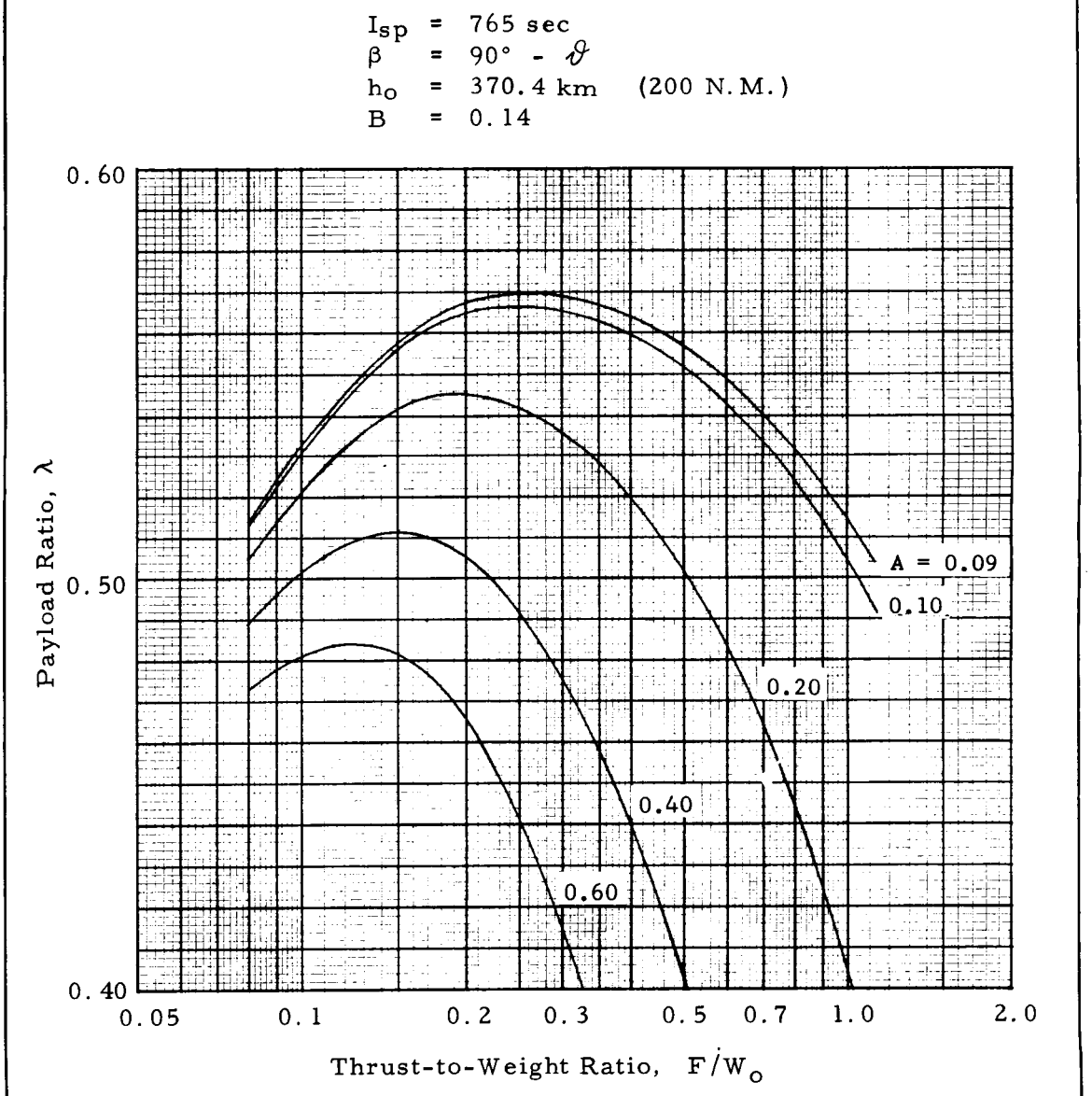

FIGURE 59. PAYLOAD RATIO AT ESCAPE

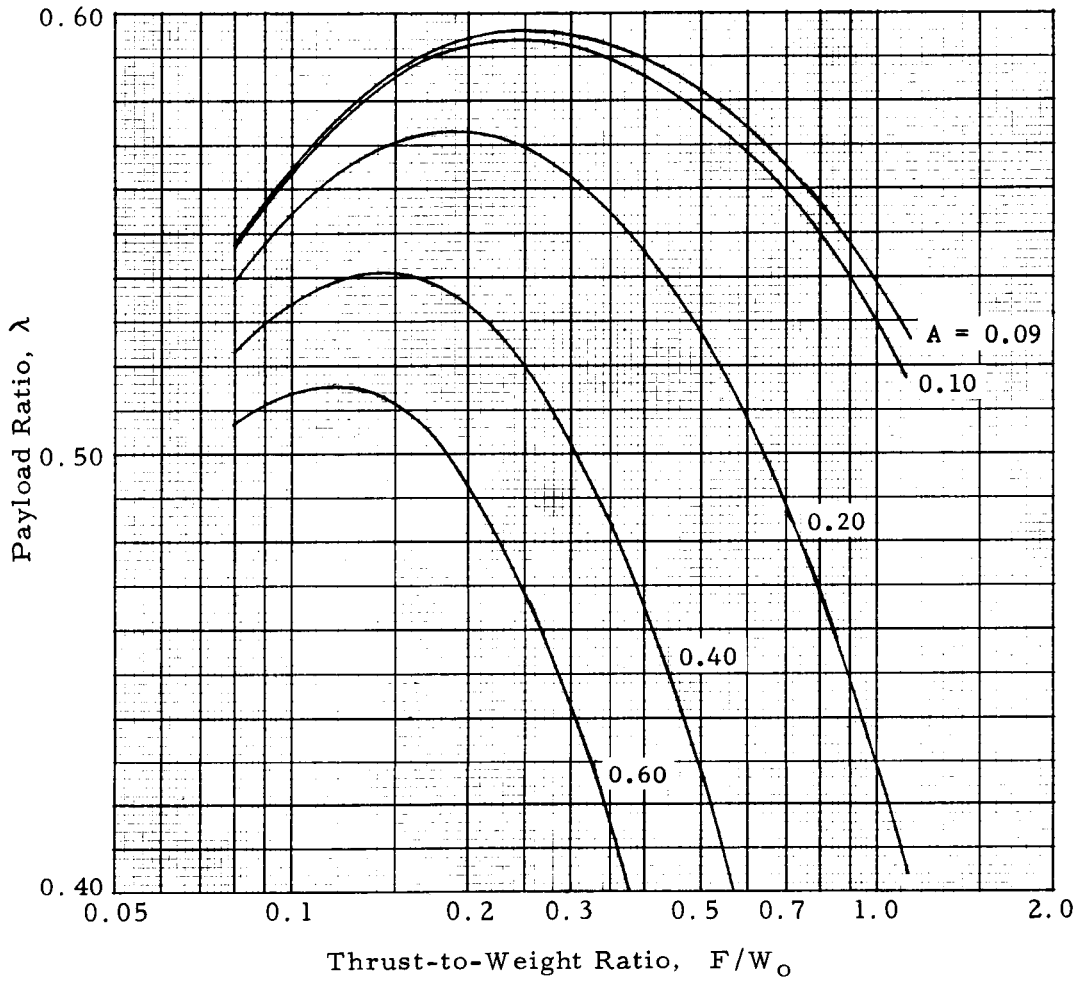

FIGURE 60. PAYLOAD RATIO AT ESCAPE

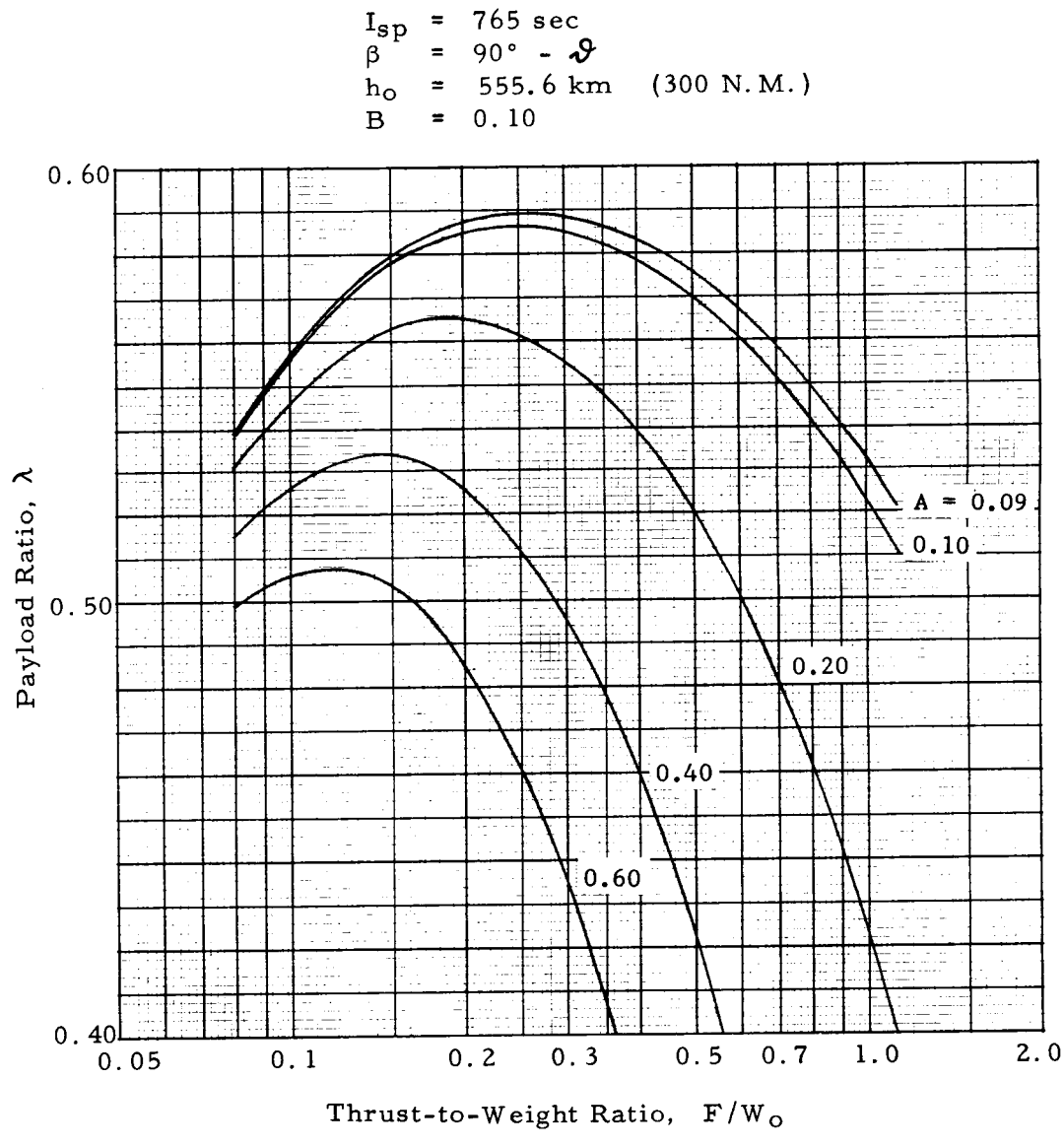

FIGURE 61. PAYLOAD RATIO AT ESCAPE

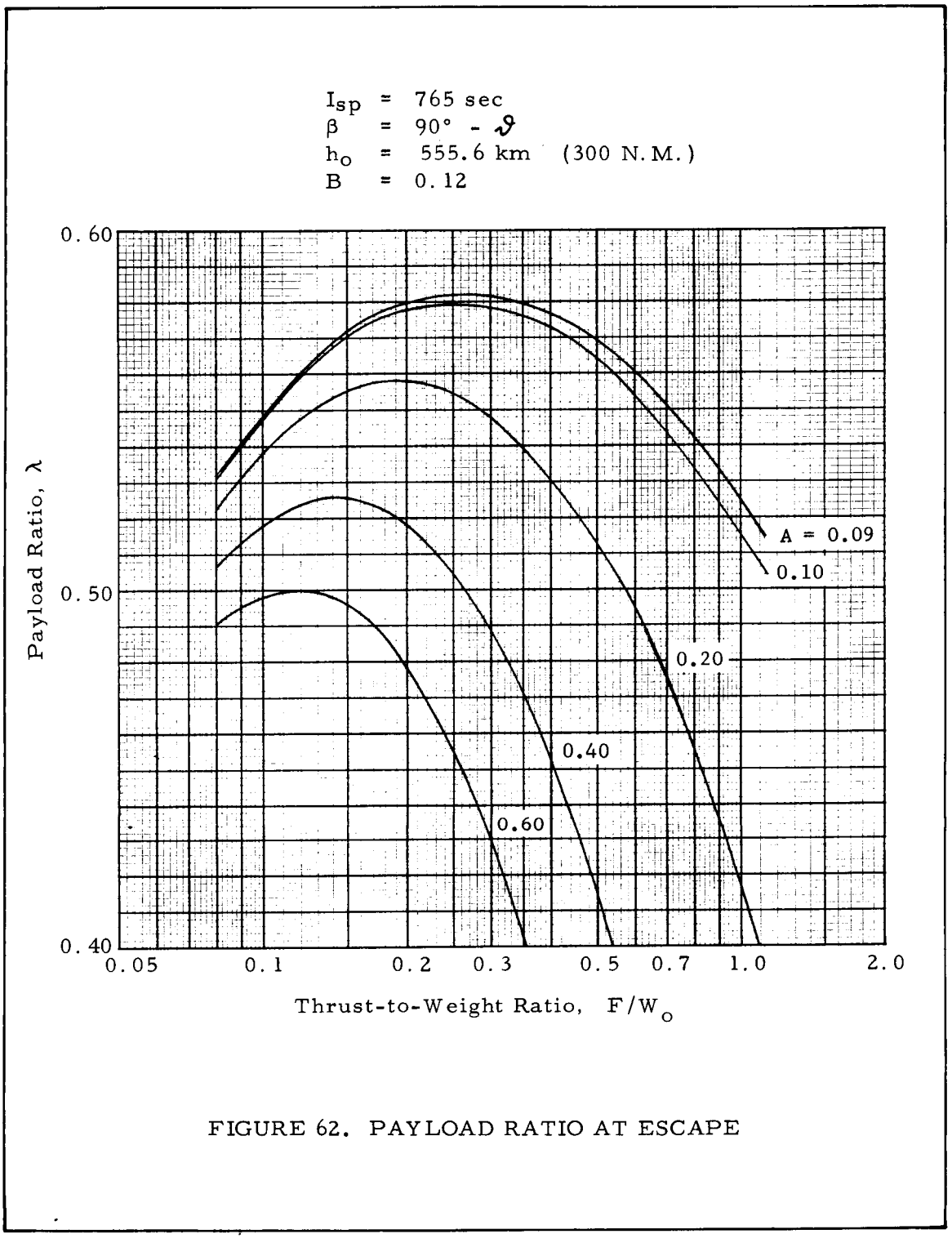

FIGURE 62. PAYLOAD RATIO AT ESCAPE

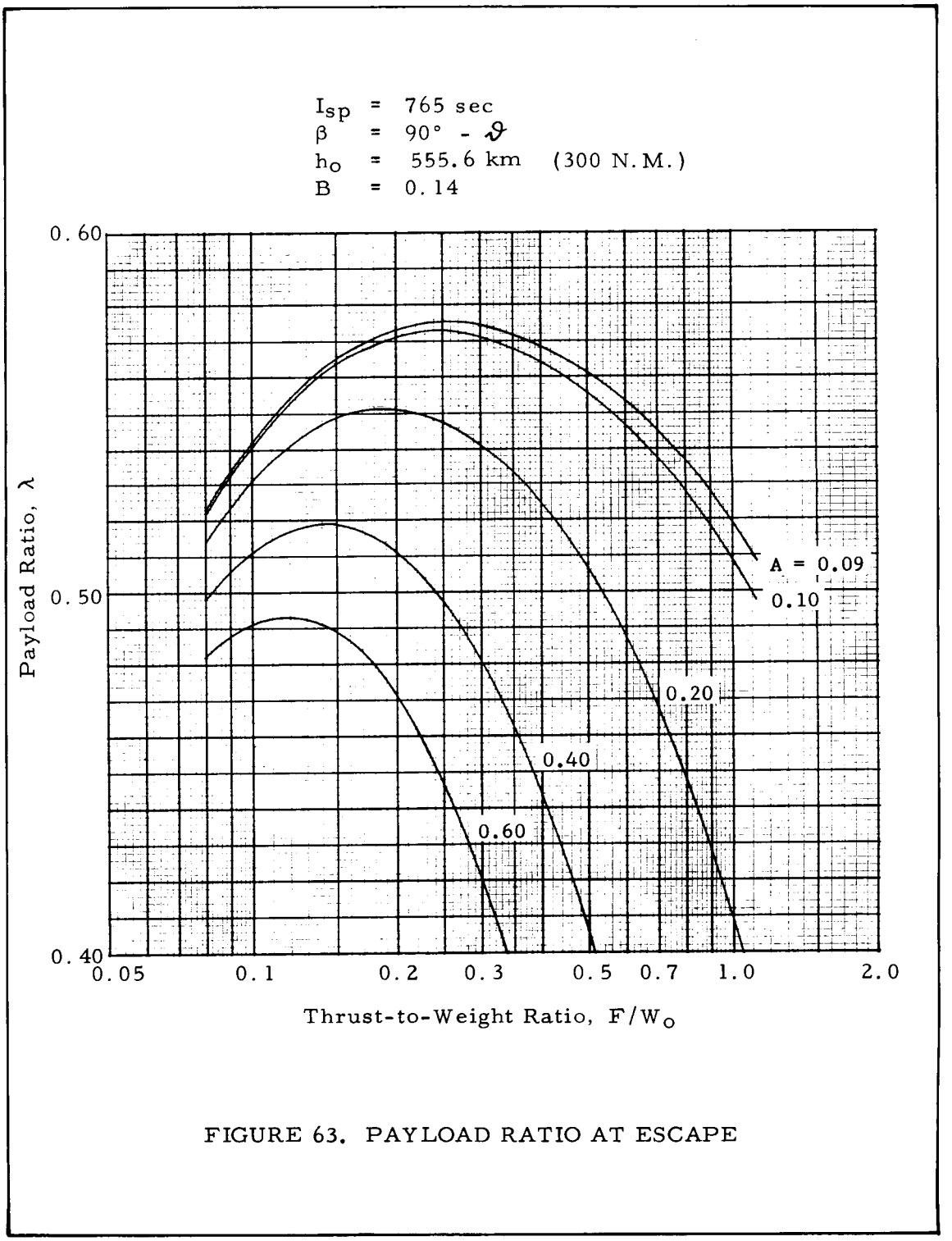

FIGURE 63. PAYLOAD RATIO AT ESCAPE

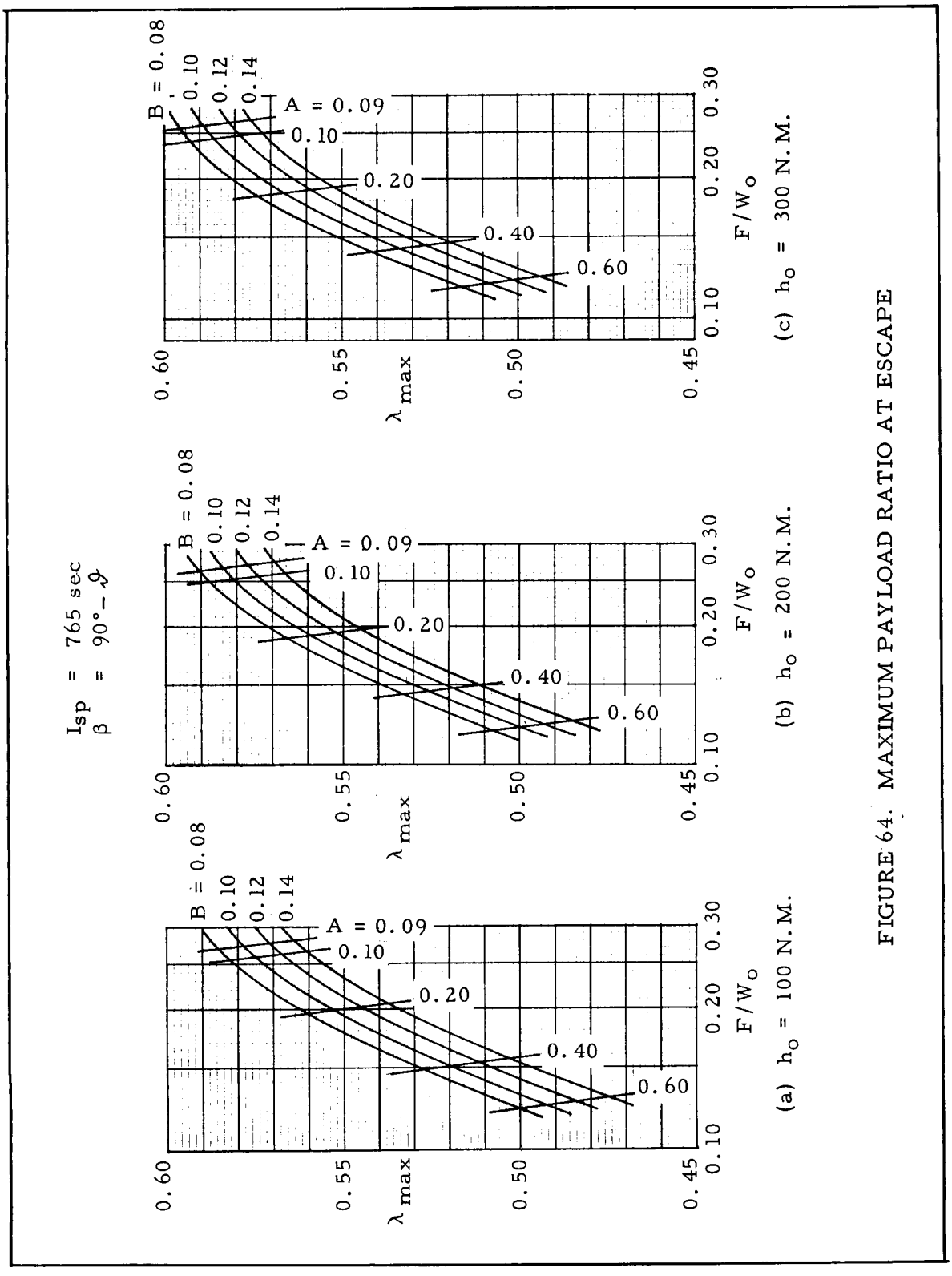

FIGURE 64. MAXIMUM PAYLOAD RATIO AT ESCAPE

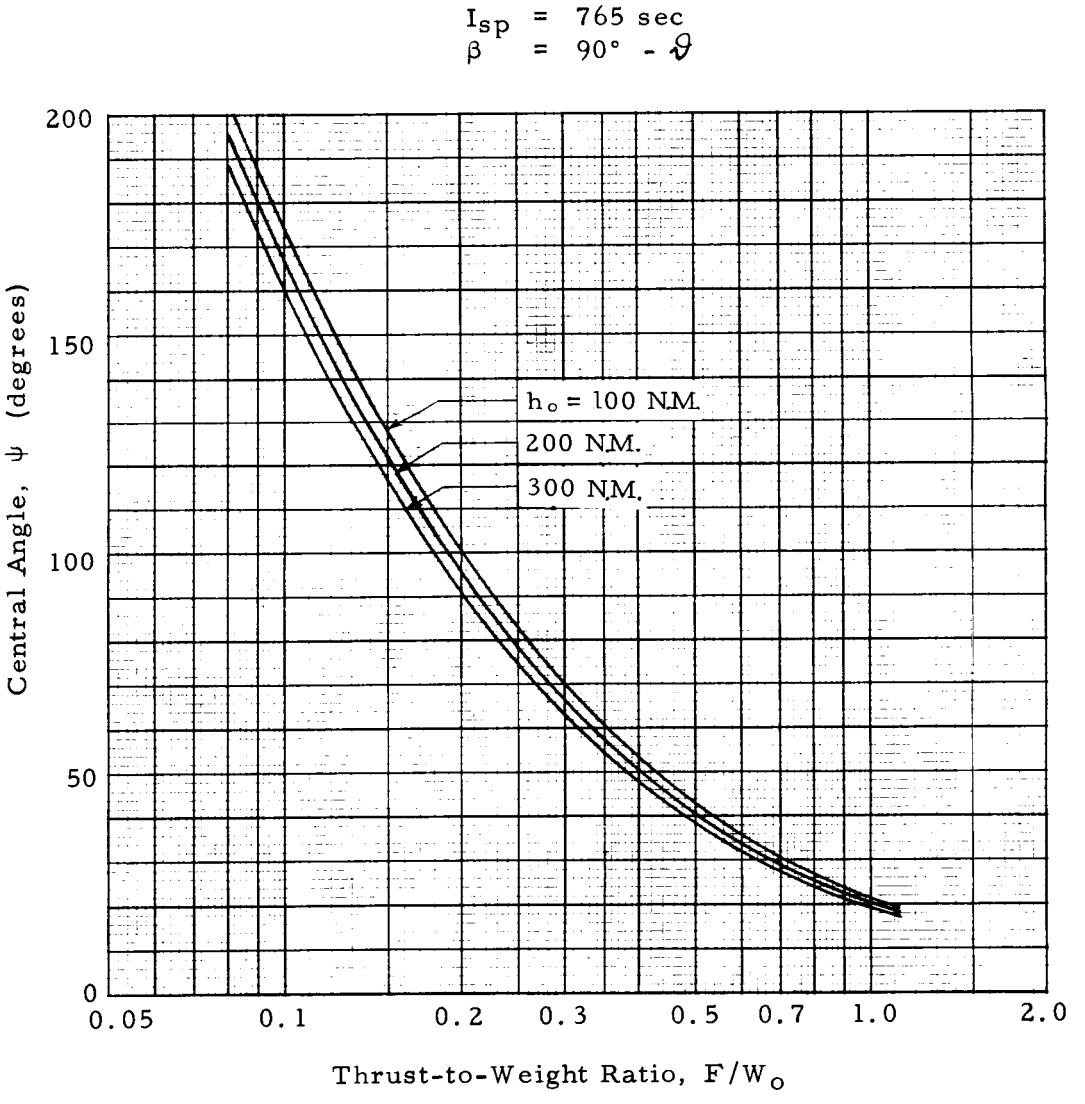

FIGURE 65. CENTRAL ANGLE AT ESCAPE

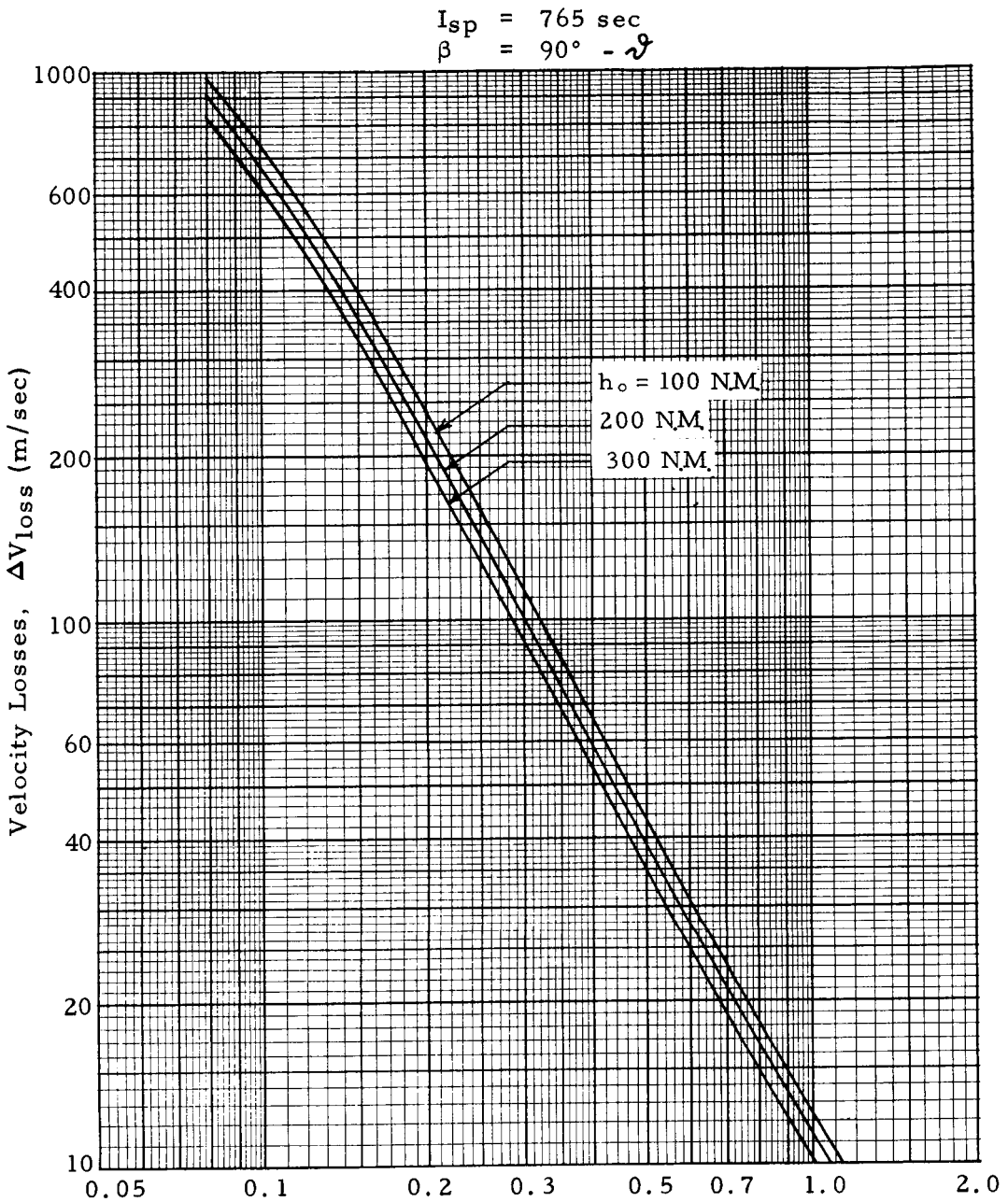

FIGURE 66. VELOCITY LOSSES FROM ORBIT TO ESCAPE

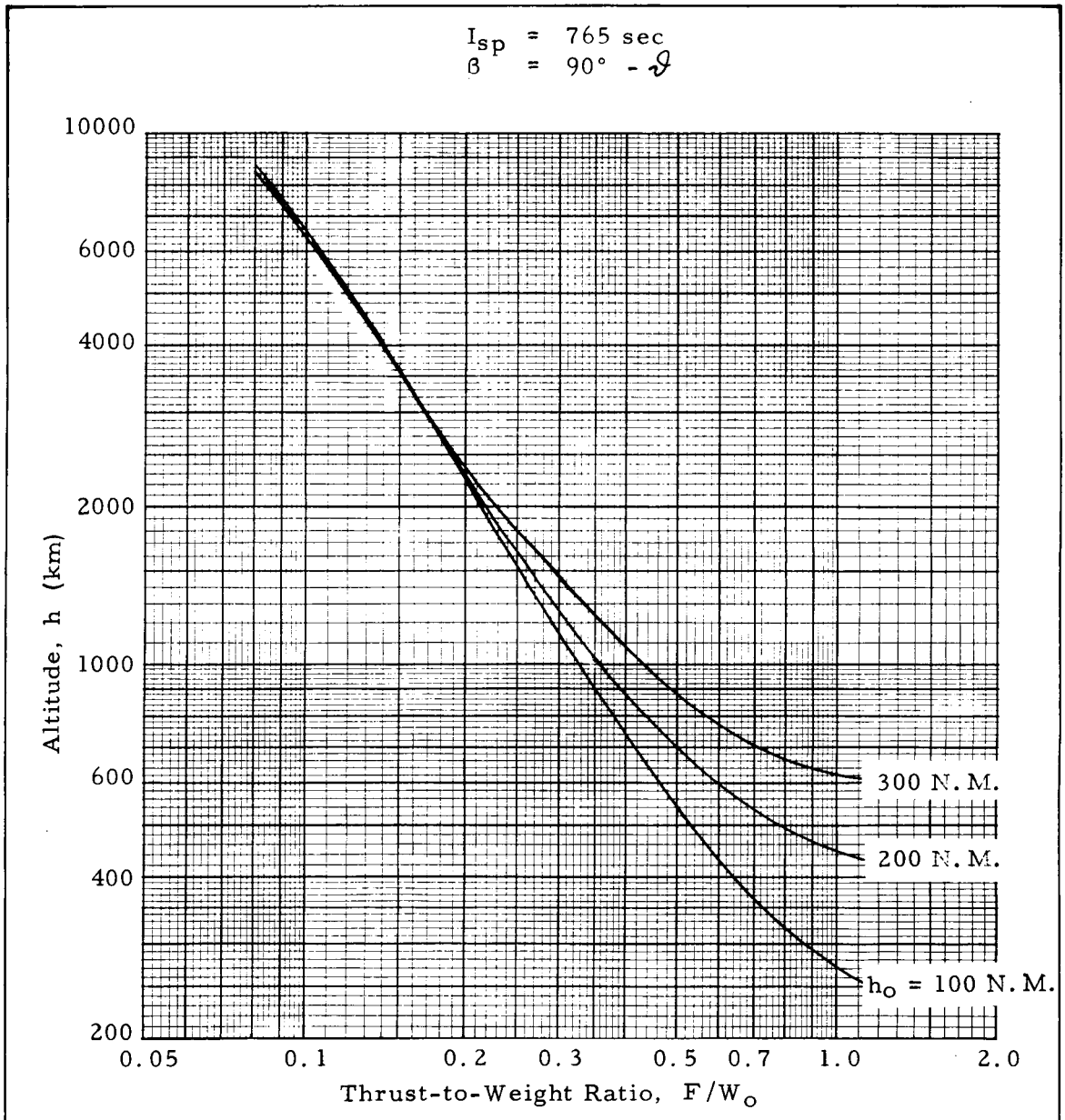

FIGURE 67. ALTITUDE AT ESCAPE

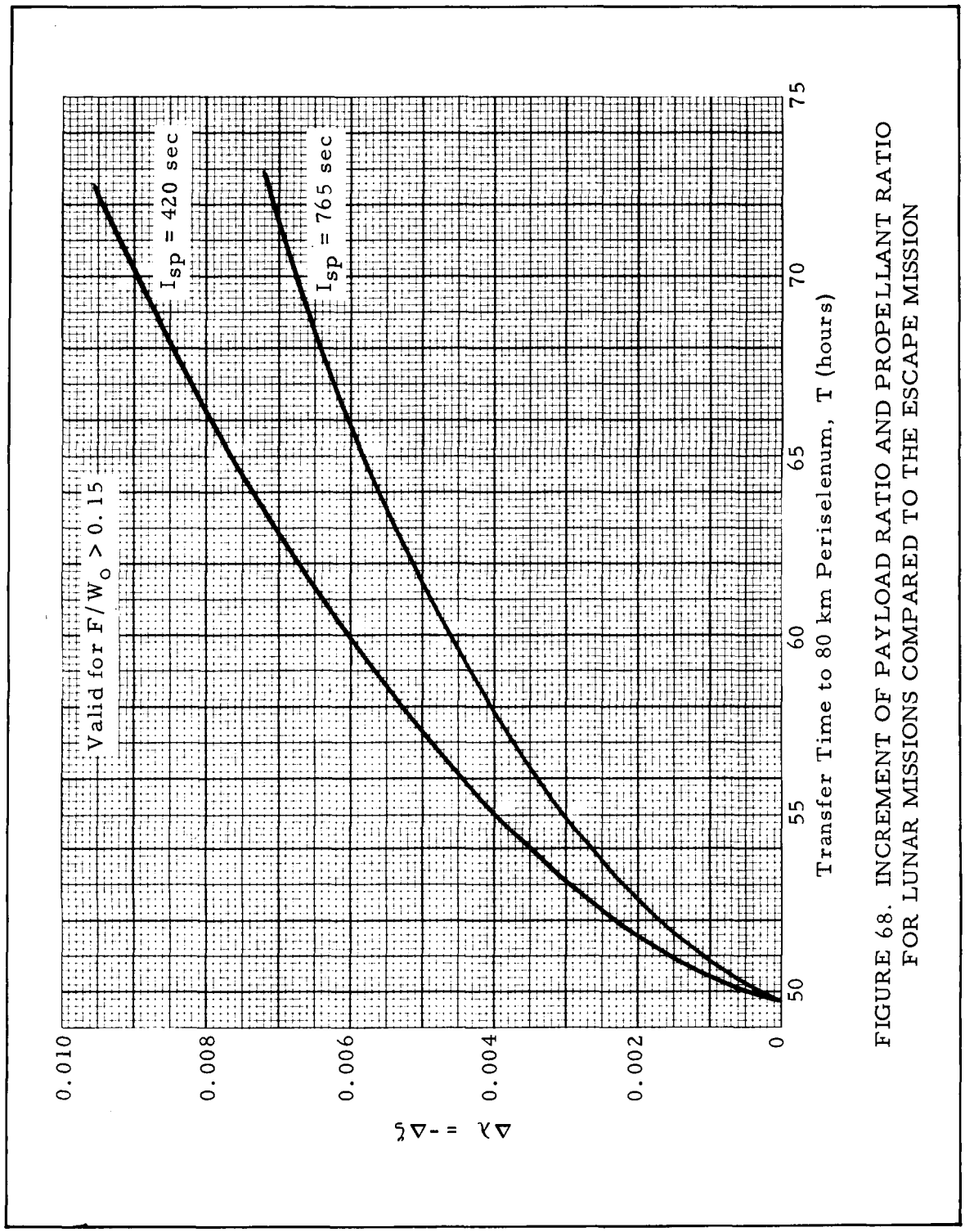

FIGURE 68. INCREMENT OF PAYLOAD RATIO AND PROPELLANT RATIO FOR LUNAR MISSIONS COMPARED TO THE ESCAPE MISSION